ABSTRACT

Title of Dissertation: **IDENTIFICATION AND CHARACTERIZATION OF IAA OXIDASES AND THEIR ROLE IN IAA HOMEOSTATIC REGULATION IN *ARABIDOPSIS***

Jun Zhang, Doctor of Philosophy, 2016

Dissertation directed by: Dr. Wendy Ann Peer, Assistant Professor, Department of Environmental Science and Technology

Auxin is a crucial plant hormone that shapes and directs plant growth. Indole-3-acetic acid (IAA) is the predominant auxin in nature. Auxin regulates cell expansion and cell division in a dose dependent way. Therefore, plants evolved an extremely complex yet highly coordinated network to maintain auxin homeostasis, including IAA biosynthesis, transport, conjugation and oxidation. Among these, the least known process is IAA oxidation. Discovering how IAA is terminated is very important in completing the whole picture of IAA homeostatic regulation.

By partial purification of IAA oxidases from *Arabidopsis*, we detected IAA oxidation activity from both microsomal fractions and soluble fractions. We first investigated the protein in microsomal fraction and identified one oxidase named as ACC oxidase 2 (ACO2), an ethylene synthetase that belongs to 2-oxoglutarate and iron (II) [2OG(Fe)] dependent dioxygenase family. *In vitro* enzyme assays with IAA showed

that ACO2 could catabolize IAA and that the product had the same retention time as indole-3-carbinal (ICA), an decarboxylative IAA oxidation product. The same enzyme assay with the ACO2 homologues ACO3 was conducted, and ACO3 showed similar activity. An *ACO2* loss-of-function allele showed ethylene related phenotypes, including longer hypocotyls and reduced apical hook angle in etiolated seedlings, and delayed bolting. Further, null aco2 mutants also showed reduced phototropic bending, a typical auxin related phenotype. These results indicate that ACO2 might be involved in both ethylene and auxin signaling.

We also investigated the soluble IAA oxidases, *AtDAO1* (*DAO1*) and *AtDAO2* (*DAO2*). *In vitro* enzyme assays showed that both recombinant DAO1 and DAO2 have IAA oxidation activity and the product is the non-decarboxylated 2-oxindole-3-acetic acid (oxIAA), the major IAA metabolite observed under normal growth conditions. Analysis of the loss-of-function null allele *dao1-1* showed that DAO1 is the predominant IAA oxidase and is responsible for 95% of oxIAA production in Arabidopsis seedlings. Dysregulation of IAA oxidation altered the IAA metabolism profile and causes accumulation of other IAA conjugates and a series of morphological alteration, including elongation of organs, increased lateral roots and delayed sepal opening. Investigation of expression patterns shows that DAO1 is a cytosolic protein that widely expressed throughout the plant, especially in the root tip, the pericycle of root, the cotyledon, and the sepal, highly correlating to the phenotypes of *dao1-1*. These results suggest that IAA oxidation plays an important role in IAA homeostasis during the whole life of *Arabidopsis*.

Identification and characterization of IAA oxidases and their role in IAA homeostatic regulation in *Arabidopsis*

by

Jun Zhang

Dissertation submitted to the Faculty of the Graduate School of the
University of Maryland, College Park, in partial fulfillment
of the requirements for the degree of
Doctor of Philosophy
2016

Advisory Committee:
  Assistant Prof. Wendy Ann Peer, Chair
  Prof. Caren Chang
  Prof. James Culver
  Prof. Zhongchi Liu
  Prof. Angus Murphy
  Associate Prof. Jianhua Zhu

Acknowledgements

Table of Contents

List of Figures

Participant contributions

The project was initiated and guided by Dr. Wendy Peer. All the LC-MS analysis was conducted by Ella Jinshan Lin and Dr. Joshua Blakeslee in Department of Horticulture and Crop Science University of Ohio. The phylogenic tree in chapter 3 was made by Fernanda Campos Mastrotti Pereira in São Paulo State University, São Paulo, Brazil. The phototropism assay was conducted by Candace Pritchard. Chinchu Harris and Fan Wu helped me with enzyme assay, constructing vectors, planting and genotyping. I designed and performed most of the experiments and analyzed the data.

Chapter 2 will be submitted to the *Journal of Experimental Botany* in August 2016. Chapter 3 was submitted to the *Proceeding of National Academy of Sciences USA* in March, 2016, and a revision was submitted in July 2016.

Chapter 1: Literature review: IAA oxidation, an auxin homeostasis guard

Abstract

Auxin (Indole-3-acetic acid, IAA) is a critical plant hormone that is involved in all kinds of developmental process throughout the whole life of the plant. IAA oxidation regulates IAA levels in the plant via reducing the active IAA. There are two forms of oxidation: decarboxylative IAA oxidation and non-decarboxylative IAA oxidation. Peroxidases and oxygenese were found to catalyze decarboxylative IAA oxidation *in vitro*, and *in vivo* studies indicate this might play a role in stress induced auxin level reduction. 2-oxindole-3-acetic acid (oxIAA), the product of IAA non-decarboxylative oxidation, was found to be the primary IAA degradation product under normal conditions across species. Recently, the oxIAA metabolic pathway was finally discovered in rice and *Arabidopsis* along with the enzymes that catalyze the reaction: DIOXYGENASE OF AUXIN OXIDATION (DAO), a subfamily of the 2-oxoglutarate and Fe(II) [2-OG Fe(II)] dependent dioxygenase superfamily. Biochemical and genetic studies revealed critical physiological functions of DAO during plant growth and development. Here, the historical and recent studies about IAA oxidation will be reviewed and the perspective of future study will be discussed.

Keywords

Indole-3-acetic acid, auxin oxidation, auxin decarboxylation, conjugation, development, DAO proteins, stress.

Introduction

The plant hormone auxin plays a critical role in plant growth, development and responses to the environment by controlling cell expansion and cell division (Gonzalez et al., 2012; Perrot-Rechenmann, 2010). The determination of the plant architecture is dependent on well pre-programmed auxin distribution in every single cell throughout the whole life of plant (Finet and Jaillais, 2012).

Auxin signaling pathway by SCF^{TIR1}-Aux/IAA complex has been thoroughly studied recently (Parry et al., 2009; Peer et al., 2011). Auxin signaling is perceived by TIR1/AFBs proteins in nuclei (Dharmasiri et al., 2005; Kepinski and Leyser, 2005). Once TIR1/AFBs is bound to auxin, it will initiate the ubiquintination of AUX/IAA, repressor proteins of downstream auxin responsive factors (Tiwari et al., 2001; Zenser et al., 2001), and thus turn on auxin responses (Parry et al., 2009; Tan et al., 2007). Cellular IAA concentrations are regulated by transport, biosynthesis, and catabolism (Normanly, 2010; Korasick *et al*., 2013). IAA is mainly synthesized by indole-3-pyruvic acid (IpyA) pathway (Mashiguchi et al., 2011) (Stepanova et al., 2011). TRYPTOPHAN AMINO TRANSFERASE OF ARABIDOPSIS (TAA) and TAA-Related (TAR) family proteins synthesize IPyA from tryptophan (Trp), and then YUCCA family proteins convert IPyA to IAA (Mashiguchi et al., 2011; Stepanova et al., 2011). The *YUCCA* family has 11 members and catalyze the rate-limiting step in this pathway (Zhao et al., 2001). Recent studies of *YUCCA* with genetic tools revealed that localized auxin biosynthesis plays a key role in plant development, especially morphogenesis of floral organs and embryos (Panoli et al., 2015; Robert et al., 2015; Vernoux et al., 2010).

Polar transport of auxin from sites of synthesis to sites of action allows auxin to respond to environmental changes like light and gravity, and form asymmetric distribution patterns during a short time period (Michniewicz et al., 2007). Auxin is conducted by cooperation of auxin influx transporters (AUX1/LAX family) and efflux facilitators and transporters (PIN family and ABCB family) located on the plasma membrane (Vanneste and Friml, 2009). Among these, PINs are well studied and their polar localization within the cell coordinates with the direction of auxin transport (Vanneste and Friml, 2009). The constitutive endocytosic recycling mediates the dynamic control of PINs polar distribution (Grunewald and Friml, 2010).

IAA catabolism controls IAA levels in the cells by reducing the free IAA levels via conjugation or oxidation. IAA can be conjugated to glucose by UDP-glucose transferases UGT84B1, UGT74E2 and UGT74D1, to produce 1-O-indole-3-acetyl-β-D-glucose (IAA-Glc) (Jackson et al., 2001; Jin et al., 2013; Tognetti et al., 2010). IAA can also be conjugated to amino acids by IAA amino acid conjugate synthases that belong to the GRETCHEN HAGEN 3 (GH3) family (Ludwig-Müller, 2011). Most of the conjugates could be hydrolyzed to free IAA by IAA-glucose hydrolases or amido hydrolases, except for IAA-Aspartic acid (IAAsp) and IAA-Glutamate (IAA-Glu) (Ludwig-Müller, 2011; Korasick et al., 2013; Ishimaru et al., 2013). The final step in IAA catabolism is IAA oxidation via oxidative decarboxylation (Reinecke and Bandurski, 1987; Barceló et al., 1990), or through non-decarboxylative oxidation (Östin et al., 1998). IAA oxidation was the least understood step in IAA metabolism. Now, as several IAA oxidases were identified from different species, we

finally are able to understand the mechanism of IAA oxidation and its role in auxin
homeostasis. This review will discuss the biochemistry, the evolution and the
physiological role of IAA oxidation *in planta*.

1. IAA decarboxylation

From the 1970s through the 1990s, the study of IAA metabolism was mainly
conducted by incubation of extracted plant proteins with IAA *in vitro*. The products
were identified mainly as IAA decarboxylation products: indole-3-aldehyde, indole-
3-carbinal, 3-methylene-2-oxindole, etc. (Figure 1; Normanly, 1997; Suzuki and
Kawarada, 1977). Peroxidases (EC 1.11.1.7) from numerous plant species have been
shown to catalyze this oxidative decarboxylation (Sembdner et al., 1981), including
horseradish peroxidase (HRP) and grape leaf peroxidase. Later, partial purification of
plant proteins identified other oxidases not in the peroxidase family were able to
decaboxylate IAA (Beffa et al., 1990). A 32.5 kDa soluble protein from maize roots
was partially purified and the product of IAA oxidation was identified as indole-3-
carbinal ((Beffa et al., 1990). Ethylene or stress treatments strongly enhanced the rate
of IAA decarboxylation. In citrus, ethylene-treated leaf discs were incubated with
IAA and more indole-3-carbinal was produced than non-treated leaf discs (Sagee et
al., 1990). Similarly, peroxide-treated *Arabidopsis* seedlings showed strong IAA
decarboxylation activity, and the products were identified via GC-MS (Murphy et al.,
unpublished data). These data indicate that decarboxylative auxin oxidation might
play a role in reducing free IAA during stress.
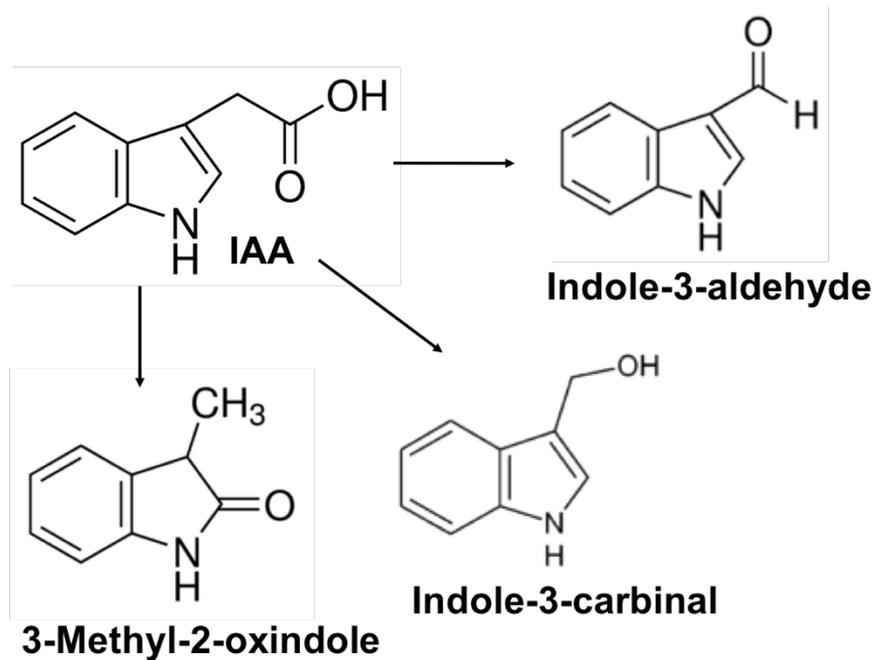
Figure 1-1. IAA decarboxylation pathway. The acetic acid group of IAA can be decarboxylated to form different side chains on the indole ring,

2. The oxIAA pathway is the major IAA catabolic pathway

With the development of [^{14}C] labeling compound tracer and mass spectrum techniques, researchers were able to identify the products of IAA metabolism *in planta*. 2-oxindole-3-acetic acid (oxIAA) was first identified as the major IAA catabolic product in maize seedlings by Reinecke et al (1981). They found that oxIAA levels were almost the same as IAA levels in maize kernels, and approximately 26% of the radiolabled IAA was turned over to oxIAA in kernels of seedlings after 4h incubation. Later, oxIAA was detected widely in higher plants, including *Arabidopsis* (Kowalczyk and Sandberg, 2001; Östin et al., 1998; Novák et al., 2012), orange (Chamarro et al., 2001), tomato (Riov and Bangerth, 1992), *Zea mays* (Reinecke and Bandurski, 1983), broad bean (Tsurumi and Wada, 1980), and

Scotch pine (*Pinus sylvestris*) (Ernstsen et al., 1987). oxIAA also exists as a predominant IAA metabolite in lower plants, including algae (Jacobs, 1993) and bryophytes (Záveská Drábková et al., 2015), although the variety and levels of IAA conjugates in lower plants are reduced compare to higher plants (Sztein et al., 1995; Záveská Drábková et al., 2015). This indicates that plants developed IAA oxidation as a strategy of IAA deactivation very early during plant evolution.

Arabidopsis seedlings fed with radiolabeled IAA primarily produce oxIAA, 1-O-(2-oxoindol-3-ylacetyl)-β-D-glucopyranose (oxIAA-Glc or oxIAA-Hex) and the conjugates indole-3-acetyl aspartic acid (IAA-Asp) and indole-3-acetyl glutamate (IAA-Glu) (Östin et al., 1998). Feeding experiments with oxIAA showed that more than 90% of the oxIAA was conjugated to glucose in 48h. UGT74D1 was recently identified as the enzyme that catalyzed glucosylation of oxIAA (Tanaka et al., 2014). In the loss-of-function line of *UGT74D1*, oxIAA-Glc decreased 85% while oxIAA increased 2.5 fold. All of these data indicated that oxIAA-Glc is mainly synthesized via glucosylation of oxIAA and not oxidation of IAA-Glc. Oxidation of IAA-amides were also detected *in planta*, although at very low levels. oxIAA-Asp and 6-OH-IAA-Asp were detected only in mature tissue or when high levels of exogenous IAA were added into the system (Östin et al., 1998). N-(6-hydroxyindol-3-ylacetyl)-phenylalanine (6-OH-IAA-Phe), and N-(6-hydroxyindol- 3-ylacetyl)-valine (6-OH-IAA-Val) were detected in *Arabidopsis* seedlings (Kai et al., 2007). oxIAA-amino acid (oxIAA-AA) or 6-OH-IAA-amino acid (6-OH-IAA-AA) could be detected after feeding with radiolabeled IAA-AA but not with oxIAA (Östin et al., 1998) or 6-OH-IAA (Kai et al., 2007), indicating oxIAA-AA and 6-OH-AA are formed by oxidation

of IAA-AA, and not from amino acid conjugation of oxidized IAA (Figure 1-2).

Consistent with this result, AtDAO1, the enzyme that catalyzes IAA oxidation in

Arabidopsis, can also oxidize IAA-Asp *in vitro*, and generated two oxidized IAA-Asp

products with same fragmentation pattern but different retention time in LC-MS

(Zhang et al., unpublished).

Among all of the catabolic products of IAA, oxIAA and oxIAA-Glc are the major

catabolic products based on direct measurements of the IAA metabolome in

Arabidopsis. In Arabidopsis seedlings, the ratio of oxIAA: IAA is around 1: 1-5 and

the ratio of oxIAA-Glc: IAA is around 1: 30-50 under normal conditions, while the

ratio of IAA-AA (IAA-amino acid conjugates) and oxidized IAA-AA with IAA is

lower than 1: 0.2 (Kai et al., 2007; Pencik et al., 2013; Tanaka et al., 2014), indicating

the oxIAA pathway is primary pathway in IAA catabolism.
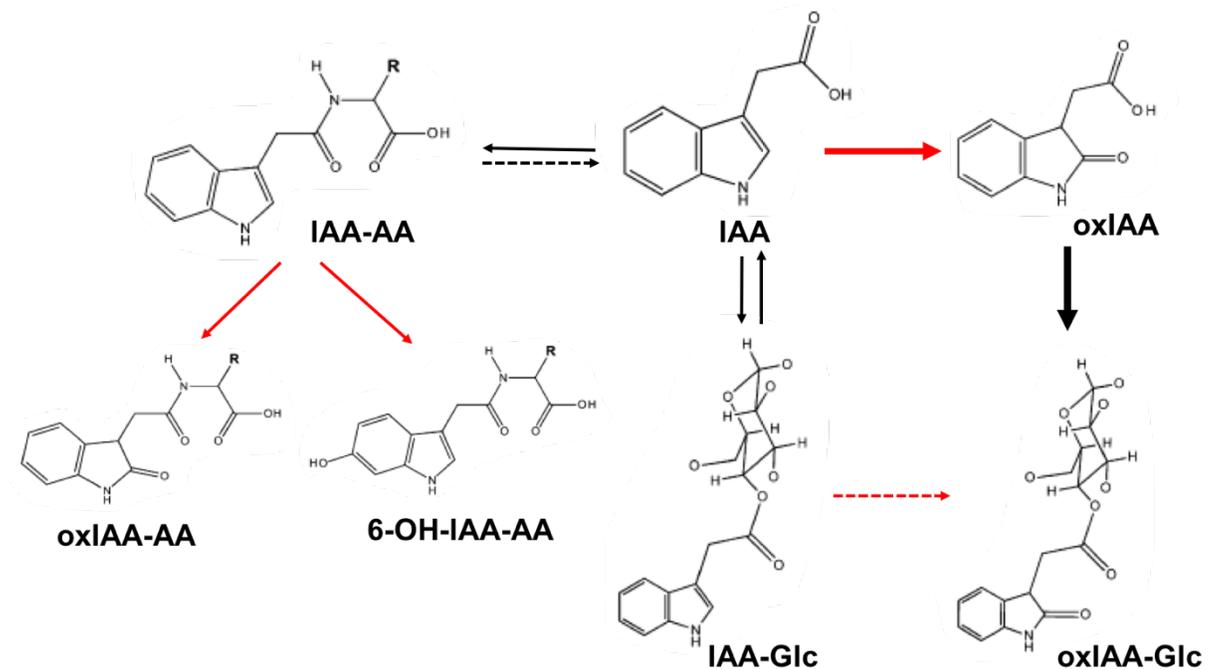
Figure 1-2. Non-decarboxylative oxidation in auxin metabolism in *Arabidopsis*. Arrows

indicate the metabolic pathway, with heavier weight indicating the primary reactions

under normal growth conditions. Black arrows indicate conjugation reactions. Red arrows indicate oxidative reactions. Black dashed arrow indicates partial hydrolysis of IAA-AA to IAA. Red dashed arrows indicate that this reaction has not been demonstrated *in planta*.

Study of oxIAA distribution in Arabidopsis seedlings shows that oxIAA in the root is much higher than in the shoot (Kowalczyk and Sandberg, 2001; Novák et al., 2012). IAA metabolite analyses of root segments show that oxIAA levels mirrors IAA levels in *Arabidopsis* roots (Pencík et al., 2013), and the highest oxIAA concentration was found in the root apex, where the IAA levels were also the highest. This indicates that IAA non-decarboxylative oxidation plays important role in IAA homeostasis. oxIAA does not have any biological activity as IAA *in planta* (Peer et al., 2013; Pencik et al., 2013). oxIAA treatment of Arabidopsis seedlings shows that oxIAA could neither promote hypocotyl elongation, inhibit root growth (Pencík et al., 2013), nor induce the expression of the IAA reporters DR5rev:GPF or 2XD0:GUS in the root tip (Peer et al., 2013). Further, oxIAA does not interact with the TIR1/AFB auxin receptors (Pencík et al., 2013). Rootward transport assays with [^{3}H]oxIAA in whole seedlings showed that oxIAA could not be transported at the root–shoot transition zone (Kubeš et al., 2012) or at the root tip (Peer et al., 2013). All of these data indicate that oxIAA has no physiological function as IAA and cannot induce the auxin signaling pathway. In sum, the oxIAA pathway is the major IAA catabolic pathway under normal growth condition.

2.1 Non-decarboxylative IAA oxidation by the DAO subfamily of dioxygenases

Although the importance of non-decarboxylative IAA oxidation was implicated in many *in vivo* assays, the enzymes that catalyze this reaction were only identified recently. The first non-decarboxylative IAA oxidase, the *DIOXYGENASE FOR AUXIN OXIDATION (DAO)* was identified in rice (*Oryza Sativa*) during a male infertility screen (Zhao et al., 2013). Then two homologs of *OsDAO* in Arabidopsis, *AtDAO1* and *AtDAO2* were newly identified (Zhang et al., Porco et al., co-submitted to *PNAS*), and one gene previously identified as an *ADVENTITIOUS ROOT RELATED OXYGENASE* in apple (*ARRO-1*) (Butler, 2000; Smolka et al., 2009) is a putative *DAO.* These proteins share a high similarity to each other and very low similarity to the other to 2-oxoglutarate/iron-dependent dioxygenase family (2-OG Fe(II) oxygenase) (Figure 1-3), making them a novel subfamily.
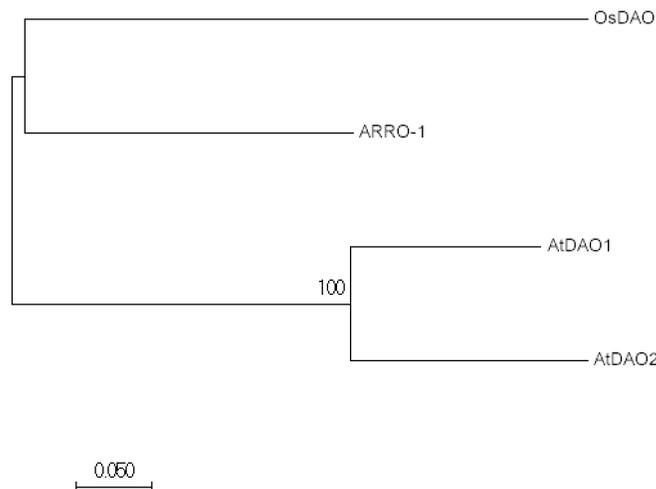
 Figure 1-3. Evolutionary relationship of identified DAO subfamily proteins. The evolutionary history was inferred using the Neighbor-Joining method (Saitou and Nei, 1987). The bootstrap consensus tree inferred from 2500 replicates (Joseph, 1985) is taken to

represent the evolutionary history of the DAO orthologs analyzed. Branches corresponding to partitions reproduced in less than 50% bootstrap replicates are collapsed. The analysis involved 4 amino acid sequences. All ambiguous positions were removed for each sequence pair. There were a total of 319 positions in the final dataset. Evolutionary analyses were conducted in MEGA7 (Kumar et al., 1965).

All of the known DAO proteins belong to 2-OG Fe(II) oxygenase, which is a highly diverse protein family involved in many different biological processes, including hormone biosynthesis and catabolism, DNA repair, oxygen sensing, and demethylation in epigenetic regulation (Farrow and Facchini, 2014; Hodges, 2002). Typically, the enzyme uses ferrous iron and oxygen to oxidatively decarboxylate 2-OG into succinate and CO_2. At the same time, another atom of oxygen is added to the primary substrate (S) and give rise to S-O (Figure 1-4) (Farrow and Facchini, 2014; Martinez and Hausinger, 2015). This protein family shares two conserved domains, the dioxygenase domain and 2OG Fe(II) oxygenase domain. Within the DAO subfamily, a motif, P(S/D/G)E(F/L)VD(A/G)EHPR, was identified as unique to DAOs, and was named the DAO motif (Zhang et al., unpublished Chapter 3). The most closely known proteins to DAOs are GA synthases in rice, apple and Arabidopsis (Butler and Gallagher, 1999; Zhao et al., 2013; Zhang, unpublished), which do not contain the DAO motif. Thus far four DAO members have been identified, with one copy in rice, two in Arabidopsis, and one in apple (Butler and Gallagher, 1999; Zhao et al., 2013; Zhang, unpublished).

$$S \longrightarrow S\text{-}O$$

$$2\text{-}OG + O_2 \quad succinate + CO_2$$
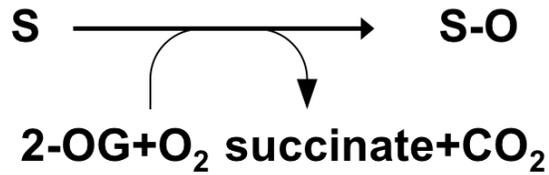
Figure 1-4. Scheme of 2-OG(Fe) dependent dioxygenase catalyzed reaction. 2-OG, 2-oxoglutarate; S, substrate.

2.2 Physiological function of identified DAOs in plant growth and development

Genetic tools have been used to investigate the physiological function and expression pattern of *DAOs* during plant growth and development. Analyses of the known *DAOs* show similar as well as species-specific phenotypes. The loss-of-function of *OsDAO* in rice leads to severe deficiencies in anther dehiscence and pollen fertility in rice. LC-MS analysis detected an increase in free IAA levels in the anther and ovary, and oxIAA was not detected in the rice *dao* mutant. GUS staining showed that *OsDAO* is highly expressed in the anthers and ovaries especially during the late stage of flowering. All of these indicate that OsDAO catalyzes IAA oxidation and plays critical role in regulation of IAA homeostasis in reproductive organs in rice.

I characterized the first *DAOs* in dicots, and another lab working in parallel independently: *AtDAO1* and *AtDAO2* in *Arabidopsis thaliana* (Zhang et al., Porco et al., co-submitted to *PNAS*). AtDAO protein sequences share 72% similarity with OsDAO. *dao1-1*, a *dao1* null mutant, contains 95% less oxIAA compared to wild type, and complementation of *dao1* restores wild-type oxIAA levels, indicating that DAO1 is the primary IAA oxidase in seedlings (Zhang et al.). Further, *dao1-1* plants

have phenotypes associated with increased auxin levels including elongated organs (hypocotyls, primary roots, rosette leaves, inflorescence stems), increased lateral root density, enhanced apical dominance, and delayed sepal opening compared to wild type, while *dao1-2D*, *DAO1* gain-of-function line, shows the opposite phenotype. Unlike *OsDAO*, both *AtDAO1* and *AtDAO2* knock-out/ knock-down lines are fertile. Native promoter driven YFP: genomic open reading frame expression fusions show that AtDAO1 is widely and constitutively expressed in the epidermis and the vascular tissue throughout the plant, and is strongly expressed in the bundle sheath cells in upper sepal during flower opening, highly correlating with the phenotype of the *AtDAO1* loss-of-function line. AtDAO2 was only detected in root cap at a very low level. All of the above data indicate that AtDAO1 is the primary IAA oxidase under normal conditions in Arabidopsis and plays important role in auxin homeostasis regulation during plant morphogenesis. However, AtDAO2 might function in specific processes. It was reported that the *AtDAO2* transcript level is regulated by circadian clock, and and oxIAA levels show circadian variation (Voß et al., 2015). This might cause variation in IAA levels during day the and further affect lateral root initiation. The root cap is sensitive to environmental changes, and it was recently reported to be involved in lateral root pre-patterning (Xuan et al., 2015). So, it is possible that the oscillating expression of *DAO2* in root cap has an impact on the lateral root initiation. To test this this hypothesis, double *dao1dao2* mutants are needed to compare the lateral root development with *dao1* under different light conditions.

The DAO1-like protein in apple, ARRO-1, shares 57% and 56% amino acid sequence identity to AtDAO1 and AtDAO2. It was isolated as an up-regulated gene in stem discs during auxin-induced adventitious root initiation (Butler and Gallagher, 1999). *ARRO-1* expression was also detected constitutively in the primary root of apple seedlings, similar to *AtDAO1* (Butler, 2000). *ARRO-1* in the primary root was highly up-regulated by indole-3-butyric acid (IBA) and IAA treatment but not by aminocyclopropyl carboxylic acid (ACC, ethylene precursor) or 2,4-dichlorophenoxyacetic acid (2,4-D, artificial auxin) treatment, indicating its function in auxin homeostasis regulation in the root of apple (Butler, 2000).

In sum, *DAOs* are low copy genes resulting different physiological processes in plant development in different plant species via IAA deactivation. In dicots like apple and *Arabidopsis*, they are mainly involved in vegetative growth, like lateral root development and leaf shape. In monocots like rice, DAO is mainly involved in reproductive growth. However, we still need more information about DAO in other plant species to draw a more complete picture about the physiological function of DAOs.

2.3 Comparison of IAA oxidation and IAA conjugation

IAA oxidation and conjugation are two different pathways to deactivate IAA. The different biochemical characteristics of DAOs and GH3s and their spatiotemporal expression patterns indicate the enzymes play the different roles during plant growth and development and responses to the environment.

Reaction rate

GRETCHEN HAGEN 3s (GH3s) have faster enzyme kinetics compared to the DAO family proteins, based on *in vitro* enzyme assays (Staswick et al., 2005; Zhang et al., submitted) and metabolic assays *in planta*. Aspartic acid is conjugated to IAA by recombinant GH3.6 at 244 nmol IAA-Asp /min/mg protein (Staswick et al., 2005), while recombinant AtDAO1 and AtDAO2 oxidizes IAA at around 5 pmol oxIAA/min/mg protein (Zhang et al., submitted), more than 10,000 times slower than GH3.6. By comparing auxin metabolism data from 11 dicots and 2 monocots, Kramer and Ackelsberg (2015) concluded that the IAA oxidation rate is between 10-40 nM/h, while the auxin conjugation rate could exceed 100 µM/h, depending on the auxin concentration applied. Therefore, DAO appears to function in a very slow manner to fine tune auxin at basal levels, in contrast to GH3.

Expression pattern

At the transcriptional level, *GH3* family genes have very low expression under normal growth conditions, unless expression is stimulated by specific conditions, such as high levels of auxin (*GH3.1, 2, 3, 4*), blue light (Takase et al., 2004) (*GH3.10*), or jasmonic acid (Khan and Stone, 2007) (*GH3.9*). *GH3* genes are among the fastest to respond to exogenous auxin, with transcript levels increasing more than 10 times within 1h (GEO accession GSM9969, http://www.ncbi.nlm.nih.gov/geo/). These suggest that the GH3 family is mainly involved in responses to environmental stimuli. In contrast, *OsDAO* and *AtDAO1,* the only two *DAO* genes that were thoroughly studied, have a constitutive background expression level in most tissues under normal conditions and have strong expression in reproductive organs during flower opening stage (Zhao et al., 2013; Zhang et al., submitted), indicating the

expression of DAOs are precisely programmed to regulate IAA homeostasis during plant growth and development. On the other hand, *DAO* could also be induced by exogenous IAA (Mellor et al., co-submitted to *PNAS*).

When Östin et al (1998) fed Arabidopsis seedlings with different amounts of IAA, they found that different metabolic profiles were obtained from feeding with 0.5 µM or 5 µM IAA. Under low IAA treatment, IAA was mainly degraded to oxIAA and oxIAA-Glc. Under the highest IAA treatment, IAA conjugation became major IAA catabolic pathway. Considering the difference of reaction rates and expression patterns between DAO and GH3, it is very easy to understand why: IAA oxidation is the guard under normal growth conditions and maintain IAA level at base level while GH3 is the firefighter that responds when environmental stimuli induce high levels of cellular IAA and a fast response is required.

2.4 Cooperation of IAA oxidation with other metabolic pathways

IAA oxidation cooperates with IAA biosynthesis and conjugation to maintain homeostasis. Detailed IAA metabolic profiling of loss-of-function *dao1-1* in Arabidopsis shows that loss of IAA oxidation does not lead to a significant change in IAA levels (Zhang et al., Porco et al., and Mellor et al., co-submitted to *PNAS*). Instead, it alters the IAA metabolic network to maintain active IAA at a normal level. IAA biosynthesis is reduced while IAA conjugation products accumulated significantly in *dao1-1*, partially compensating for the loss of IAA oxidation. This demonstrates that regulation of IAA homeostasis by the IAA metabolic pathway is redundant to some extent.

Another kind of cooperation is by the timing of expression. In the sepals of Arabidopsis, *YUC1* and *YUC4*, encoding two key IAA biosynthetic enzymes, are expressed during early stages of flower development, while *DAO1* is highly expressed during the late stages just before flower opening (Zhang et al., submitted; Cheng et al., 2006). Measurements of IAA in the sepal shows that IAA levels are in the sepals of very young flowers (42 ± 3.4 pg mg^{-1}) and are reduced (6.7 ± 2.9 pg mg^{-1}) at the time of bud opening (Zhang et al., submitted). Double *yuc1yuc4* mutants failed to develop normal sepals, and *dao1-1* shows delayed sepal opening. Taken together, the precise cooperation between IAA biosynthesis and IAA oxidation regulates dynamic IAA levels required for flower development and opening.

3. IAA oxidation and ROS

During stress or ROS treatment, IAA signals are attenuated. Blomster et al. (2011) showed that a ROS burst could cause a down regulation of initial auxin signaling genes including the auxin co-receptors *TIR/AFBs* and *IAA/AUXs* and the ARF transcription factors. This leads to stress-induced morphogenetic response in Arabidopsis. Lack of ROS scavengers in the triple *ntra ntrb cad2* mutant causes auxin related phenotypes and reduced IAA levels (Bashandy et al., 2010). Some evidence indicates that ROS could increase the level of IAA oxidation to reduce free IAA. In Arabidopsis, oxIAA levels are higher in mutants that lack ROS-scavenging flavonoids (*tt4*) and lower in mutants that accumulate excess flavonols (*tt3*) (Peer et al., 2013). A mitochondrial ATP-dependent protease, FtH4, is identified as a modulator between H_2O_2 and auxin homeostasis to regulate plant growth and development (Zhang et al., 2014). The *ftsh4-4* mutation has decreased free IAA,

perturbed auxin signaling, and elevated H_2O_2 and peroxidase levels. The dwarfism and increased in axillary branching of the *ftsh4-4* mutant could be reversed by expressing the IAA synthetase *iaaM* gene or by knocking down the peroxidase genes *PRX34* and *PRX33*, resulting in elevated auxin levels in *ftsh4-4* mutant. Peroxidases are activated by hydrogen peroxide which is formed under stress conditions (Gazaryan et al., 1996), and horseradish and tobacco peroxidases were shown to decarboxylatively oxidize IAA *in vitro*. Microarray data in the root of Arabidopsis seedlings show that *AtDAO1* and *AtDAO2* both respond to multiple abiotic stresses, including salt, drought and UV-B (Affymetrix ATH1 microarray data from Kilian et al., 2007). All of this indicates that IAA oxidation is involved in ROS-induced auxin signaling attenuation. However, the mechanism underlying IAA oxidation in stress and the purpose has not been fully elucidated.

4. Perspective

Substantial progress has been made with the recent identification of IAA oxidases and made the understanding of IAA metabolism much more complete. However, there are still puzzles that are waiting to be answered. For example, is auxin oxidation involved in hormonal crosstalk? How does ethylene enhance IAA decarboxylation rate? Jasmonic acid (JA) is involved in flower opening, which also involves auxin (Nagpal et al., 2005), and *DAO1* expression can be strongly induced by JA (microarray data from AtGenexpress, NASCARRY174). Further efforts are needed to explain the mechanism of the hormone crosstalk involved by IAA oxidation. Also how do plants regulate the expression and post-transcriptional regulation of IAA oxidases? A better understanding of IAA oxidation could eventually be applied to agricultural

17

production as a tool to manipulate crops growth and improve resistance to

environmental stress.

Chapter 2: Two ACC oxidases exhibit IAA oxidation activity *in vitro*

Abstract

The phytohormone auxin (indole-3-acetic acid, IAA) is widely involved in plant developmental and physiological processes. Auxin oxidation has been suggested to be one of the crucial ways IAA levels are regulated in plant developmental and physiological processes.

Discovering how IAA oxidation terminates auxin signal transduction events is important to efforts to manipulate auxin signaling. Both soluble and membrane associated auxin oxidation have been described. Recently, I purified an ethylene biosynthetic enzyme, 1-aminocyclopropane-1-carboxylate oxidase 2 (ACC oxidase 2, ACO2) from Arabidopsis microsomal membranes, that has IAA oxidation activity *in vitro*. ACO2 is a member of a 2-oxoglutarate and iron (II)-dependent dioxygenase family that catalyzes the last step in ethylene biosynthesis converting ACC to ethylene. ACO2 is induced by IAA treatment, indicating that ACO2 is a point of convergence in ethylene – auxin crosstalk. Enzyme activity of ACO2 homologues ACO1 and ACO3 were also tested *in vitro* and ACO3, the closest member to ACO2, showed similar IAA oxidase activity. *ACO2* loss-of-function lines exhibited reduced phototropic bending compared to wild type.

Introduction

Auxin, like a commander in chief, coordinates plant growth by regulating cell division and cell expansion (Perrot-Rechenmann, 2010). Therefore, plants developed a redundant system to control auxin homeostasis in every individual cell, including auxin biosynthesis, transport, conjugation, and oxidation (Peer et al., 2011). The least understood process among these is auxin oxidation. Both soluble and membrane associated auxin oxidation have been described (Peer et al., 2013). One type of IAA oxidation is decarboxylation of the carboxyl group of IAA by peroxidase and oxygenases (Sembdner et al., 1980). The products of the *in vitro* reaction include indole-3-carbinal, 3-methylene-2-oxindole, 3-hydroxymethyl-2-oxindole, et al., as identified by mass spectrometry (Normanly, 1997; Suzuki and Kawarada, 1977). The other type is non-decarboxylation oxidation of IAA by addition of one oxygen on the C2 position of IAA, generating 2-oxoindole-3-acetic acid (oxIAA), which may be further conjugated to glucose to form 1-O-(2-oxoindol-3-ylacetyl)-β-D-glucopyranose (oxIAA-Glc or oxIAA-Hex) (Christie et al., 2011; Kai et al., 2007; Kowalczyk and Sandberg, 2001; Östin et al., 1998; Pencik et al., 2013). A soluble 2-oxoglutarate and iron (II)-dependent *DIOXYGENASE FOR AUXIN OXIDATION* (*DAO*) was identified in rice (Zhao et al., 2013). Under normal growth conditions, oxIAA is the major IAA metabolic product. However, IAA decarboxylation might also play an important role in stress-induced IAA signaling attenuation. In citrus, ethylene treated leaf discs incubated with IAA produced more indole-3-carbinal than non-treated leaf discs (Sagee et al., 1990), and peroxide treated Arabidopsis showed strong IAA decarboxylation activity via LC-MS (Murphy et al., pers. comm.).

Determination of how IAA oxidation terminates auxin signal transduction events is important to efforts to manipulate auxin signaling. Here, we show that ACO2, a membrane-associated ethylene biosynthetic enzyme, exhibits IAA oxidase activity *in vitro*, and loss-of-function lines were used to investigate the physiological function of ACO2 *in planta*.

Results

IAA oxidase activity assay of microsomal protein and soluble protein from Arabidopsis seedlings

To identify membrane-associated IAA oxidase, gel filtration with Sephacryl-S200 and anion exchange were conducted to purify fractions with IAA oxidase activity from microsomal proteins and soluble proteins extracted from 7 day old Arabidopsis seedlings. Enzyme assays of each fraction were conducted by incubating with IAA for 1h at 30℃. Mn^{2+} or Fe^{2+} was added to the reaction as cofactors. Ultra Performance Liquid Chromatography (UPLC) was utilized to detect the product of the enzyme assay. As shown in Figure 2-1, in enzyme activity assays with both microsomal and soluble proteins fractions, the oxIAA peak occurred in fraction 50, corresponding to 30-40 k Da proteins. The IAA oxidation activity peak was almost equal in both soluble and microsomal fractions, indicating that either the IAA oxidase might be a peripheral protein or there are both soluble and membrane IAA oxidases.
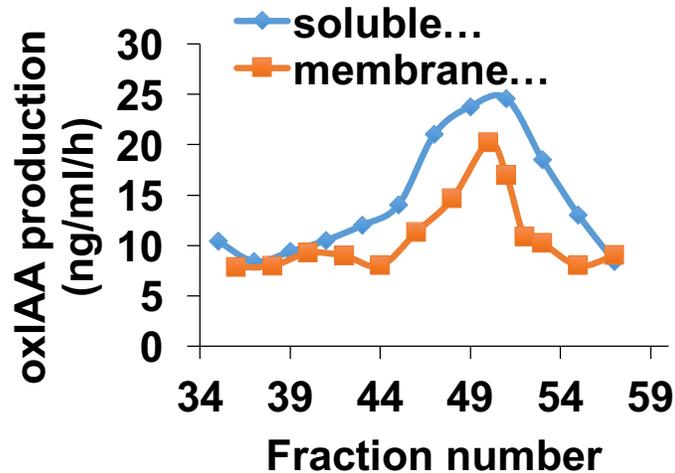
Figure 2-1. Analyze of IAA oxidation activity of fractions from gel filtration of membrane proteins and soluble proteins respectively. Fractions were incubated with IAA for 1h and the products were analyzed by HPLC. Both soluble and membrane proteins show IAA oxidation activity in fractions 49-50 which contain 35-40 kDa proteins.

Screen of IAA oxidase candidates

A candidate gene approach was used to identify auxin oxidases. According to the partial protein purification results (Figure 2-1), IAA oxidases are 30-40 kDa proteins. Since oxIAA mainly accumulates in the quiescent center and columella cells in *Arabidopsis* root tips (Pencík et al., 2013), the search was narrowed to 30-40 kDa oxidases and peroxidase that are expressed in this region. Based on a search of the Arabidopsis genome, 634 genes have oxidation reduction activity. After using the constraints of protein size, the expression levels of all these genes were investigated before and after 1µM IAA treatment for 30 min, 1h and 3h (NASCArray, IAA

treatment time course). The tissue-specific localizations of these genes in Arabidopsis

roots were also investigated using the Arabidopsis gene expression database

(www.arexdb.org). Finally, only 4 candidates, AT5G64100 (peroxidase),

AT5G43450 (2-oxoglutarate and iron (II)-dependent dioxygenase, ACC oxidase-

like), AT1G71695 (peroxidase), AT5G39580 (peroxidase), satisfied all of these

conditions. T-DNA insertion lines were obtained from the Salk Institute. Seeds were

bulked up, genotyped and sent to Dr. Karin Ljung's lab (Umeå Plant Science Centre,

Sweden) to be analyzed for IAA metabolite concentrations in roots and shoots of 7

days seedlings. However, the results showed no significant difference in the IAA and

oxIAA levels between wild type (Col-0) and the mutants (Figure 2-2), indicating

these genes were unlikely to function in IAA oxidation during seedling growth.
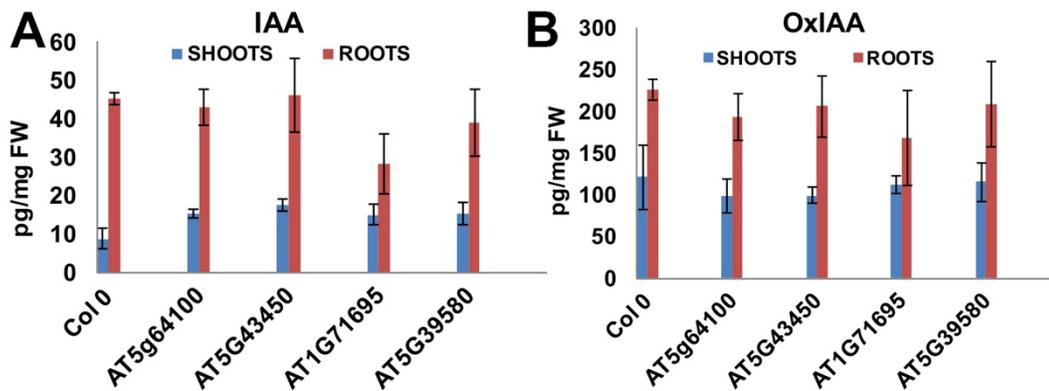
Figure 2-2. IAA and oxIAA level were not altered in T-DNA insertion mutants of candidate genes. IAA (A) and oxIAA level (B) of wild type and candidate mutants in the roots and shoots of 7-day-old seedlings. Data are means and standard deviations of at least independent 6 experiments.

Protein sequencing of the purified IAA oxidase fraction

After gel filtration and ion exchange chromoatography, purified IAA oxidation activity fractions were sent for tryptic digests and sequencing analyses in Dr. Jiri Ademec's lab at the University of Nebraska by Mass Metabolic Profiling/Mass Spectroscopy facility (Christie et al., 2011). The only identifiable protein with an oxidative enzymatic activity is 1-aminocyclopropane-1-carboxylic oxidase 2 (ACC oxidase 2, ACO2), which catalyzes the last step in the biosynthesis of the plant hormone ethylene. It has been reported that ACO2 is involved in IAA and ethylene interactions. *ACO2* expression is up-regulated by auxin and down-regulated by ethylene (Chae et al., 2000). Accumulation of mRNA for *AtACO2* occurred within cells predominantly located on the outer-side of the hook (Raz and Ecker, 1999), while auxin accumulates mainly on the inner side of the hook (Zádníková et al., 2010), which indicates that ACO2 might be involved in apical hook development. All of this indicates that ACO2 is possible candidate to also be an auxin oxidase in *Arabidopsis*.

Cloning and expression of recombinant ACO2 in E. coli.

To study the enzyme activity of ACO2 *in vitro*, I cloned *AtACO2* and expressed recombinant ACO2 (rACO2) with 6 x his tag in *E. coli* BL21 plsyE (Figure 2-3A, B). rACO2 was purified by his-spin trap column and SDS-PAGE analysis and western blot with anti-His antibody showed that rACO2 was around 40 kDa (Figure 2-3A, B). ACO2 was crystallized as a tetramer, and it was not known if ACO2 is a monomer or

oligomer *in planta* (Heinemeyer et al., 2007). Blue native gel analysis indicated that rACO2 is a monomer (Figure 2-3C).
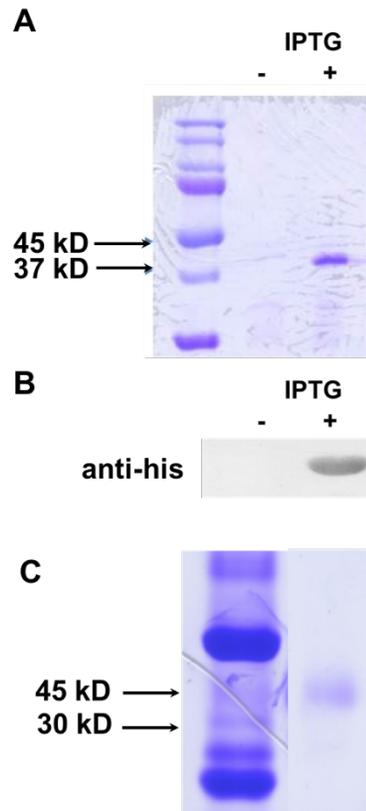
Figure 2-3. SDS-PAGE gel and western blot of expressed rACO2. (A) Commassie blue stain of un-induced or IPTG-induced protein expression after purification. Lanes: 1, protein ladder. 2, control (extracted protein from un-induced cells). 3. IPTG induced expression of rACO2. (B) Western blot of non-induced or induced rACO2 expression with anti-his tag antibody. (C) Blue native gel of recombinant ACO2.

Determination of ACC oxidation activity and IAA oxidation activity of rACO2

To determine if rACO2 has biological activity, I conducted enzyme assays with ACC as substrate (Yoo et al., 2006) and detected ethylene generation using a gas chromatograph. The assay showed that recombinant ACO2 ACC oxidase activity is 1.2 ppm ethylene mg protein^{-1} min^{-1}, indicating that it has the biological function as an ethylene producer *in vitro* (Figure. 2-4A).

Further, ACO2 IAA oxidase activity was analyzed by incubation with IAA as a substrate, and an auxin oxidative product was detected with HPLC. FeSO$_4$ and NaHCO$_3$ were added as cofactors to the enzyme reaction buffer. Indole-3-propionic acid (IPrA) was added as an internal standard. Figure 2-4A shows that IAA was reduced to 45% in the reaction system after 2h incubation in the dark, indicating that ACO2 might also function as an IAA oxidase. Detailed HPLC analysis of the enzymatic product was compared to the boiled enzyme control. The enzymatic product showed a peak at 15.5 min retention time which is the same as the indole-3-carbinol (ICA) standard, indicating that rACO2 can decarboxylate IAA (Figure 2-4B). However, addition of 10 mM ascorbic acid to the assay buffer completely blocked IAA decarboxylation by rACO2 (Table. 1). Ascorbic acid was previously reported to be the inhibitor of peroxidase-mediate IAA oxidation. In contrast, ascorbic acid is a required cofactor for ACC oxidase activity. It is possible that ascorbic acid is essential for regulating ACO2 enzyme activity.
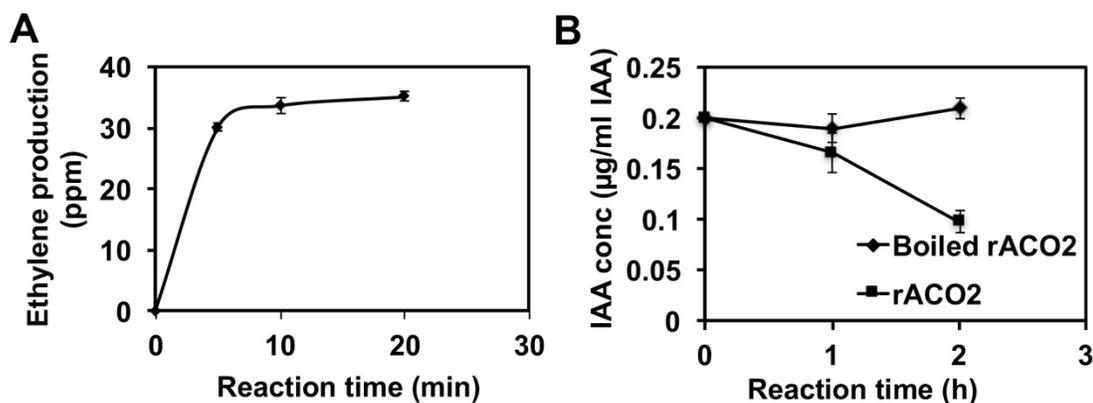
Figure 2-4. rACO2 enzyme activity assay with ACC or IAA as substrate. (A) Time course of ethylene production byACO2 ACC oxidase activity. (B) Time course of IAA consumption by ACO2 IAA oxidase activity. Each data time point is the mean value and standard deviation of 6 independent replicates.

Table 1. IAA oxidation activity of rACO2 with or without Asc

Product (µg/ml)	Bolied rACO2	rACO2
-Asc	0.028	0.049
+Asc	0	0

10 mM Asc was added to the enzyme buffer and products were analyzed by HPLC. Each data time point is the mean value of 3 independent replicates.

Enzyme assay of ACO2 homologs

There are 13 homologs of ACC oxidase homologs in Arabidopsis. To investigate if other ACC oxidases have IAA oxidation activity, two homologs, ACO1 (AT2G19590) and ACO3 (AT1G12010) were heterologously expressed in *E.coli*.IAA oxidation assays were conducted under the same conditions as for rACO2. The result show that ACO1 had no IAA oxidation activity (apendix A) while ACO3 exhibited

the activity, and the product has the same retention time as indole-3-carbinol, similar to ACO2 (Fig.2-5).
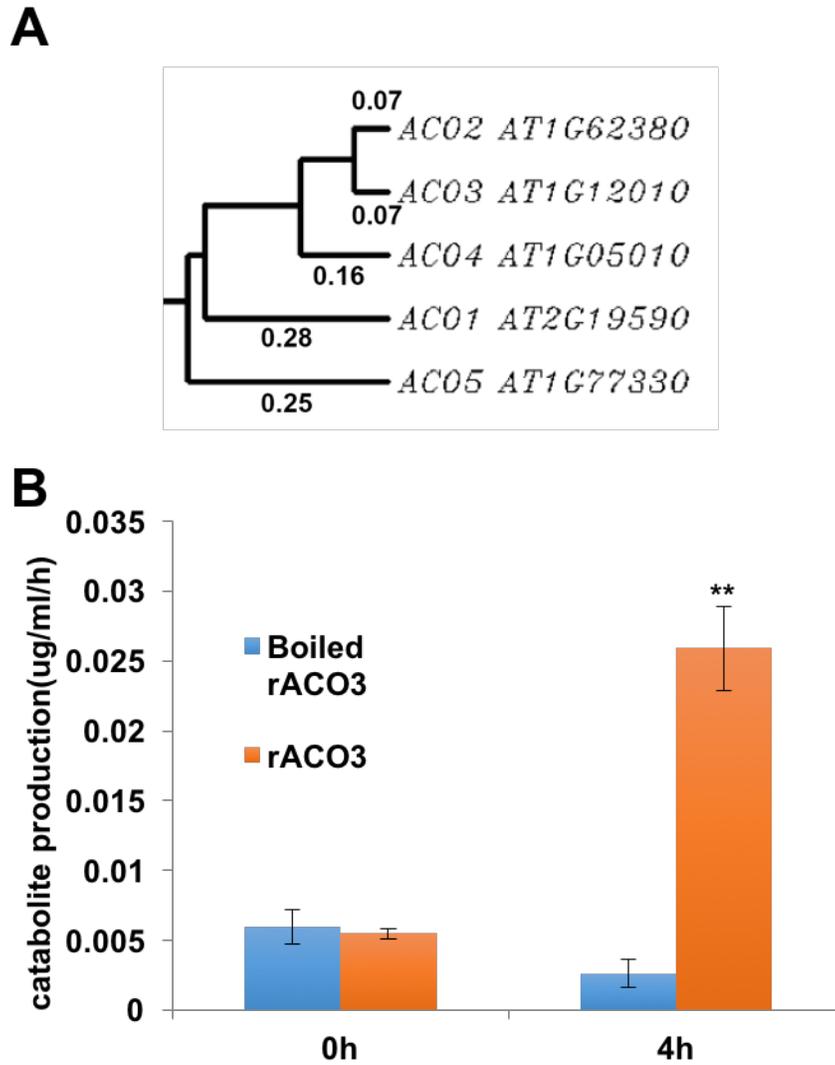
Figure 2-5. rACO3 exhibits IAA oxidation activity *in vitro* as rACO2. (A) Phylogenic tree of ACO family and subcellular distribution of ACOs. (B) IAA oxidation activity assay with rACO3.

Identification of ACO2 knock-down lines

Two *ACO2* T-DNA insertion lines, *aco2-1* (Salk_027311C) and *aco2-2*
(Salk_044146C) were obtained from the Salk Institution. *aco2-1* has a T-DNA
insertion is in the intron, and *aco2-2* has an insertion in the 3' untranslated region
(Figure 2-6A). Quantitative real-time PCR was conducted to identify if the T-DNA
insertions were null or weak alleles of *ACO2*. *ACO2* expression was reduced 95.7%
in *aco2-1* and 75% in *aco2-2* (Figure 2-6B). Western bot analysis showed that the
ACO2 protein was not detectable in *aco2-1*, while protein levels were reduced in
aco2-2 (Figure 2-6C).
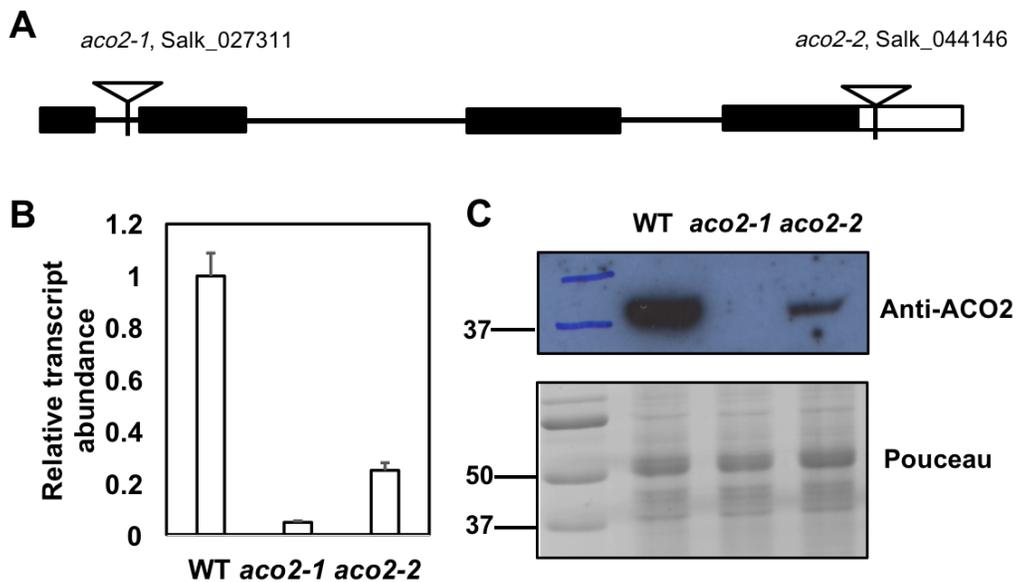
Figure 2-6. Characterization of *aco2* T-DNA insertion mutants. (A) Schematic diagram
of the genomic region flanking the T-DNA insertion site in *aco2* mutants. The inverted
triangles represent the T-DNA insertion sites in the genomic DNA. Black boxes represent the
exons in the genomic DNA, intervening lines represent the intron, the white box represents
the 3' untranslated region. (B) *ACO2* gene transcription levels in two *ACO2* T-DNA insertion

lines. 7-day-old seedlings were used to extract RNA and quantitative real-time PCR was conducted to detect *ACO2* gene transcription level. PP2A was employed as an internal standard. The data represent quantitative real-time PCR experiments conducted 3 biological replicates. (C) ACO2 protein level in two ACO2 T-DNA insertion lines is detected by western blot with anti-ACO2 antibody provided by Prof. Ranjan Swarup in University of Nottingham.

Phenotypes of aco2 mutants

To investigate the physiological function of *ACO2 in planta*, the phenotypes of *aco2-1* and *aco2-2* were analyzed. Etiolated *aco2-1* and *aco2-2* mutants showed reduced apical hook and longer hypocotyl length (Figure 2-7), and delayed bolting, all of which are typical ethylene-related phenotypes (Johnson and Ecker, 1998; Ogawara et al., 2003), indicating that ACO2 functions as an ethylene synthase *in planta*. Neither light grown mutants showed significant differences compared to wild type, nor differences in gravitropic bending assays (Figure 2-8). However, they showed a slight but statistically significant reduction of phototropic bending (Figure 2-9). To study the possible function of ACO2 in IAA metabolism, the IAA metabolome assay with 7-day-old seedlings was conducted. IAA levels were not disrupted in the mutants compared to wild type (Figure 2-10). Taken together, *ACO2* functions mainly as an ethylene synthetase under normal growth condition *in planta*.
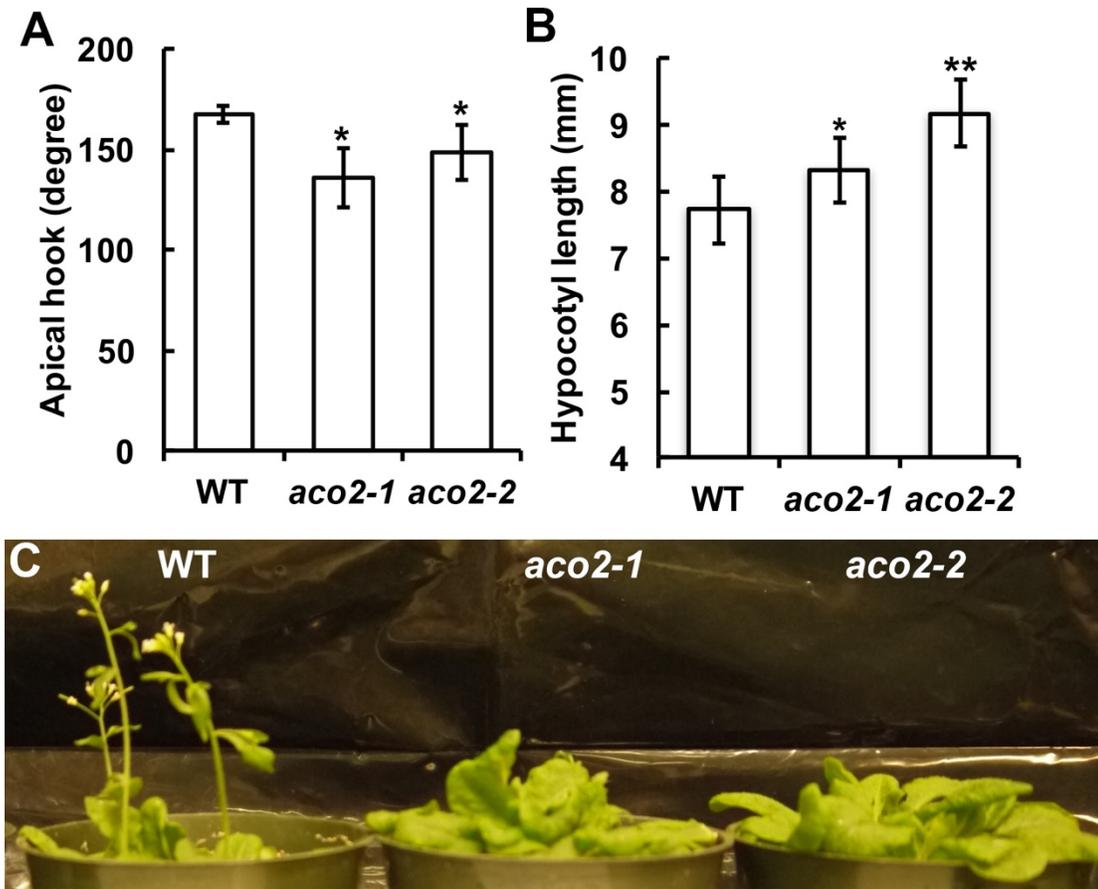
Figure 2-7. ACO2 knock out mutants show ethylene-related phenotypes. (A) Apical hook of 3-day-old etiolated wild type (WT) and *aco2* knock down lines. (B) Hypocotyls of etiolated WT and *aco2* null and knock-down lines. (C) Both *aco2-1* and *aco2-2* showed delayed bolting time compare to wild type. Picture was taken at 25 days after sowing. Image J was used to measure the apical hook and length of hypocotyls and roots.
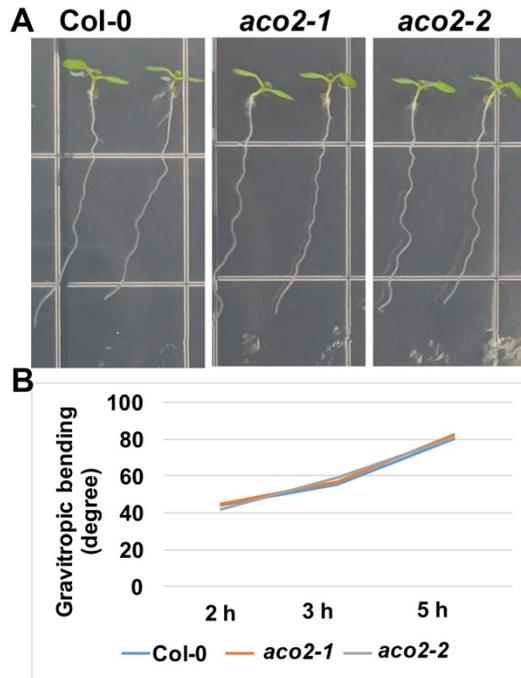
Figure 2-8. aco2 mutants grown under light does not show difference with wild type. (A) 7-day-old seedlings of Col-0, *aco2-1*, *aco2-2*. (B) Gravitropic bending of Col-0, *aco2-1* and *aco2-2*. 5-day-old seedlings grown vertically on MS plates were rotated 90 degrees to analyze the gravitropic bending.
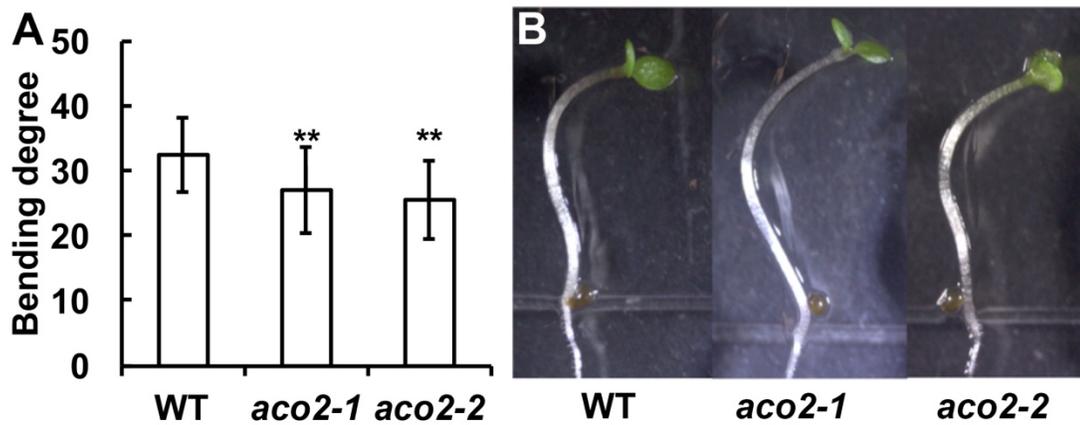
Figure 2-9. *aco2* knock out lines show reduced phototropic bending. 2-day-old seedlings were subjected to blue light for 12 hours and the bending angle was analyzed by ImageJ. At least 40 seedlings were measured for each data point.
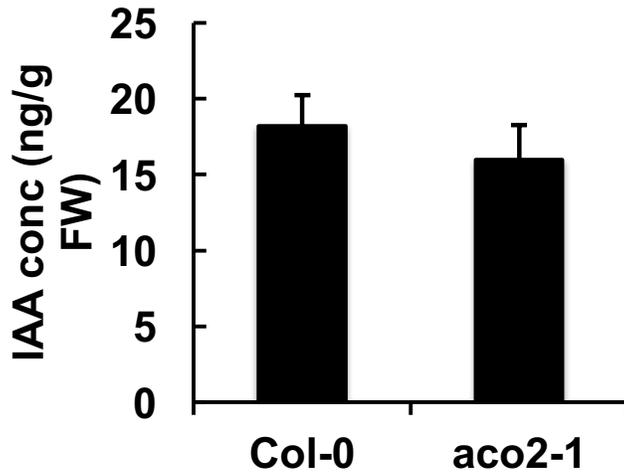
Figure 2-10. IAA level in Col-0 and *aco2-1* mutant. 7-day-old seedlings grown under 24 h light were collected and analyzed by LC-MS. n = 3. No statistical difference was shown in student t-test.

Discussion

Herein, we demonstrate that ACC oxidase 2 and 3 can catabolize IAA *in vitro* and the activity can be inhibited by ascorbic acid. The product is not oxIAA. Instead, the product has the same retention time as indole-3-carbinal in UPLC, indicating ACO mediated IAA decarboxylation. Our previous data has shown that IAA decarboxylative oxidation activity is mainly detected in microsomal fractions (Murphy, unpublished). On the other hand, ascorbic acid can inhibit the IAA decarboxylation activity of ACO2, in contrast to the activating role ascorbic acid

plays in ACC oxidation, suggesting that the presence of ascorbate might regulate

ACO2 enzymatic activity.

The endoplasmic reticulum (ER) is considered to be a very important compartment

for IAA metabolism. PIN5 and PIN8 are auxin efflux transporters that are located on

ER and transport auxin from the cytosol into ER (Mravec et al., 2009). *PIN5* over-

expression (OE) lines show reduced levels of free IAA while *PIN8* OE lines have

increased free IAA levels and reduced IAA conjugates (Ding et al., 2012). It is

possible that the ER is a storage place that regulates IAA levels in the cytosol. ACO2

is an ACC oxidases that is localized on the ER membrane and also shows IAA

decarboxylation activity. This suggests a possible connection between the subcellular

distribution and an IAA oxidation function under stress conditions where free IAA

levels increase.

By utilizing genetic tools, we demonstrated that ACO2 is involved in ethylene

responses in Arabidopsis, including apical hook formation, hypocotyl elongation of

dark-grown seedlings. *ACO2* is also involved in phototropism, a typical auxin

response. However, *aco2* loss-of-function lines did not show other obvious auxin-

related phenotypes. It has been reported that IAA decarboxylation is present at low

levels in plants under normal conditions (Nonhebel et al., 1983; Östin et al., 1998),

which may explain why obvious auxin related phenotypes or alteration in auxin levels

in *ACO2* loss-of-function lines were not observed. It is possible that ACO2 might

play a role during responses to the environment. Ethylene treatment enhanced IAA

decarboxylation activity in citrus leaves (Sagee et al., 1990). Since IAA

decarboxylation activity is not highly specific and many peroxidases could oxidize IAA *in vitro*, it is difficult to test this hypothesis definitively.

Materials and Methods

Plant material

All the Arabidopsis lines used in this research were in Columbia-0 background. *aco2-1* (SALK_027311) and aco2-2 (SALK_044146) were obtained from Arabidopsis Biological Resource Center. Plants were grown as previously described (Peer et al., 2013). Briefly, seeds were surface-sterilized and planted on 1/4 Murashige and Skoog (MS) medium (RPI Corp.) containing 0.5% sucrose and 0.8% agar, pH 5.5. Seeds were stratified at 4°C for 3 d and then placed in growth chambers at 22°C, 24 h at 100 µmol m^{-2} s^{-1} light except as indicated for specific treatments. Plants on soil were grown in growth chambers at 22°C, at 100 µmol m^{-2} s^{-1} light (16 h light/8 h darkness).

Protein extraction and purification

Seedlings were grown in the vertical mesh transfer apparatus (Murphy and Taiz, 1995) under continuous light. Microsomal preparations of 7-d-old Arabidopsis seedlings were prepared and assayed for purity as described previously (Murphy and Taiz, 1999) with the exception that 500 μM benzamide and 500 μM benzamidine were added to the original homogenization buffer. Prepared membranes were stored in liquid nitrogen. Membrane proteins were detergent solubilized by incubation with

gentle shaking at 4°C for 30 min in a buffer consisting of 0.1% (w/v) Brij 35, 0.05% (w/v) CHAPS {3-[(3-cholamidopropyl) dimethylammonio]-1-propanesulfonic acid}, 10 mM BisTris propane-MES (pH 7.8), 250 mM Suc, 20% (w/v) glycerol, and 1 mM DTT followed by centrifugation at 100,000 x g for 30 min. All subsequent purification steps were performed at room temperature unless otherwise noted and fractions were stored at −70°C. The supernatant was filtered through a 0.45um syringe filter and applied to a 48 × 1.2 cm Sephacryl S-200 column (Pharmacia Biotech, Piscataway, NJ) that had been precalibrated with molecular mass standards (Aldolase, 158,000D; Albumin 68,000D; Albumin 45,000D; Cytochrom C 12,500D from Boehringer Mannheim, Germany) and eluted utilizing a running buffer (RB) containing 5% (w/v) glycerol, 0.025% (w/v) Triton X-100, 20 mM HEPES, pH 7.0 plus 150 mM KCl.

  For soluble protein, soluble fractions were collected during microsomal preparation. Ammonium sulfate was added to the soluble fraction slowly till its concentration arrived 80%. Centrifuge the sample at 12,000 g for 10 min under 4C, and pour out the supernatant. Resuspend the pellet with 50mM HEPES pH 7, 3mM DTT. Dialysis was conducted against pH 7 HEPES buffer 3mM DTT overnight at 4C. Change the buffer the second day. After that, concentrate the protein by dialysis against PEG powder. Then the sample was run through Sephacrly S-200 column as described above with the exception that Triton x-100 were not added to the running buffer. Fractions from 35 min to 60 min (0.5 ml per fraction) were collected and enzyme activity assay were conducted under following condition: 40 mM PBS, pH 5.5, 0.05 mM $MnCl_2$, IAA 0.001mg/ml,100 μl enzyme.

Cloning and protein expression in E. coli

Plasmids with cDNA of *AtACO1*, *AtACO2* and *AtACO3* were obtained from ABRC

(Ohio State University). The cDNA fragments were subcloned into

pET23B+ (Novagen, Nottingham, UK) between the EcoR I and Xho I using the

restriction sites introduced by the PCR primers (Table S2) and sequenced. The

plasmid was transformed into *E. coli* BL21 (DE3) plysE and protein expression

optimized. In the preparative procedure, *E. coli* containing the plasmid were grown in

shaker flasks (250 rpm, 37 °C) containing LB media supplemented with 15 ug/ml of

ampicillin to late exponential phase (A_{600} ca. 0.8). Recombinant protein production

was induced by the addition of isopropyl-D-thiogalactopyrano-side (IPTG) to a final

concentration of 0.4 mM. Cells were grown for a further 4 hr in 27 °C and then

harvested. Cell paste was stored at - 80 ºC. Thawed cell pellets were suspended in

lysis buffer contain 20 mM PBS, pH 7.4,10% glycerol, 0.02 mg/ml DNaseI, 1 mM

$MgCl_2$, 1 mM PMSF, 20 mM imidazole, 500 mM NaCl. Unbroken cells, cell debris

and precipitated nuclei were then removed by centrifugation at 14,000 g at 4 °C for

15 min. The supernatant was run through his spin trap column (GE), washed with

buffer A (20 mM imidazole, 500 mM NaCl, 20mM PBS pH 7.4) and eluted with

buffer B (buffer A plus 250 mM imidazole). The elute was concentrated with

Millipore Amicon 30 kb membrane by centrifugation at 14,000 rpm at 4 °C for 10

min.

SDS-PAGE and western blot analyses

SDS loading buffer (LAEMMLI, 1970) was added to the cell pellet or purified enzyme and boiled for 5 min. Samples were centrifuged at 12,000 x g for 5 min. Then supernatant was loaded on a 12% SDS-PAGE gel (LAEMMLI, 1970). After running the gels, the gels were either blotted or stained with Coomassie blue. For western blot analyses, proteins were transferred onto nitrocellulose by wet electroblotting. For detection of recombinant protein, a mouse monoclonal 6x HIS antibody (Abcam) and an anti-mouse antibody conjugated to peroxidase (Sigma) were used at 1: 1,000 and 1: 5, 000 dilutions, respectively. Blots were developed using the HyGLO™ Quick Spray, and chemiluminescence emitted from the filter was exposed to a Kodak film for 10-30 sec and then developed. Anti-ACO2 antisera was provided from Prof. Ranjan Swarup in University of Nottingham.

ACC oxidase activity assay

The reaction mixture contained 40 mM PBS, pH 7.4, 10 % glycerol, 20 mM ascorbic acid, 1 mM ACC, 20 uM $FeSO_4$, 10 mM $NaHCO_3$. 10 μg boiled or unboiled protein were added to 0.5 ml reaction buffer in HPLC tube, then rotated under 30 ℃ for 0, 5, 10, 20, 40 min. 0.1 ml air was injected from the top space into the gas chromatograph with a porapak N 80/100 column. The oven temperature was set to 100°C; injection port, 110 °C; detector 250°C. The carrier flow was 22 ml/min.

IAA oxidase activity assays

The reaction mixtures contained 40 mM PBS, pH5.5, 0.5 mM Fe $(SO_4)_2$ in a final volume of 500 μl. 0.002 mg/ml IAA and 6 μg boiled or unboiled enzyme was added to the mixtures and incubated under in the dark at 30 ℃ for 4 hr. Then 2 volumes of acetone mixed with 0.001 mg/ml indole-3-propionic acid as a standard were added to the sample and placed in -20 °C overnight to precipitate protein. After centrifugation at 14,000 x g, 10 min, the supernatants were dried with speed vac and dissolved with 50 μl 10% methanol, 0.3% acetic acid. 20 μl samples were introduced by an autosampler onto a C18 column (EC 150/3, 3μm Nucleodur, Macherey Nagel) housed in a HPLC chromatography (1260 infinity, Agilent). The mobile phase was delivered at a flow rate of 0.3 ml/min with an initial mixture of 34% methanol in water (with 0.3% acetic acid in both solvents) for 5 min, followed by a 20 min linear gradient to 90% methanol. A diode array detector (1260 infinity, Agilent) were set up to detect the effluence absorbance at 200, 254, 280 and 325 nm.

Liquid chromatography tandem mass spectroscopy analyses

For enzyme assays: Samples were injected into an Agilent 1260 infinity LC system, and compounds were separated using an Agilent Poroshell 120EC-C18 (3.5 × 50 mm, 2.7 μm) column and an acidified water: methanol buffer system (Solvent A: 0.1% acetate, 5% MeOH in water; Solvent B: 0.1% acetate in methanol). Gradient conditions were as follows: 1 minute 0-10% B, 5 minutes 10-60% B, 5minutes 60-100% B, hold at 100% B for 3 minutes and then back to 0% B in 2 minutes. Eluted compounds were further separated and quantified using an Agilent 6460 triple quadrupole dual mass spectrometer equipped with an electrospray ionization source.

Compounds were quantified in positive ion mode, MS/MS settings were as described (Novák et al., 2012) conducted by Agilent G6460.

For plant tissue: Arabidopsis seedling samples were collected, weighed and chilled in liquid nitrogen before storing in -80 °C. Samples were ground in liquid nitrogen and 1 mL 50 mM sodium-phosphate buffer (pH 7.0, contains 1% DETC) was immediately added into each tube afterwards. 25 ng d5-indole-3 acetic acid (d5-IAA, OlChemIm, Ltd., Olomouc, Czech Rebuplic, part #0311532) and 25 ng d3-Tryptophan (d3-Trp, CDN isotopes, Quebec, Canada, part #D-7419) were added into each tube as internal standards (ISTD). Samples were vortexed, extracted for 20 min at 4 °C on a lab nutator and finally centrifuged at 12,000 x G for 15 min at 4 °C. The pH value of the supernatant was adjusted to 3 using 1N HCl, and the supernatants were purified using HLB column (column conditioned with 1 mL methanol (LC-MS/MS grade, Fisher Scientific, Pittsburgh, PA, part #A456-1), followed with 1 mL water and 0.5 mL 50 mM pH 2.7 Na-Phosphate buffer, after loading the sample, column was washed with 2 mL 5% methanol and finally eluted with 2 mL 80% methanol). The eluted samples were dried under nitrogen gas, re-dissolved with 500 µL methanol and filtered through 4 mm 0.2 µm PTFE filters (Fisher Scientific, Pittsburgh, PA, part #03-391-4E). 1 µL of each sample was injected for LC-MS/MS analyses

RNA extraction and transcription analysis

Total RNA was extracted from designated tissues using the RNeasy Plant Mini kit (Zymo Research). After treatment with DNaseI (Invitrogen), 2 μg of total RNA was used for the synthesis of the first-strand cDNA using thermoscript RT-PCR system

and oligo(dT) as primers (Invitrogen). Quantitative PCR was performed using SYBR Green on a CFX96 Touch Real-Time PCR Detection System (Bio-Rad). PCR was performed in 96-well optical reaction plates heated for 5 min to 95°C, followed by 40 cycles of denaturation for 10 s at 95°C and annealing-extension for 30 s at 60°C. All quantitative RT-PCR experiments were performed in triplicate, and the values presented represent means ± SE.

Gravitropism assay

Seedlings were grown vertically on plates as above for 4 days. After reorienting the plates by 90 degrees, the root tip position was marked every 3 h over a 24-h time period. The angles of curvature were measured using the Image J (Schneider et al., 2012), and the data were analyzed by Microsoft Excel. Averages and standard deviations were calculated from 50 seedlings.

Phototropism assay

Seeds are placed on 50-70 mesh sand (Sigma Cat. 274739) with water, covered with a clear vented lid, and light treated for 12 hours. Subsequently, seeds are placed in dark until 2 days old, or until about 0.4 cm in height. Seedlings then undergo light treatment at 65 μM m^{-2} s^{-1} light (Philips f32t8/tl741; Philips, NV) at 24°C for 12 hours to undergo photomorphogenesis, then returned to dark 12 h. The vented lid was removed and seedlings are placed in front of a 450 nm 100 LED light source (Rothner Laser Technic; Vienna, Austria) between 0.9- 0.6 μM m^{-2} s^{-1} at 24°C. Video was

captured using an MTI ccd72 (DAGE-MTI; Michigan City, IN) camera, the image was snapped every 5 minutes. The bending angles were measured using Image J.

Chapter 3: Oxidative inactivation of auxin by DAO1 regulates growth in Arabidopsis thaliana

Abstract

Tight homeostatic regulation of the phytohormone auxin is essential to plant growth and survival. The *Arabidopsis thaliana* enzymes that function in auxin biosynthesis and conjugation to sugars and amino acids for temporary or permanent inactivation have been identified, but the enzyme that catalyzes oxidation of IAA to its primary catabolite 2-oxindole-3-acetic acid (oxIAA) remains uncharacterized. Here we show that DIOXYGENASE for AUXIN OXIDATION1 (DAO1) catalyzes formation of oxIAA *in vitro* and *in vivo* and that this mechanism regulates auxin homeostasis and plant growth. Null *dao1-1* mutants contain 95% less oxIAA compared to wild type, and complementation of *dao1* restores wild-type oxIAA levels, indicating that DAO1 is the primary IAA oxidase in seedlings. Further, *dao1-1* plants have phenotypes associated with increased auxin levels including elongated organs (hypocotyls, primary roots, rosette leaves, inflorescence stems), increased lateral root density and delayed sepal opening compared to wild type. These phenotypes are complemented by transformation with *DAO1pro*:YFP-DAO1. The dominant *dao1-2D* overexpression line has increased oxIAA levels and has shorter leaves and inflorescence stems, thus supporting DAO1 IAA oxidase function *in vivo*. *DAO1pro*:YFP-DAO1 expressed in *dao1-1* produces signals in the root tip as well as in all juvenile and mature vascular and epidermal tissues, especially in the sepal. A

second isoform, DAO2, is very weakly expressed in seedling root apices. Together, these data confirm that IAA oxidation by DAO1 is the principal auxin catabolic process in Arabidopsis and that DAO1 is an important regulator of auxin homeostasis during plant morphogenesis.

Introduction

The phytohormone auxin (indole-3-acetic acid, IAA) regulates plant growth and development, including plant architecture and tropisms. The spatiotemporal distribution of auxin is regulated at the cellular level by control of biosynthesis, transport, reversible conjugation, compartmentalization, and catabolism. Loss of any one of these mechanisms is often balanced by compensatory homeostatic responses, but can also produce morphological or physiological changes. The enzymes that catalyze auxin biosynthesis via the indole-3-pyruvic acid (IpyA) pathway (Mashiguchi et al., 2011), (Stepanova et al., 2011) and the UDP-glucose transferases (Jackson et al., 2002, 2001; Tognetti et al., 2010) and amido synthetases that inactivate IAA by conjugation to small molecules (Ludwig-Muller, 2011; Staswick et al., 2005) are well characterized (Fig. 3-1A). Most IAA conjugation is reversible and functions in compartmentation or storage (Ishimaru et al., 2013; Korasick et al., 2013; Ludwig-Muller, 2011). Exceptions are the formation of the irreversible catabolites

44

IAA-aspartic acid (IAA-Asp) and IAA-glutamate (IAA-Glu) in discrete plant tissues (LeClere et al., 2002; Östin et al., 1998; Rampey et al., 2004).

Oxidation of IAA has long been known to be the primary mechanism of auxin catabolism (Ray, 1958). Arabidopsis seedlings contain 10-100 times more 2-oxindole-3-acetic acid (oxIAA) than the major IAA conjugates IAA-Glu and IAA-Asp (Kowalczyk and Sandberg, 2001; Östin et al., 1998; Pencik et al., 2013), but the enzymes catalyzing oxIAA formation have been elusive. In part, this has been due to early implication of peroxidases and oxygenases in auxin oxidative processes (Hu and Dryhurst, 1997; Ray, 1958; Reinecke and Bandurski, 1988; Sandberg and Ernstsen, 1987). However, re-examination by liquid chromatography mass spectroscopy (LC-MS) of the reaction products from previously published horseradish and grape leaf peroxidases, as well as two Arabidopsis peroxidases, showed that these reactions produce the decarboxylation products indole-3-carbinol, 3-methylene-2-oxindole and 3-hydroxymethyl-2-oxindole present in low levels in plants (Normanly, 1997), but not oxIAA (Peer et al., 2013). In *Zea mays*, oxIAA was reported to be produced by an oxygen-requiring soluble enzyme and a more active detergent-soluble, stable component (Reinecke and Bandurski, 1988). A correlation of cellular oxIAA and IAA levels (Peer et al., 2013; Pencik et al., 2013) and with expression of a gene with similarity to a rice gene named *DIOXYGENASE for AUXIN OXIDATION* (*DAO*) (Voß et al., 2015; Zhao et al., 2013) (Porco et al., and Mellor et al. co-submitted to *PNAS*) suggested that similar genes in Arabidopsis, *DAO1* and *DAO2*, encode the enzymes that produce oxIAA. Here we show that DAO1 is the major IAA oxidase in Arabidopsis and demonstrate that IAA oxidation plays an important role in IAA

homeostasis and regulation of plant morphogenesis by balancing IAA levels
throughout the life of the plant.

Results

Phylogenetic analysis of Arabidopsis 2-oxoglutarate and Fe(II)-dependent oxygenase superfamily

AtDAO1 (At1g14130) and AtDAO2 (At1g14120) in Arabidopsis *thaliana* were identified as homologues of rice OsDAO (Os04g0475600) (Fig. 3-1B, C). AtDAO1 (DAO1) has 71.7% similarity and 45% identity and AtDAO2 (DAO2) has 71.9% similarity and 43% identity to OsDAO, and DAO1 and DAO2 show 72% identity to each other. They are all members of the 2-oxoglutarate and Fe(II)-dependent [2OG Fe(II)] oxygenase superfamily. The superfamily is characterized by the conserved dioxygenase and 2OG Fe(II) oxygenase domains (Fig. 3-1B, C). A further conserved sequence P(S/D/G)E(F/L)VD(A/G)EHPR, without any known motifs, was identified among the rice and Arabidopsis DAO proteins and examined further (Fig. 3-1B, C). Sequence alignment with Viridiplantae (taxid:33090) suggests that this motif is specific to proteins in a subset of the 2-oxoglutarate and Fe(II)-dependent oxygenase superfamily annotated as DAO and DAO-like (See Apendix C). Motif analysis (Dinkel et al., 2015) (Durek et al., 2010) showed μ Adaptor Protein and actin binding motifs (Fig. 3-1C), and twelve putative serine/threonine phosphorylation sites in DAO1 and fifteen in DAO2.

The majority of the proteins in the 2OG Fe(II) oxygenase superfamily have not been characterized, and a phylogenetic analysis of the superfamily in Arabidopsis

was undertaken to identify any nearest neighbors to DAO1 and DAO2 (Fig. 3-1B; Appendix A). The nearest neighbors are AT5G58660, an uncharacterized 2OG Fe(II) superfamily member, AT1G50960 (GA2OX7) and AT4G21200 (GA2OX8), all of which lack the DAO motif (Fig. 3-1B).
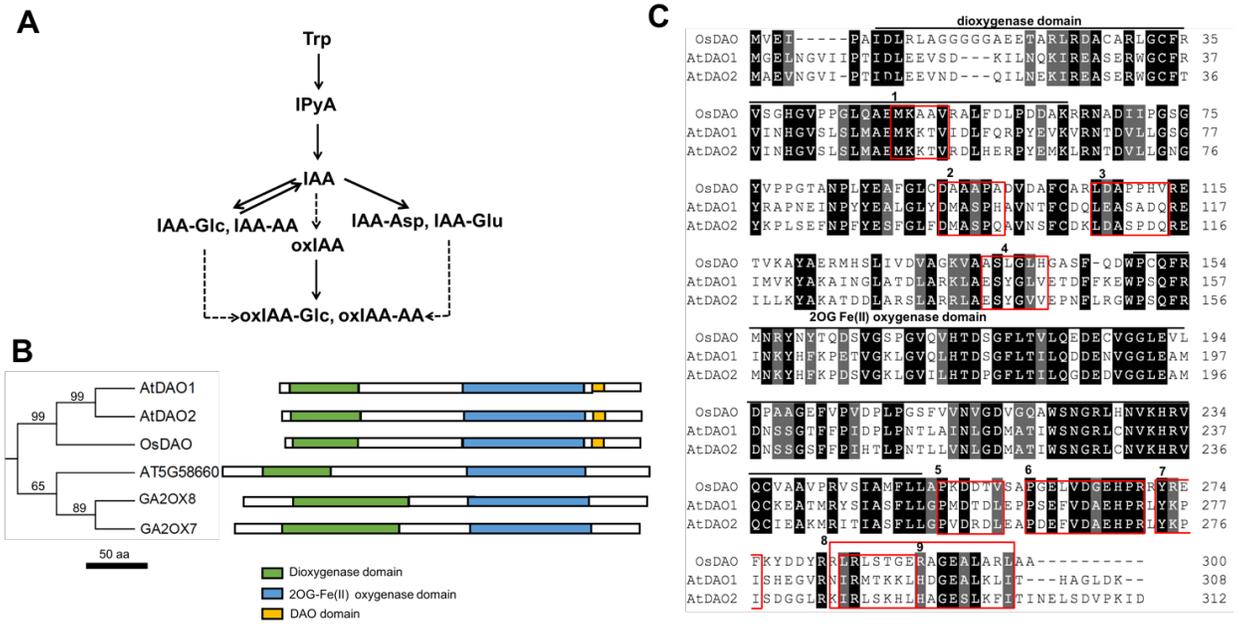
Figure 3-1. Identification and characterization of 2-oxindole acetic acid synthetases in *Arabidopsis thaliana*.

(*A*) Auxin metabolic pathway via IPyA. Trp, tryptophan; IPyA, indole-3-pyruvic acid; IAA, indole-3-acetic acid; IAA-Glc, IAA-glucose; IAA-AA, IAA-amino acid conjugate; IAA-Asp; IAA-aspartate; IAA-Glu, IAA-glutamate; oxIAA, 2-oxindole-3-acetic acid; oxIAA-Glc, oxIAA-glucose; oxIAA-AA, oxIAA-amino acid conjugate. (*B*) Pictogram conserved domains among OsDAO, AtDAO1, AtDAO2, and the nearest clade of a subfamily of 2-OG oxygenases in Arabidopsis. *(C)* Protein sequence alignment of AtDAO1, AtDAO2 and OsDAO with Clustalx2.1. Conserved residues, dark rectangles; residues with similar properties, grey rectangles; (-), gap inserted to maximize the alignment. Bars, oxygenase or dioxygenase domains; triangles, Fe binding residues; open circle putative phosphorylation

sites in AtDAO1, closed circles putative phosphorylation sites in AtDAO2; boxes, putative motifs. 1. μ Adaptor Protein motif. 2. CK2 phosphorylation site. 3. DAO motif. 4. μ Adaptor protein motif. 5. Actin cleft binding motif.

rDAO can catalyze the formation of oxIAA

Enzyme assays of recombinant DAO (rDAO) with indole-3-acetic acid (IAA) as a substrate were conducted. *DAO1* and *DAO2* cDNA were subcloned into expression vectors, heterologously expressed in *E. coli*, and purified with anti-His spin trap columns, and the proteins were the expected 36 kDa (Fig. 3-2A). *In vitro* enzyme assays were conducted with 10 μM IAA, 5 mM 2-oxoglutarate, and 0.5 mM $Fe(SO_4)_2$. Liquid chromatography tandem mass spectroscopic (LC-MS/MS) analyses showed one major peak with the same retention time and fragmentation pattern as the 2-oxindole-3-acetic acid (oxIAA) standard (Fig. 3-2B). Non-enzymatic oxIAA production was observed when IAA was incubated with denatured enzyme (Fig. 3-2B, C), accounting for 20% of oxIAA production *in vitro*. Previous reports have shown that oxidases in bacteria can catabolize IAA to methyl-oxindole or indole-3-carbinol (Egebo et al., 1991). Therefore, enzyme assays from the empty vector extracts were also performed to determine if the observed IAA oxidation was due to the activity of a co-purifying bacterial enzyme. Fig. 3-2C shows that the purified extracts from the empty vector control do not exhibit auxin oxidase activity. The enzyme activity of rDAO1 is 4.8 ± 0.3 pmol $oxIAA^{-1}$ min^{-1} mg protein, and rDAO2 is 4.3 ± 1.1 pmol $oxIAA^{-1}$ min^{-1} mg protein under the conditions used (see methods).

These rates are consistent with the IAA oxidation rate previously observed *in planta*, which is between 10-40 nM^{-1} h (Kramer and Ackelsberg, 2015).
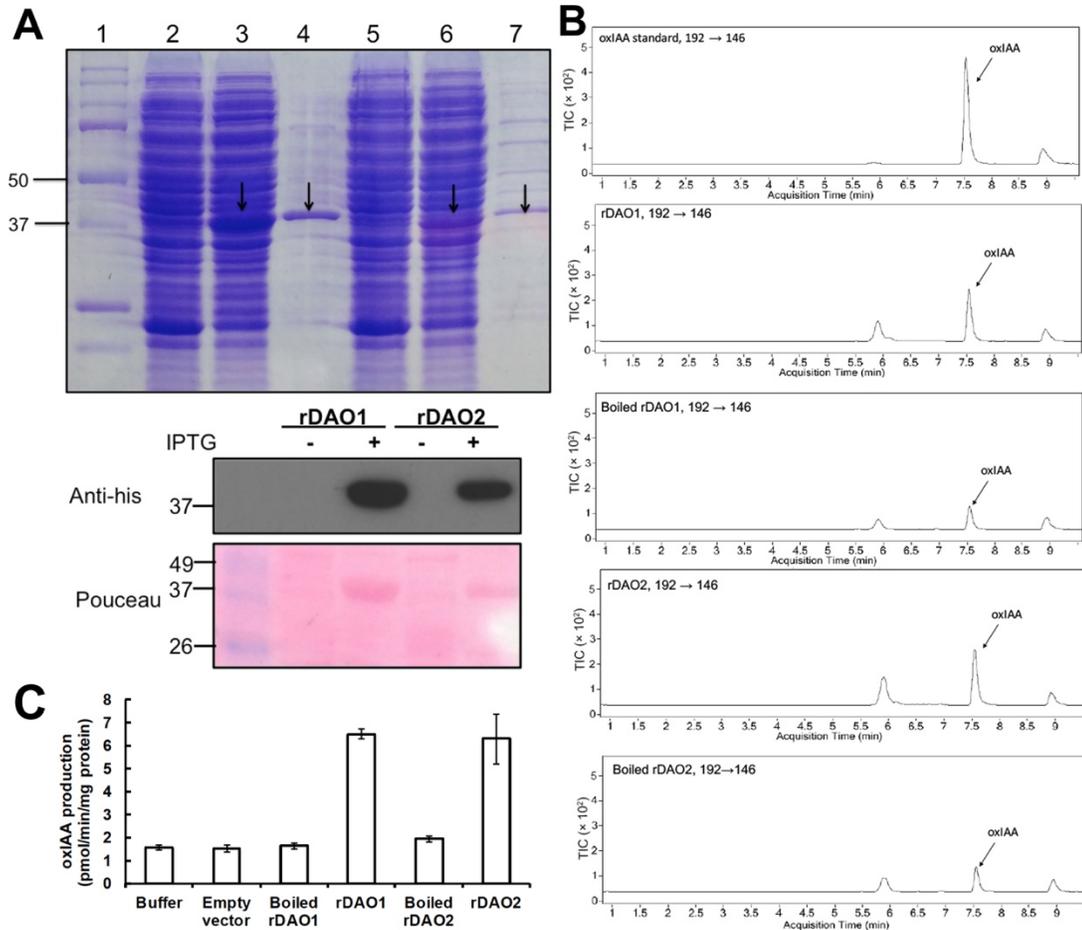
Figure 3-2. Heterologous expression and enzyme assay of rDAO1 and rDAO2.

(A) Heterologous expression of rDAO1 and rDAO2. Commassie stained SDS-PAGE of recombinant AtDAO1 and AtDAO2 expression in *E. coli* induced by IPTG. Lane 1. Molecular weight marker (Bio-Rad). 2. Control, non-induced BL21 plsy/pET AtDAO1. 3. IPTG induced BL21 plsy/pET AtDAO1. 4. His-spin trap column purified protein from IPTG induced BL21 plsy/pET AtDAO1. 5. Enzymatic activity of control, non-induced BL21 plsy/pET AtDAO2. 6. IPTG induced BL21 plsy/pET AtDAO2. 7. His-spin trap column purified protein from IPTG induced BL21

plsy/pET AtDAO2. *(B)* LC-MS/MS analysis of the genuine oxIAA standard and the *in vitro* product of rDAO1 and rDAO2. Total ion counts (TIC) showing a product peak (m/z 192→146) at 7.5 min, which is identical to oxIAA standard. (*C*) Enzyme assays of recombinant DAO (rDAO1 and rDAO2) with buffer control, empty vector control, and heat-inactivated (boiled) enzyme control with IAA as a substrate. Data are means and standard deviations of at least independent 10 experiments.

DAO1 loss-of-function and gain-of-function plants show altered auxin metabolites

DAO1 and *DAO2* are located in tandem on chromosome 1, with 1091 bp between the end of *DAO1* and the beginning of *DAO2*. T-DNA insertional mutants for *DAO1* and *DAO2* were obtained (Alonso et al., 2003) and verified (Fig. 3-3A, B). Quantitative real-time PCR (qPCR) showed *DAO1* expression was not detected in *dao1-1* (first exon insertion) and increased 1.7 fold in *dao1-2D* (intergenic region) (Fig. 3-3B). qPCR showed that *DAO2* expression was 61% less in *dao2-1* (Fig. 3-3B). Seven-day-old mutants were analyzed for altered auxin metabolism, and *dao1-1* mutants exhibited a 94.3% decrease in oxIAA production ($P < 0.01$; Fig. 3-3C) while *dao1-2D* overexpression lines showed a 42% increase in oxIAA levels compared to wild type (Col-0), ($P < 0.01$; Fig. 3-3D). oxIAA accumulation in *dao2-1* was the same as wild type (Fig. 3-3E)*,* indicating DAO1 is the major IAA oxidase during seedling establishment*.* Therefore, we focused on *DAO1*.

Although the amount of free IAA was not significantly altered in *dao1-1* ($P >$ 0.05, Fig. 3-3C), one of the major IAA-amino acid conjugates, IAA-Asp, showed a 1 x 10^6-fold increase in *dao1-1* compared to wild type (Fig. 3-3C). Further, *GH3.3*, which can synthesize IAA-Asp, was up-regulated in *dao1* loss-of-function mutants (Fig. 3-4). These data suggest that the IAA conjugation pathway was induced to compensate for loss of DAO-mediated attenuation of auxin signaling.
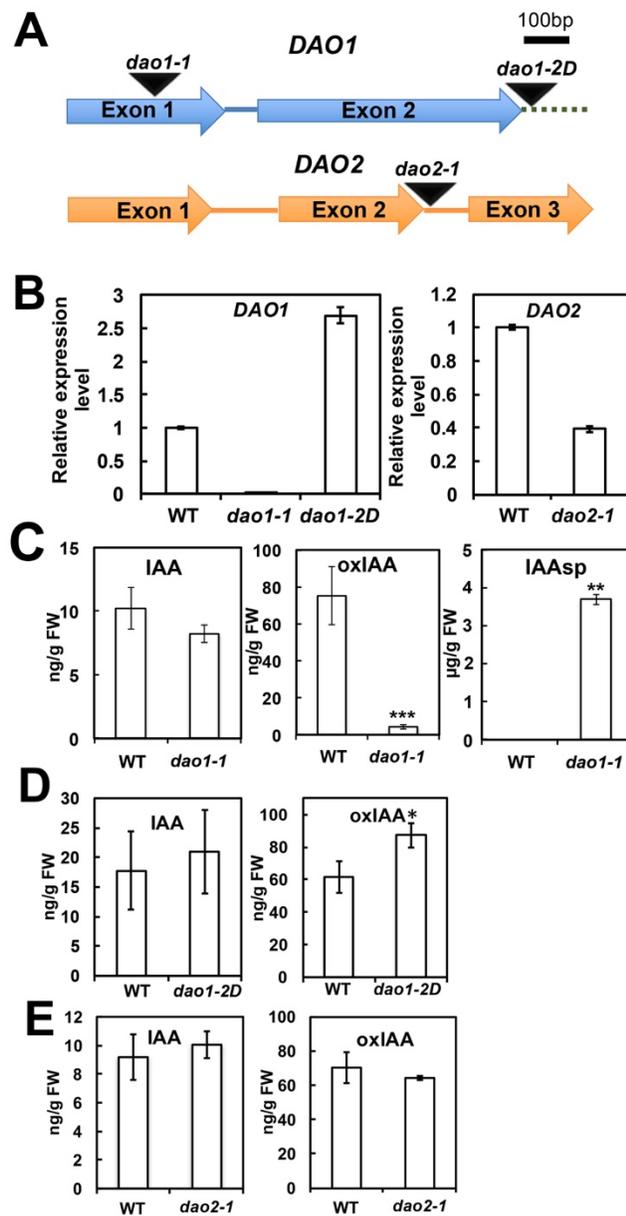
Figure 3-3. Identification and IAA metabolites analyze of DAO mutants. (*A*) Gene organization and schematic representation of T-DNA insertion lines of *DAO1* (At1G14130) and *DAO2* (At1G14120). Arrows represent the exon and the intervening lines indicate the introns. The site of the T-DNA is indicated by triangles: Salk_093162 (*dao1-1*), SAIL_349_D02 (*dao1-2D*) and Salk_205223 (*dao2-1*). The dotted line indicates the 1091 bp interval between *DAO1* and *DAO2*. (*B*) Relative expression of *DAO1* and *DAO2* in T-DNA insertion lines compared to Col-0. (*C*) IAA and IAA metabolite concentrations in 7d Col-0 (wild type) and *dao1-1* seedlings. (*D*) IAA and oxIAA concentrations in 9d Col-0 *and dao1-2D* seedlings. (*E*) LCMS analysis of oxIAA and IAA concentrations in 7-day-old Col-0 and the *DAO2* knock-down *dao2-1* mutant seedlings. Data represent mean value ± SD of 4 replicates. No significant difference, Student's *t*-test.
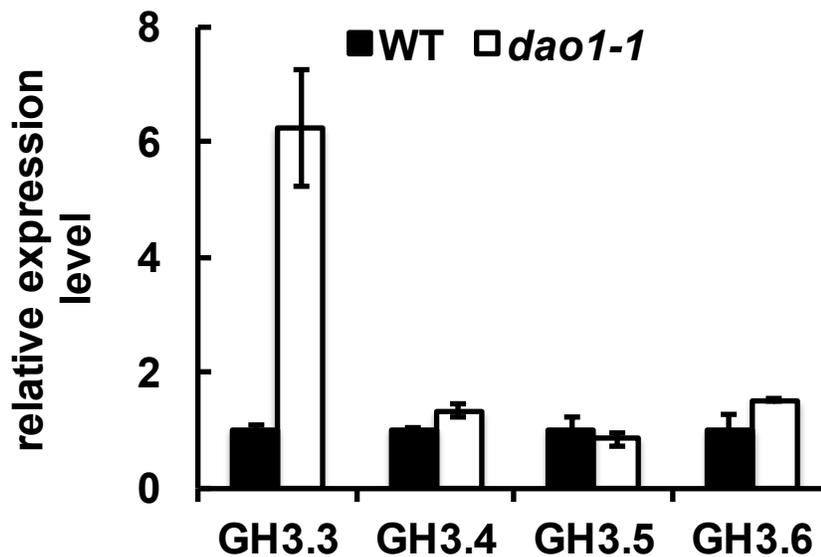
Figure 3-4. Relative expression of *GH3* genes in Col-0 (WT) and *DAO1* loss-of-function mutant. RNA was extracted from 7-day-old seedlings of wild type and *dao1-1* and qRT-PCR was conducted with *ACTIN2* as an internal standard. Data represent means ± SD of 6 replicates.

DAO1 loss-of-function and gain-of-function plants show morphological changes

The observed increases in terminal IAA conjugation were not sufficient to complement the loss of IAA oxidase activity since *dao1-1* showed altered morphological phenotypes (Fig. 3-5). To investigate the role of altered auxin metabolism in the observed *dao1-1* phenotypes, *yuc6-1D* (*kidari*), a reported IAA overproducing line (Kim et al., 2011, 2007), was compared to *dao1-1* at different growth stages. Both *dao1-1* and *yuc6-1D* had longer hypocotyls and inflorescences, and increased lateral root density compared to wild type (Fig. 3-5A, B, G, H). Primary roots were initially longer in *dao1-1* seedlings and by 11 days were similar to wild type (Fig. 3-5B), and lateral root density in *dao1-1* increased one-fold compared to wild type ($P < 0.001$; Fig. 3-5B). In *dao1-1* the hypocotyls were 43% longer in light-grown seedlings ($P < 0.01$; Fig. 3-5B), and 48% longer in etiolated seedlings, and the apical hook angle was reduced 20% in 3-day-old etiolated seedlings compared to wild type ($P < 0.001$, $P < 0.001$; Fig. 3-5C), suggesting DAO1 might contribute to apical hook maintenance. The *dao1-1* rosette leaves were 21% larger than wild type ($P < 0.01$; Fig. 3-5E, F, H), in contrast to the narrow and curling rosette leaves in *yuc6-1D*, suggesting that *DAO1* might play a role in leaf shape. The primary inflorescences of *dao1-1* plants were 42% longer at 45 days ($P < 0.001$; Fig. 3-5G, H. Sepal and petal opening were delayed at floral stages 13-15 in *dao1-1* mutants (Fig. 3-5I), and more failed or shorter siliques were observed in primary infloresence of *dao1-1*(Fig. 3-5G) at 35 days. In contrast, the *dao1-2D* overexpression line had smaller rosette leaves and shorter inflorescence stems (Fig. 3-5E, G). Tropic

responses were also altered in *dao1-1*, and root gravitropic bending and phototropic

bending in post-photomorphogenic seedlings were faster in *dao1-1* than wild type at

the initial stages of the tropic response ($P < 0.01$, $P < 0.03$; Fig. 3-5D).
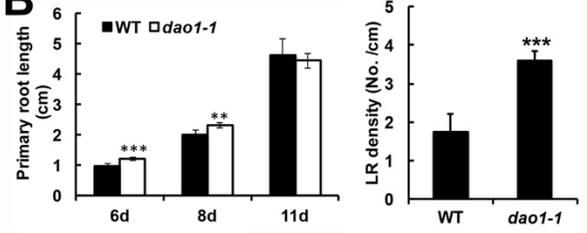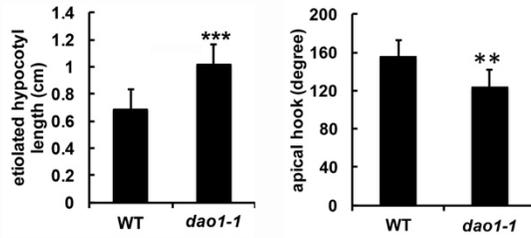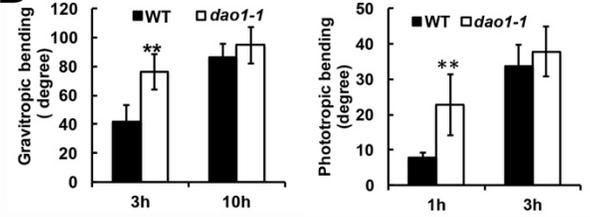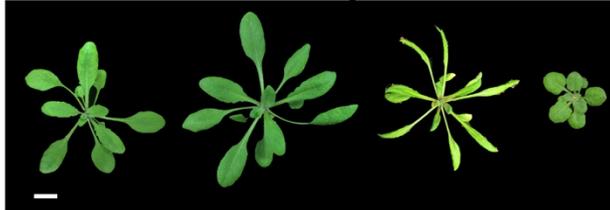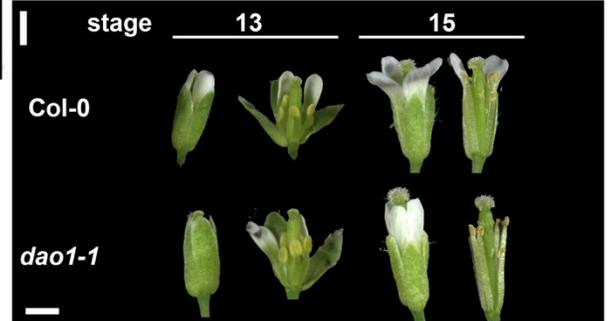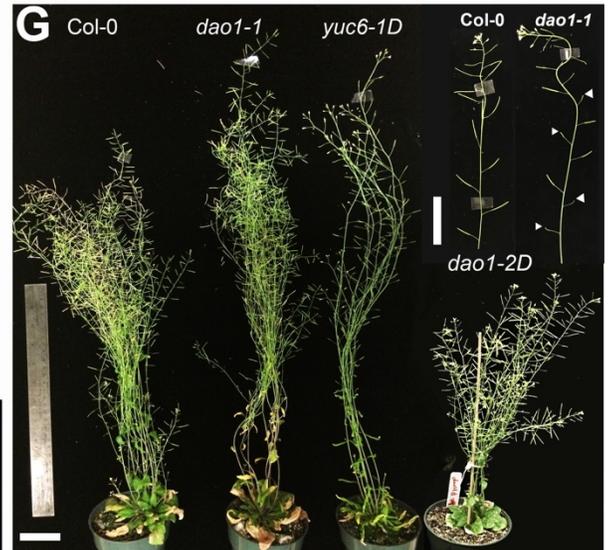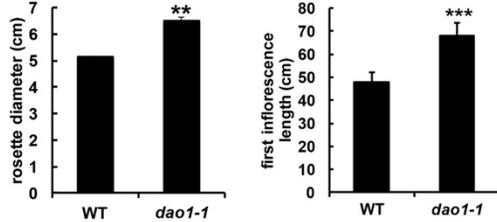
Figure 3-5. *DAO1 loss-of-function plants and gain-of-function plants show altered*

phenotypes. (*A*) 9-day-old light grown seedlings of Col-0, *dao1-1*, *yuc6-1D* and *dao1-2D*. (*B*)

Phenotypic quantification of light grown seedlings: primary root length of seedlings of wild

type and *dao1-1* at 6d, 8d and 11d after sowing; lateral root density in 11-day-old seedlings;

hypocotyl length of 5-day-old light-grown seedlings. (*C*) 3-day-old etiolated Col-0 *dao1-1,*

yuc6-1D and *dao1-2D* seedlings; quantification of hypocotyl length and apical hook angle of

3-day-old etiolated Col-0 and *dao1-1* (lower panel)*.* (*D*) Tropism analyses of Col-0 and *dao1-*

1. Gravitropic bending assay: 5-day-old seedlings grown on MS plates were rotated 90

degrees and images were taken at 3h and 10h respectively; Phototropism assay: 3-day-old

post-photomorphogenic seedlings grown on sand slurry were treated with unilateral blue light

and images were taken every 5 min. (*E*) Rosette leaves of Col-0, *dao1-1*, *yuc6-1D* and *dao1-*

2D at bolting. Bar = 1cm. (*F*) Separated rosette leaves of Col-0 and *dao1-1*. (*G*) 55-day-old

Col-0, *dao1-1, yuc6-1D,* and *dao1-2D* plants. Bar = 5cm. (*G*) upper right: primary

inflorescence from 35-day-old Col-0 and *dao1-1*. White arrows indicate failed silliques. Bar

= 1 cm. (*H*) Rosette diameter at bolting and the primary inflorescence length of 45-day-old

plants. (*I*) Individual flowers of Col-0 and *dao1-1* at stages 13 and 15 respectively. Bar =

1mm. All of data were measured with ImageJ. Error bars show standard deviation. n ≥ 10.

Asterisks represent the statistical significance between wild type and *dao1-1* analyzed by

Student's *t*-test. **, P < 0.01; ***, P < 0.001.

To verify that the phenotypes of *dao1-1* were due to loss of *DAO1* function, a

DAO1 native promoter driv ing the *DAO1* genomic coding sequence was fused to a

fluorescent protein reporter to make the *DAO1*pro:YFP-DAO1 construct, and

transformed into *dao1-1*. *DAO1* transcript (Fig.3-6A) and oxIAA levels (*P* > 0.05;

Fig.3-6B) were restored to wild type in the complemented lines. Furthermore, the

morphological phenotypes of *dao1-1*, such as bigger rosette leaves, were also

complemented (Fig.3-6C, D). Together these results support that DAO1 functions as

an IAA oxidase *in vivo* and regulates plant morphogenesis.
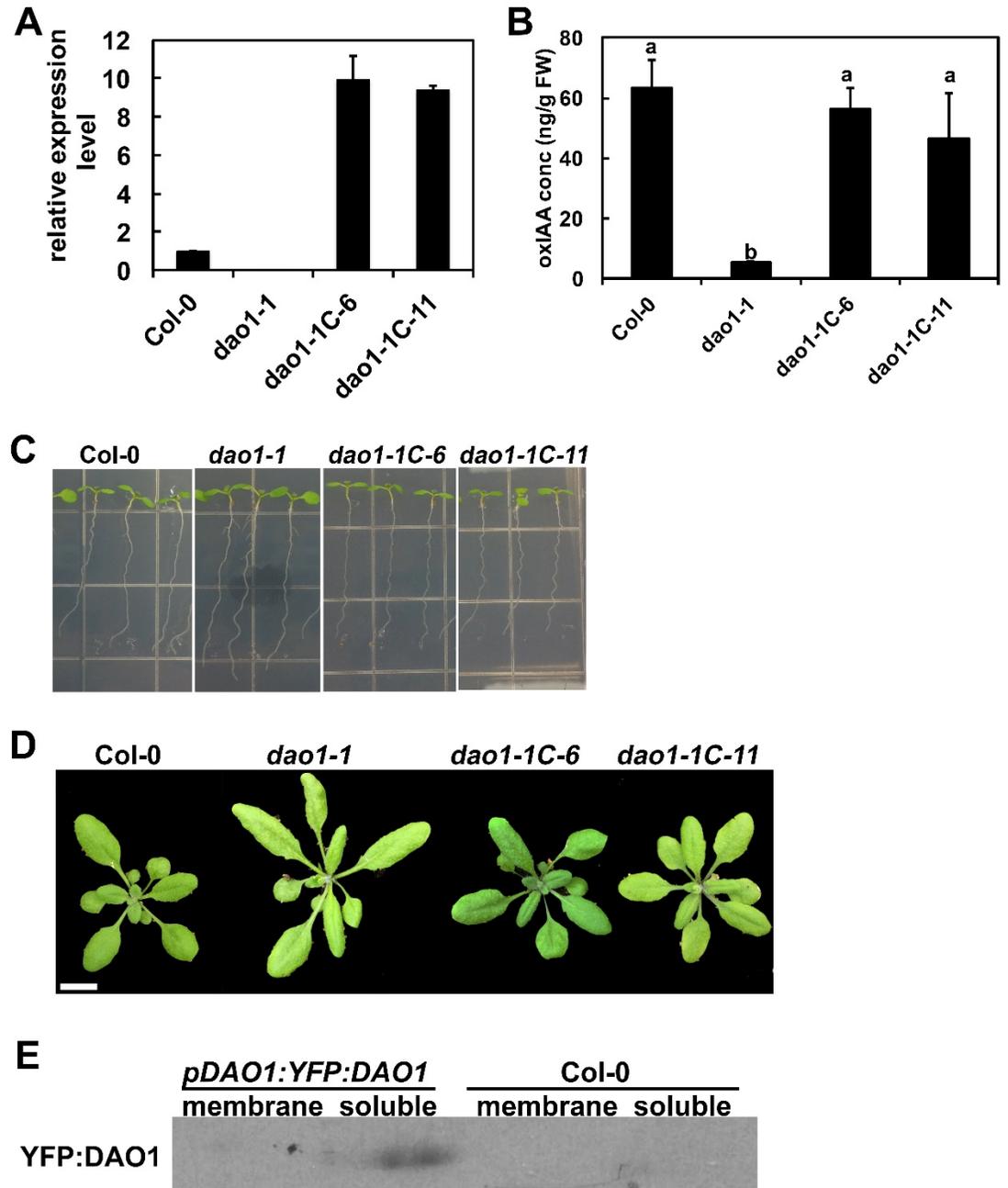
Figure 3-6. *DAO1pro*:YFP-DAO1 in *dao1-1* complemented the phenotypes of *dao1-1*.

Comparison among Col-0, *dao1-1*, and *DAO1* complemented lines 6 and 11 (*dao1-1c-6*,

dao1-1c-11). (*A*) Relative expression of *DAO1* in 7-day-old seedlings, (*B*) oxIAA levels in 7-day-old whole seedlings, (*C*) 7-day-old seedlings, (*D*) Rosette leaves at bolting. (*E*) Western blot with anti-YFP antibody shows YFP-DAO1 is in soluble fraction in the *DAO1pro*: YFP-DAO1 line.

DAO1 is expressed throughout the plant

A native promoter driven GUS construct (*DAO1*pro:GUS) and a functionally fluorescent protein fusion, *DAO1*pro:YFP-DAO1, were made to study the expression pattern of DAO1. Figure 3a shows the *DAO1pro*:GUS expression in 7d old seedling. Strong and constitutive GUS activity was observed at the leaf margin, epidermis of the upper part and the end of hypocotyl, epidermis and vascular tissue of upper root, and comparable weak expression in epidermis of cotyledon, vascular tissue of lower root and root tip. Interestingly, the expression of *DAO1pro*:GUS has a distinct change at the root-shoot transition zone, where the root side has almost no expression while the shoot side has a strong expression in the epidermis. These are consistent to the florescence signal of *DAO1*pro:YFP-DAO1 in seedlings. Confocal microscopy images (Fig. 3-7B-G) of 7d seedlings further showed *DAO1*pro:YFP-DAO1 signal in the cytosol and signals were present in the pavement cells of cotyledon, the epidermis and pericycle in the root, and in the root cap. The *DAO1* expression pattern in the seedling reflects the altered leaf and root phenotypes observed in *dao1-1* seedlings. Figure 3h shows that *DAO1* expression is greater inside of apical hook where there are strong DR5:GFP signal, suggesting DAO1 participates in auxin homeostasis in apical hook maintenance (Fig. 3i). In floral organs, *DAO1* has strong expression in the vascular tissue and epidermis in the sepasl and petals, epidermis of anthers and

carpels (Fig. 3-7J-M). Intriguingly, *DAO1* reached highest expression in bundle

sheath cells near the top of the sepal from flower stage 12 (Fig. 3-7J), the final stage

before the buds open (Smyth et al., 1990). Before this stage, DAO1's expression

remains background level in the sepal (Fig. 3-7J). This correlates with the delayed

flower opening observed in *dao1-1*. The autoflorescence image are shown in

Appendix B. These data strongly support the idea that DAO1 is involved in plant

morphogenesis via auxin oxidation.
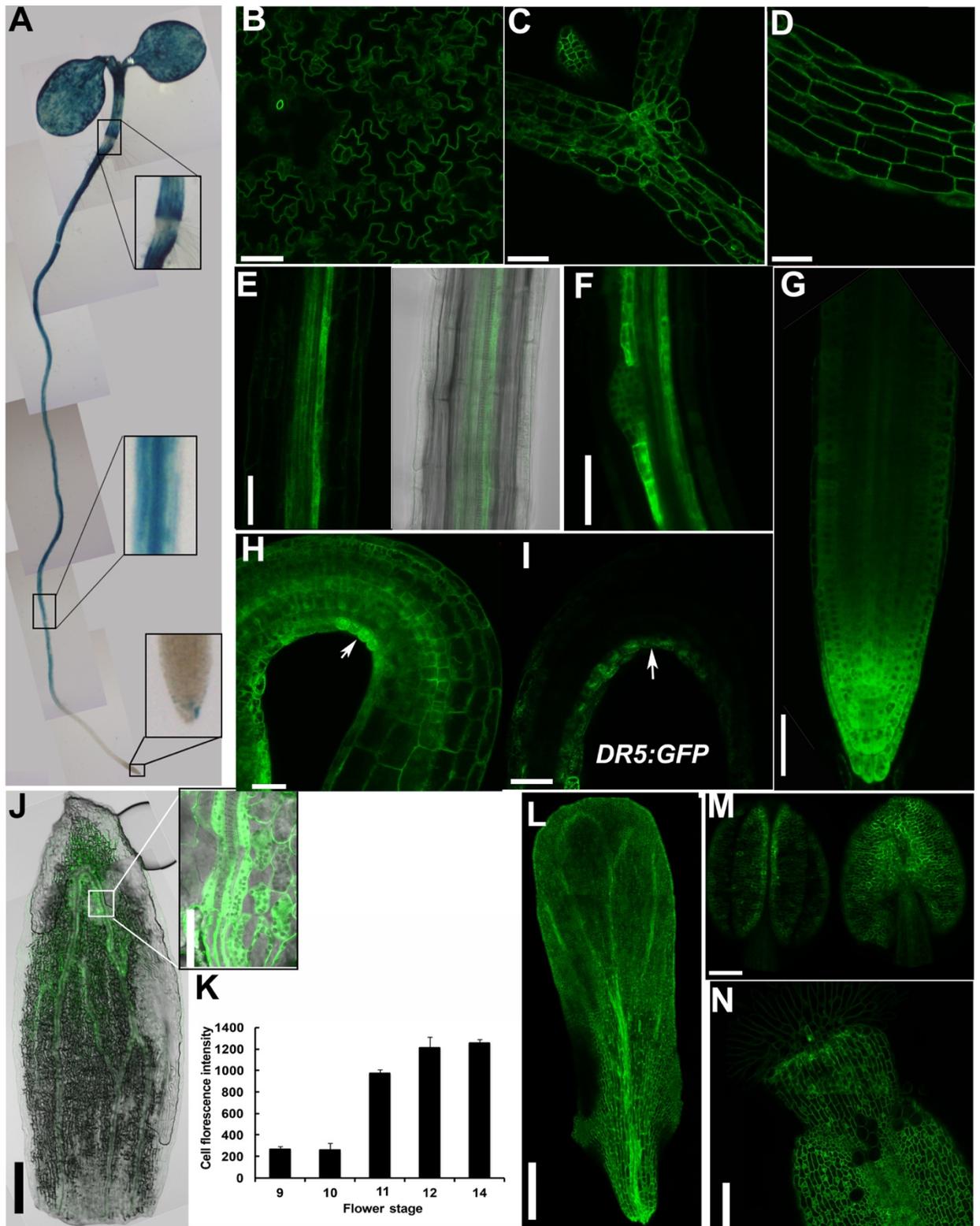
Figure 3-7. Spatial and temporal expression pattern of *DAO1*. (*A*) GUS-staining of 7-day-

old *DAO1pro*:GUS seedling. The boxes show magnified regions as indicated. *(B-E, G)*

60

DAO1pro:YFP-DAO1 signal in 5-day-old seedlings. (*B*) cotyledon, (*C*) shoot apex, (*D*) hypocotyl, (*E*) upper root, (*F*) upper root with a lateral root primordium in 9-day-old seedlings, (*G*) root tip. H, I Apical hook of 3-day-old etiolated seedlings, *DAO1pro*:YFP-DAO1 signal complemented line (*H*) DR5:GFP signal (*I*). Bar = 0.05 mm. (*J-N*) *DAO1pro*:YFP-DAO1 signals in reproductive tissues. (*J*) sepal, bar = 0.2 mm; magnification (box, right), bar = 0.05 mm. (*K*) Florescence intensity of *DAO1pro*:YFP-DAO1 in the upper sepal during flower development. The florescence intensity of at least six bundle sheath cells in the upper sepal from each stage were quantified with the histogram analyses tool in the ZEN Lite 2012 software. n = 3. All the images were taken under the same conditions (see methods). Data are mean value ± standard deviation. (*L*) petal, bar = 0.1 mm; (*M*) stamen, bar = 0.2 mm; (*N*) stigma, bar = 0.1 mm. (*J, L,N*) flower stage 12, (*M*) flower stage 13.

DAO2 is expressed weakly in root cap

To investigate the spatio-temperal expression pattern of DAO2, a native promoter driven YFP:DAO2 genome was made and transferred into both wild type and *dao2-1*. qRT PCR shows that *dao2/DAO2* line recovered DAO2 transcript level to normal level (Fig. 3-8A). Unlike expression pattern of DAO1, DAO2's expression was only detected in cytosol of root cap in 7d seedlings (Fig. 3-8B, C). This is consistent with microarray data (M. Yamada and P. Benfey, personal communication).
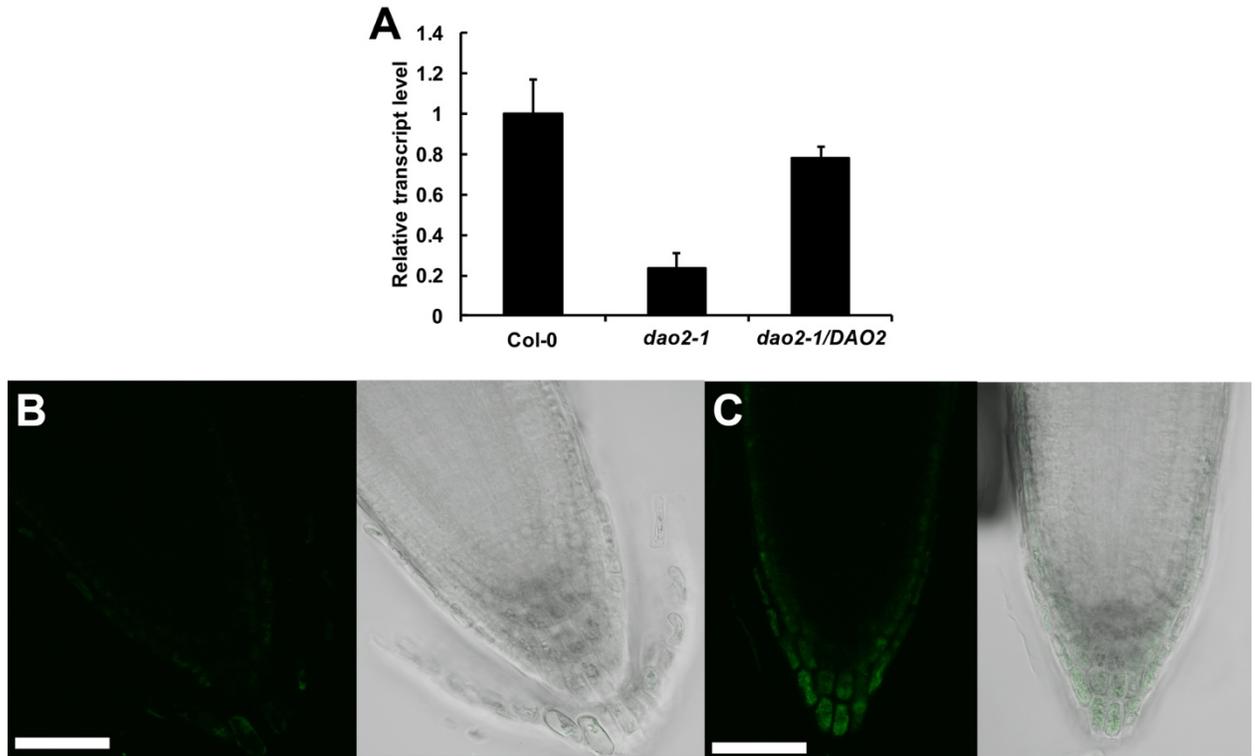
Figure 3-8. *DAO2*pro:YFP-DAO2 expression in root cap. (*A*) Relative transcript

level of DAO2 in wild type, *dao2-1* and *dao2/DAO* lines. *(B)* autoflorescence control

with wild type; (*C*) *DAO2*pro:YFP-DAO2 signal in root tip. Bar = 0.05mm.

Discussion

Previous studies on auxin catabolism emphasized auxin conjugation to glucose or

amino acids in large part due to the identification of metabolic mutants in genetic

screens. In contrast, studies on IAA oxidation *in planta* were constrained because of

lack of identification of IAA oxidases in these screens, and only recently was an IAA

oxidase identified in rice (Zhao et al., 2013). However, the lack of readily available

genetic tools in rice makes it difficult to fully analyze IAA oxidase function in rice, and there may be difference between monocots and dicots. Here we identified two IAA oxidases in *Arabidopsis thaliana*, DAO1 and DAO2, and studied the biochemical and physiological function of the major IAA oxidase, DAO1, using genetic tools.

According to Zhao et al. (2013), rice *dao* plants showed no obvious differences during the seedling, tillering, and flowering (heading) stages compared to wild type plants. Our data suggest that DAO1 plays important role in restriction of tissue size throughout the life of the plant (Fig. 3-5), which is different from the role of OsDAO in rice. On the other hand, rice *dao* plants have severe defects in anther dehiscence, pollen germination and growth, and seed development. Though DAO1 has a strong expression in epidermis of ovary and stamen (Fig. 3-7m, n), no significant defects in fertility were observed in *dao1-1*. It is possible that *DAO2* might compensate the loss of function of *DAO1* in the flower. Double *dao1 dao2* mutants could shed a light on this.

However, rice and Arabidopsis *dao* mutants have one thing in common: defective flower opening, lemma and pale in rice and sepals in Arabidopsis. One thing our data clearly showed is that *DAO*1 has a distinct expression pattern in the sepal compare to other leaf tissues. While DAO1 was mostly evenly distributed in other leaf tissue, like cotyledon (Fig. 3-5A, B) and petal (Fig. 3-5K), DAO1 was strikingly expressed near the top of the sepal, especially the bundle sheath cells. YUC1 and YUC4 have been reported to play important roles in sepal development at the early flower stage, and *YUC4* is expressed at the apex of the sepal (Cheng et al.,

2006), while their expression is turned off at later stage. Taken together, we can deduce that: at early stage before the bud opening, the sepal is tight around the flower and high auxin level is needed to maintain the closed flower that protects the developing reproductive organs (Tekada et al., 2013 Plant Physiology). But at the later stage (from stage 12) that high level auxin becomes an obstacle to flower opening, therefore auxin biosynthesis is turned off and IAA oxidation is initiated to reduce the IAA level and release the sepal. That would explain why DAO1 is highly expressed there and *dao1-1* shows deficiency in sepal opening.

While *DAO2* expression is much lower compared to *DAO1* under normal growth conditions, it is possible that DAO2 might be involved in some specific biological processes. *DAO2* expression was reported to be regulated by the circadian clock which is involved in lateral root initiation(Voß et al., 2015). Recently, IAA derived from the root cap was found to be involved in pre-patterning of lateral root formation(Xuan et al., 2015). *DAO2* null mutants are needed to fully characterize the role in lateral roots development, as the knock-down mutation did not show significant changes in the number of lateral roots (data not shown).

Our results show that one of the "irreversible" major IAA conjugates, IAA-Asp occurs at higher levels in *dao1*(Fig. 2C), in consistent with data from Porco et al., and Mellor et al. (co-submitted to *PNAS*). So why did plants evolve two different pathways to diminish auxin in the cell? Comparison of their functions suggests an explanation. On transcriptal regulation level, *GH3* family genes have very low expression level under normal growth conditions, unless expression is stimulated by specific conditions, such as high levels of auxin (*GH3.1, 2, 3, 4*), blue light (*GH3.10*),

or jasmonic acid (*GH3.9*). *GH3* genes are among the fastest to respond to exogenous auxin, with transcript levels increasing more than 10 times within 1h (GEO accession GSM9969, http://www.ncbi.nlm.nih.gov/geo/). Most *GH3* knock-out mutants are hypersensitive to long-term treatment of exogenous IAA (Staswick et al., 2005). In contrast, *DAO1* has a constitutively high expression level in most tissues under normal conditions. In addition, GH3s have faster enzyme kinetics compared to DAO1, from *in vitro* enzyme assays (Staswik et al 2005; Fig. 1). Asp was conjugated to IAA by GH3.6 at 244 nmol IAA-Asp /min/mg protein (Staswik et al 2005), while DAO1 oxidizes IAA at 15.4 pmol oxIAA/min/mg protein, more than 10,000 times slower than GH3.6. Therefore, DAO1 appears to function in a very slow and consistent manner to fine tune auxin levels during development, in contrast to GH3, which responds quickly to environmental factors. This also explains why increased *GH3* expression levels in *dao1-1* could not compensate the morphogenic phenotypes. Taken together, our results demonstrate that DAO1-mediated IAA oxidation plays important role in IAA homeostatic regulation. DAO1 regulates plant vegetative growth and flower development in a different manner compared to IAA conjugation.

Materials and Methods

Plant material

All the *Arabidopsis* lines used in this research are in Columbia-0 background. *dao1-1* (SALK_093162), *dao1-2D* (CS816250), and *dao2-1* (SALK_205223) were obtained from Arabidopsis Biological Resource Center. Plants were grown as previously

described (Peer et al., 2013). Briefly, seeds were surface-sterilized and planted on 1/4 Murashige and Skoog (MS) medium (RPI Corp.) containing 0.5% sucrose and 0.8% agar, pH 5.5. Seeds were stratified at 4°C for 3 d and then placed in growth chambers at 22 °C, 24 h at 100 μmol m^{-2} s^{-1} light except as indicated for specific treatments. Plants on soil were grown in growth chambers at 22°C, at 100 μmol m^{-2} s^{-1} light (16 h light/8 h darkness).

Cloning and protein expression of AtDAO1 and AtDAO2

Plasmids with *AtDAO1* (At1g14130, U50705) and *AtDAO2* (At1g14120, C105263) cDNA were obtained from ABRC (Ohio State University). The cDNA fragments were subcloned into pET23B+ (Novagen, Nottingham, UK) between the EcoR I and Xho I using the restriction sites introduced by the PCR primers (Table S2) and sequenced. The plasmid was transformed into *E. coli* BL21 (DE3) plysE and protein expression optimized. In the preparative procedure, *E. coli* containing the plasmid were grown in shaker flasks (250 rpm, 37 °C) containing LB media supplemented with 15 ug/ml of ampicillin to late exponential phase (A$_{600}$ ca. 0.8). Recombinant protein production was induced by the addition of isopropyl-D-thiogalactopyrano-side (IPTG) to a final concentration of 0.4 mM. Cells were grown for a further 4 hr in 27 °C and then harvested. Cell paste was stored at -80 ºC. Thawed cell pellets were suspended in lysis buffer contain 20 mM PBS, pH 7.4,10% glycerol, 0.02 mg/ml DNase, 1 mM MgCl$_2$, 1 mM PMSF, 20 mM imidazole, 500 mM NaCl. Unbroken cells, cell debris and precipitated nuclei were then removed by centrifugation at 14,000 g at 4 °C for 15 min. The supernatant was run through his spin trap column

(GE), washed with buffer A (20 mM imidazole, 500 mM NaCl, 20mM PBS pH 7.4)

and eluted with buffer B (buffer A plus 250 mM imidazole). The eluate was

concentrated with Millipore Amicon 30kb membrane by centrifugation at 14,000 rpm

at 4 °C, 10 min.

SDS-PAGE and western blot analyses

SDS loading buffer (LAEMMLI, 1970) was added to the cell pellet or purified

enzyme and boiled for 5 min. Samples were centrifuged at 12,000 x *g* for 5 min. Then

supernatant was loaded on a 12% SDS-PAGE gel (LAEMMLI, 1970). After running

the gels, the gels were either blotted or stained with Coomassie blue. For western blot

analyses, proteins were transferred onto nitrocellulose by wet electroblotting. For

detection of recombinant protein, a mouse monoclonal 6x HIS antibody (Abcam) and

an anti-mouse antibody conjugated to peroxidase (Sigma) were used at 1: 1000 and 1:

5 000 dilutions, respectively. Blots were developed using the HyGLO™ Quick Spray**,**

and chemiluminescence emitted from the filter was exposed to a Kodak film for 10-

30 sec and then developed.

Enzyme assays

The reaction mixtures contained 40 mM PBS, pH7.4, 5 mM 2-oxoglutarate, and 0.5

mM Fe $(SO_4)_2$ in a final volume of 500 μl. 0.002 mg/ml IAA and 6 μg boiled or

unboiled enzyme was added to the mixtures and incubated under in the dark at 30 ºC

for 1 hr. Then 2 volume of acetone mixed with 0.001 mg/ml indole-3-propionic acid

as a standard were added to the sample and placed in -20 °C overnight to precipitate

protein. After centrifugation at 14,000 x *g*, 10 min, the supernatants were dried with speed vac and dissolved with 50 µl 10% methanol, 0.3% acetic acid. 20 µl samples were introduced by an autosampler onto a C18 column (EC 150/3, 3 µm Nucleodur, Macherey Nagel) housed in a HPLC chromatography (1260 infinity, Agilent). The mobile phase was delivered at a flow rate of 0.3 ml/min with an initial mixture of 34% methanol in water (with 0.3 % acetic acid in both solvents) for 5 min, followed by a 20 min linear gradient to 90% methanol. A diode array detector (1260 infinity, Agilent) were set up to detect the effluence absorbance at 200, 254, 280 and 325nm. Boiled or unboiled rDAO1and rDAO2were incubated with 0.2, 1, 2, 5 µmol/L IAA for 30min and oxIAA production was quantified by HPLC. Each data point is the average of at least 6 repeats.

Liquid chromatography tandem mass spectroscopy analyses

For enzyme assays: Samples were injected into an Agilent 1260 infinity LC system, and compounds were separated using an Agilent Poroshell 120EC-C18 (3.5 × 50 mm, 2.7 µm) column and an acidified water:methanol buffer system (Solvent A: 0.1% acetate, 5% MeOH in water; Solvent B: 0.1% acetate in methanol). Gradient conditions were as follows: 1 minute 0-10% B, 5 minutes 10-60% B, 5minutes 60-100% B, hold at 100% B for 3 minutes and then back to 0% B in 2 minutes. Eluted compounds were further separated and quantified using an Agilent 6460 triple quadrupole dual mass spectrometer equipped with an electrospray ionization source. Compounds were quantified in positive ion mode, MS/MS settings were as described (Novák et al., 2012) conducted by Agilent G6460.

For plant tissue: Arabidopsis seedling samples were collected, weighed and chilled in liquid nitrogen before storing in -80 °C. Samples were ground in liquid nitrogen and 1 mL 50 mM sodium-phosphate buffer (pH 7.0, contains 1% DETC) was immediately added into each tube afterwards. 25 ng d5-Indole-3 Acetic acid (d5-IAA, OlChemIm, Ltd., Olomouc, Czech Rebuplic, part #0311532) and 25 ng d3-Tryptophan (d3-Trp, CDN isotopes, Quebec, Canada, part #D-7419) were added into each tube as internal standards (ISTD). Samples were vortexed, extracted for 20 min at 4 °C on a lab nutator and finally centrifuged at 12,000 x G for 15 min at 4 °C. The pH value of supernatant was adjusted to 3 using 1N HCl, and the supernatants were purified using HLB column (column conditioned with 1 mL methanol (LC-MS/MS grade, Fisher Scientific, Pittsburgh, PA, part #A456-1), followed with 1 mL water and 0.5 mL 50 mM pH 2.7 Na-Phosphate buffer, after loading the sample, column was washed with 2 mL 5% methanol and finally eluted with 2 mL 80% methanol). The eluted samples were dried under nitrogen gas, re-dissolved with 500 μL methanol and filtered through 4 mm 0.2 μm PTFE filters (Fisher Scientific, Pittsburgh, PA, part #03-391-4E). 1 μL of each sample was injected for LC-MS/MS analyses

RNA extraction and transcription analysis

Total RNA was extracted from designated tissues using the RNeasy Plant Mini kit (Zymo Research). After treatment with DNaseI (Invitrogen), 2 μg of total RNA was used for the synthesis of the first-strand cDNA using thermoscript RT-PCR system and oligo(dT) as primers (Invitrogen). Quantitative PCR was performed using SYBR Green on a CFX96 Touch Real-Time PCR Detection System (Bio-Rad). PCR was

performed in 96-well optical reaction plates heated for 5 min to 95°C, followed by 40 cycles of denaturation for 10 s at 95°C and annealing-extension for 30 s at 60°C.

The gene-specific primers used to detect the transcripts were as follows: RTDAO1-F:ATCCGTTGCAAGTCCATTGA; RTDAO1-R: GTTACAGAGCTCCAAACGAAA; RTDAO2-F: AAAATTGGGCTCTACCACTCC; RTDAO2-R: TTGTGATAAACTCGACGCCTC. RTGH3.3-F: ACAATTCCGCTCCACAGTTC; RTGH3.3-R: ACGAGTTCCTTGCTCTCCAA. Expression levels were normalized to actin-2 using the following primers: AtACT2- F: ACACTGTGCCAATCTACGAGGGTT; AtACT2- R : ACAATTTCCCGCTCTGCTGTTGTG. All quantitative RT-PCR experiments were performed in triplicate, and the values presented represent means ± SE.

Generation of transgenic lines

Gateway vector pUBNYFP-dest (Grefen et al., 2010) was digested with SacI and SpeI followed by ligation of *AtDAO1* promoter (1.8 kb) or *AtDAO2* promoter (2.0 kb) respectively in the vector. *DAO1* and *DAO2* genomic coding sequences were PCR amplified and ligated into modified pUBN-YFP vector for pDAO1: YFP: DAO1 and pDAO2: YFP: DAO2. Transformation of *Arabidopsis thaliana* with *Agrobacterium tumefasciens* (GV3101) was performed as described previously (Clough and Bent, 1998). All complementation experiments were performed with two independent homozygous T$_3$ lines.

70

Gravitropism assay

Seedlings were grown vertically on plates as above for 4 d. After reorienting the plates by 90 degrees, the root tip position was marked every 3 h over a 24-h time period. The angles of curvature were measured using the Image J (Schneider et al., 2012), and the data were analyzed by Microsoft Excel. Averages and standard deviations were calculated from 50 seedlings.

Phototropism assay

Seeds are placed on 50-70 mesh sand (Sigma Cat. 274739) with water, covered with a clear vented lid, and light treated for 12 hours. Subsequently, seeds are placed in dark until 2 days old, or until about 0.4 cm in height. Seedlings then undergo light treatment at 65 μM m-2 s-1 light (Philips f32t8/tl741; Philips, NV) at 24°C for 12 hours to undergo photomorphogenesis, then returned to dark 12 hours. The vented lid is removed and seedlings are placed in front of a 450 nm 100 LED light source (Rothner Laser Technic; Vienna, Austria) between 0.9- 0.6 μM m^{-2} s^{-1} at 24°C. Video is captured using an MTI ccd72 (DAGE-MTI; Michigan City, IN) camera, the image is snapped every 5 minutes. The bending angles are measured using Image J.

GUS staining

β-Glucuronidase (GUS) staining was as described in Geisler et al. (Geisler et al., 2005). Briefly, seedlings or adult plant tissues were incubated in GUS substrate for 12

h at 37 °C, then destained in 70% ethanol prior to imaging.

Microsomal membrane preparations

Microsomal preparations of 7-d-old Arabidopsis seedlings were prepared and assayed for purity as described previously(Murphy and Taiz, 1999) with the exception that 500 μM benzamide and 500 μM benzamidine were added to the original homogenization buffer. Prepared membranes were stored in liquid nitrogen. Membrane proteins were detergent solubilized by incubation with gentle shaking at 4°C for 30 min in a buffer consisting of 0.1% (w/v) Brij 35, 0.05% (w/v) CHAPS {3-[(3-cholamidopropyl)dimethylammonio]-1-propanesulfonic acid}, 10 mM BisTris propane-MES (pH 7.8), 250 mM Suc, 20% (w/v) glycerol, and 1 mM DTT followed by centrifugation at 100,000g for 30 min.

Microscopy

Protein localizations in Arabidopsis seedlings were visualized using an LSM 710 laser spectral scanning confocal microscope (Zeiss, http://corporate.zeiss.com) with either 20× lens or a 40× water immersion lens and pixel dwell time of 0.01 ms. The master gain was always set to less than 893, with a digital gain of 1.5. For YFP acquisition: 514 nm (5%) excitation and 519-560 nm emission. For GFP: 488 nm (5%) excitation and 493-598 nm emission. Quantification of florescence intensity was analyzed using ZEN Lite 2012. Briefly, representative images from 3 sepals in each flower stage were selected for analysis. Six cells from each images were selected in

each images. All images were processed with ZEN Lite 2012 (Zeiss) and Photoshop (Adobe, http://www.adobe.com).

Sequence and phylogenetic analysis

Translated BLAST (tBLASTn) was used to identify homologous genes of *OsDAO* (Os04g0475600) in *Arabidopsis thaliana* (ncbi.nlm.nih.gov). Protein sequences of the 2-oxoglutarate and Fe(II)-dependent oxygenase super family in *Arabidopsis thaliana* were obtained from The Arabidopsis Information Resource (TAIR, version 10) (https://www.arabidopsis.org). The sequences were aligned using the CustalW 2.0 (Larkin et al., 2007). The alignment file was used to generate an unrooted tree with MEGA 6.0 (Tamura et al., 2013) applying the neighbor-joining method, with 10,000 bootstrap replications and handling gaps with pairwise deletion.

for providing the auxin quantitation data in the sepals, helpful discussions and critically reading the manuscript.

Chapter 4.

Conclusion and perspective

In this dissertation, I identified and characterized IAA oxidases that deactivate IAA by decarboxylative or non-decarboxylative oxidation in Arabidopsis. The long-term goal is to acquire the knowledge of how IAA oxidation affects plant growth and to improve the crop traits by genetic engineering.

I first demonstrated that IAA can be decarboxylated by ACO2, a membrane localized ethylene synthase. Ascorbic acid inhibits IAA decarboxylation activity, while it is essential for ethylene synthesis activity. *ACO2* loss-of-function lines showed ethylene related phenotypes, including longer hypocotyls and reduced apical hook angles in etiolated seedlings, and delayed bolting. They also showed reduced phototropic bending, a typical auxin response. High ascorbic acid levels might explain why *ACO2* mutants did not have auxin related phenotype during plant growth and development. However, ACO2 might be involved in stress induced auxin degradation.

Then I identified two cytosolic IAA oxidases, AtDAO1 and AtDAO2. Both of them could catalyze IAA oxidation and produce oxIAA *in vitro*, the major IAA metabolite *in planta*. DAO1 is the dominant IAA oxidase *in planta* and is responsible for 95% of oxIAA production in Arabidopsis. The IAA metabolome in *DAO1* loss-of-function lines indicates that IAA conjugation partially compensated disruption of IAA oxidation and maintained total IAA levels similar to wild type.

Expression patterns of *DAO1* and *DAO2* were studied by native promoter driven YFP-protein fusions and GUS. *DAO1* was strongly expressed in young cotyledons, root vascular tissue and the root cap in Arabidopsis seedlings. *DAO1* was also expressed in all four whorls of flower, in which sepals had the highest expression from floral stage 11, just before the flower opening. My results indicate that localized IAA oxidation by DAO1 plays an important role in plant morphogenesis, including regulation of cotyledon size, lateral root density, and floral organ size and subsequent fertility. My results also indicate that the plant might maintain the required auxin levels by a delicate cooperation of IAA synthesis and IAA oxidation during sepal opening.

A T-DNA insertion in 3' UTR of *DAO1* caused elevated transcript levels of *DAO1* (*dao1-2D*) with a corresponding increase in oxIAA. However, complemented lines which have an even higher transcript level (10 times) showed oxIAA levels similar to wild type, indicating that some post-translational regulation might be involved in *DAO1* expression levels. The mutation in the 3'UTR might impact the mRNA stability of *DAO1*. Transcriptional inhibitors could be utilized to test the stability of *DAO1* mRNA in *dao1-2D* and wild type. Further, yeast two-hybrid assays could be employed to investigate transcription factors that bind to 3'UTR area or factors that affect translation of the mRNA in *dao1-2D*. These experiments will improve our understanding of molecular mechanism of *DAO1* expression regulation during different development programs and further benefit the future crop improvement.

Although the physiological function of DAOs during plant development were well studied in the presented research, further research is needed to understand the role of

76

DAOs in response to environmental change. It was reported that the oxIAA level was elevated while IAA levels were reduced under different stress conditions. Our preliminary data (Appendix E) and the microarray data showed that *DAO1* and *DAO2* gene transcription levels are rapidly induced by salt sand ABA treatment (Schmid et al., 2005). However, what specific role they play in stress resistance has not been investigated. Studies of stress resistance in different *DAO* mutants could shed a light on this.

DAO1 could also be strongly induced by jasmonic acid (JA), indicating it might be involved in JA-auxin interactions (Goda et al., 2008). However, the exact physiological function of this interaction has not been investigated. This could be investigated by focusing on the biological processes in which both JA and auxin are involved, especially the ones where auxin needs to be degraded, like flowering, senescence, etc.

Appendices
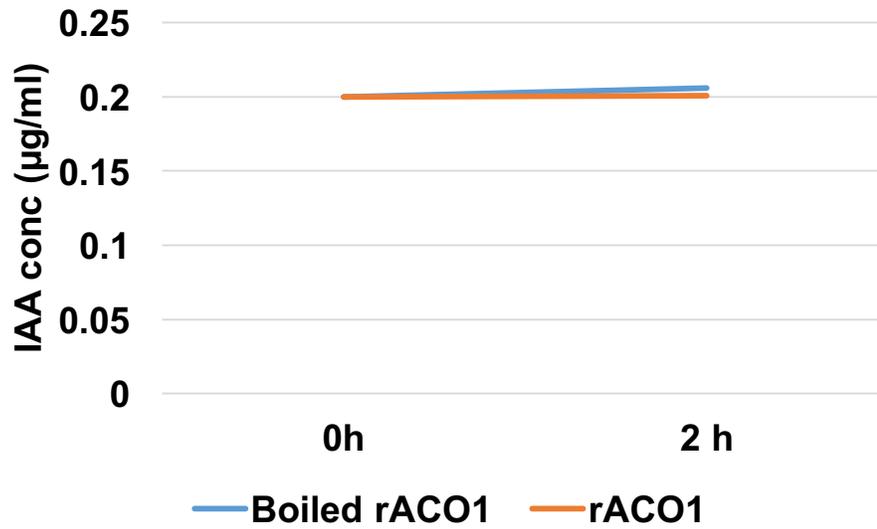
Appendix A. rACO1 does not have IAA oxidation activity. rACO1 was incubated

with IAA for 2 h and the IAA concentration was detected with HPLC.
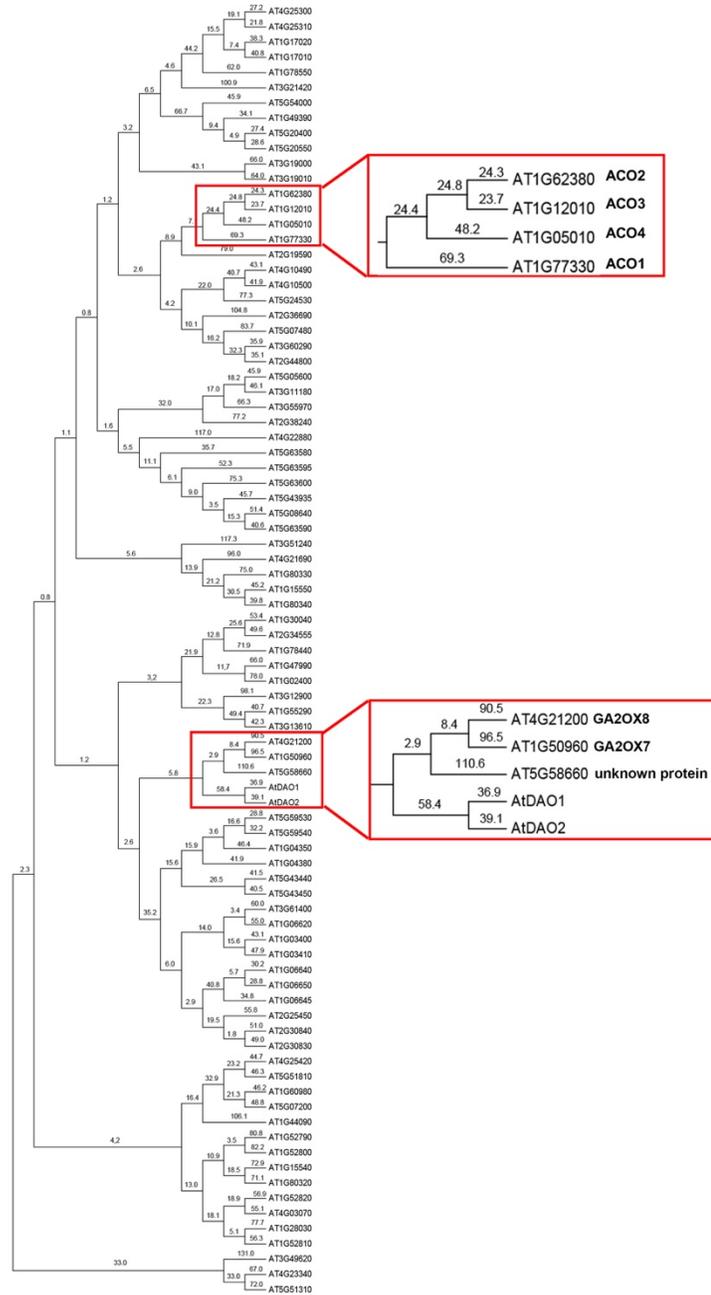
Appendix B. Phylogenetic analysis of 2-oxoglurate Fe(II)-dependent oxygenase superfamily in *Arabidopsis thaliana*. The evolutionary history was inferred using the Neighbor-Joining method in MEGA 6.0. The bootstrap consensus tree inferred from 10,000 replicates is taken to represent the evolutionary history of the taxa

analyzed. Branches corresponding to partitions reproduced in less than 50% bootstrap

replicates are collapsed. The evolutionary distances were computed using the number

of differences method and are in the units.
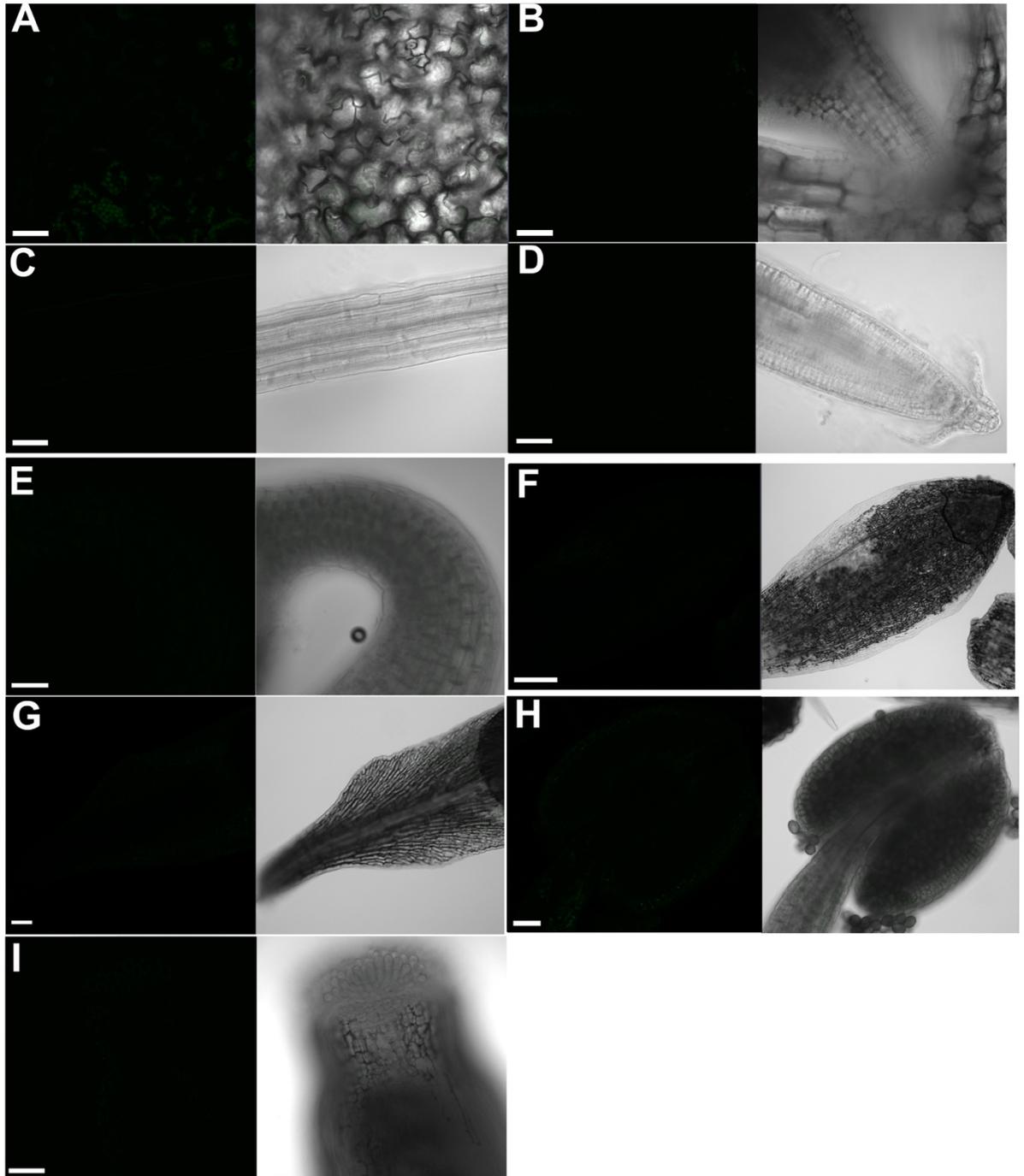
Appendix C. Autofluorescence controls of wild type plants corresponding to confocal images Figure 3. (A-D), 5-day-old seedlings, (*A*) cotyledon, (*B*) shoot apex, (*C*) upper root, (*D*) root tip. E. Confocal image of apical hook of 3-day-old etiolated seedling. Bar = 0.05mm. f-i, Autofluorescence signal in reproductive tissues: (*F*) sepal, bar = 0.5 mm; (*G*) petal, bar = 0.05 mm; (*H*) stamen, bar = 0.05 mm; (*I*) stigma, bar = 0.05 mm. (*F-H*) are from one flower at stage 12, (*I*) is from one flower at stage 13. Images were taken on an LSM710 confocal spectral laser scanning microscope. All the images were taken under the same conditions corresponding images in Figure 3.

Appendix D. Viridiplantae (taxid:33090) Blast analyses of a degenerate DAO motif PSELVDAEHPR. Rice DAO was identified in the search (highlighted in bold). Sequences in GENBANK annotated as DAO or DAO-like are highlighted in grey.

GI number	Sequence	% Identity
>gi|460374964|ref|XP_004233278.1|:259-269 PREDICTED: 2-oxoglutarate-dependent dioxygenase DAO-like [Solanum lycopersicum]	PSELVDAEHPR	100
>gi|674243627|gb|KFK36392.1|:216-226 hypothetical protein AALP_AA4G118300 [Arabis alpina]	PSELVDADHPR	90.909
>gi|661890588|emb|CDP06085.1|:258-268 unnamed protein product [Coffea canephora]	PSELVDSEHPR	90.909
>gi|698552242|ref|XP_009769574.1|:214-224 PREDICTED: 2-oxoglutarate-dependent dioxygenase DAO-like isoform X2 [Nicotiana sylvestris]	PPELVDAEHPR	90.909
>gi|723676585|ref|XP_004233915.2|:214-224 PREDICTED: 2-oxoglutarate-dependent dioxygenase DAO-like [Solanum lycopersicum]	PPELVDAEHPR	90.909
>gi|698552236|ref|XP_009769572.1|:259-269 PREDICTED: 2-oxoglutarate-dependent dioxygenase DAO-like isoform X1 [Nicotiana sylvestris]	PPELVDAEHPR	90.909

>gi|697104708|ref|XP_009606157.1|:259-269 PREDICTED: 2-oxoglutarate-dependent dioxygenase DAO-like isoform X2 [Nicotiana tomentosiformis]	PPELVDAEHPR	90.909
>gi|565398913|ref|XP_006365008.1|:259-269 PREDICTED: probable 2-oxoglutarate-dependent dioxygenase AOP1-like [Solanum tuberosum]	PPELVDAEHPR	90.909
>gi|565398911|ref|XP_006365007.1|:259-269 PREDICTED: probable 2-oxoglutarate-dependent dioxygenase AOP1-like [Solanum tuberosum]	PPELVDAEHPR	90.909
>gi|697104706|ref|XP_009606156.1|:266-276 PREDICTED: 2-oxoglutarate-dependent dioxygenase DAO-like isoform X1 [Nicotiana tomentosiformis]	PPELVDAEHPR	90.909
>gi|674907065|emb|CDY26052.1|:24-34 BnaC06g05720D [Brassica napus]	PEELVDAEHPR	90.909
>gi|703112634|ref|XP_010100168.1|:264-274 Gibberellin 3-beta-dioxygenase 4 [Morus notabilis]	PSELVDDEHPR	90.909
>gi|674951431|emb|CDX81613.1|:134-144 BnaC08g39880D [Brassica napus]	PSEFVDAEHPR	90.909
>gi|922508960|ref|XP_013590817.1|:247-257 PREDICTED: LOW QUALITY PROTEIN: probable 2-oxoglutarate-dependent dioxygenase AOP1.2 [Brassica oleracea var. oleracea]	PEELVDAEHPR	90.909
>gi|923832425|ref|XP_013698039.1|:262-272 PREDICTED: 2-oxoglutarate-dependent dioxygenase DAO-like [Brassica napus]	PSEFVDAEHPR	90.909
>gi|923818163|ref|XP_013693229.1|:262-272 PREDICTED: 2-oxoglutarate-dependent dioxygenase DAO-like [Brassica napus]	PSEFVDAEHPR	90.909
>gi|685316161|ref|XP_009148694.1|:262-272 PREDICTED: 2-oxoglutarate-dependent dioxygenase DAO-like [Brassica rapa]	PSEFVDAEHPR	90.909
>gi|674883357|emb|CDY49110.1|:262-272 BnaA06g08960D [Brassica napus]	PSEFVDAEHPR	90.909
>gi|923874821|ref|XP_013710739.1|:263-273 PREDICTED: 2-oxoglutarate-dependent dioxygenase DAO-like [Brassica napus]	PSEFVDAEHPR	90.909
>gi|923825585|ref|XP_013695754.1|:263-273 PREDICTED: 2-oxoglutarate-dependent dioxygenase DAO-like [Brassica napus]	PSEFVDAEHPR	90.909
>gi|923763987|ref|XP_013677797.1|:262-272 PREDICTED: 2-oxoglutarate-dependent dioxygenase DAO-like [Brassica napus]	PSEFVDAEHPR	90.909
>gi|923719998|ref|XP_013664686.1|:263-273 PREDICTED: 2-oxoglutarate-dependent dioxygenase DAO-like [Brassica napus]	PSEFVDAEHPR	90.909
>gi|923693597|ref|XP_013657373.1|:262-272 PREDICTED: 2-oxoglutarate-dependent dioxygenase DAO-like [Brassica napus]	PSEFVDAEHPR	90.909

|		
>gi|922545847|ref|XP_013600713.1|:263-273 PREDICTED: 2-oxoglutarate-dependent dioxygenase DAO-like [Brassica oleracea var. oleracea]	PSEFVDAEHPR	90.909
>gi|922491820|ref|XP_013585242.1|:263-273 PREDICTED: 2-oxoglutarate-dependent dioxygenase DAO-like [Brassica oleracea var. oleracea]	PSEFVDAEHPR	90.909
>gi|685350016|ref|XP_009110557.1|:262-272 PREDICTED: 2-oxoglutarate-dependent dioxygenase DAO-like [Brassica rapa]	PSEFVDAEHPR	90.909
>gi|685316165|ref|XP_009148696.1|:263-273 PREDICTED: 2-oxoglutarate-dependent dioxygenase DAO-like [Brassica rapa]	PSEFVDAEHPR	90.909
>gi|923915368|ref|XP_013727221.1|:263-273 PREDICTED: 2-oxoglutarate-dependent dioxygenase DAO-like [Brassica napus]	PSEFVDAEHPR	90.909
>gi|674883356|emb|CDY49109.1|:263-273 BnaA06g08970D [Brassica napus]	PSEFVDAEHPR	90.909
>gi|702482924|ref|XP_010033632.1|:260-270 PREDICTED: 2-oxoglutarate-dependent dioxygenase DAO-like [Eucalyptus grandis]	PEELVDAEHPR	90.909
>gi|674899181|emb|CDY33774.1|:264-274 BnaA09g45800D [Brassica napus]	PSEFVDAEHPR	90.909
>gi|727432894|ref|XP_010495771.1|:262-272 PREDICTED: 2-oxoglutarate-dependent dioxygenase DAO-like [Camelina sativa]	PSEFVDAEHPR	90.909
>gi|565492802|ref|XP_006304040.1|:262-272 hypothetical protein CARUB_v10009839mg [Capsella rubella]	PSEFVDAEHPR	90.909
>gi|297849816|ref|XP_002892789.1|:262-272 hypothetical protein ARALYDRAFT_471571 [Arabidopsis lyrata subsp. lyrata]	PSEFVDAEHPR	90.909
>gi|15223096|ref|NP_172865.1|:263-273 2-oxoglutarate (2OG) and Fe(II)-dependent oxygenase-like protein [Arabidopsis thaliana]	PSEFVDAEHPR	90.909
>gi|923874876|ref|XP_013710756.1|:280-290 PREDICTED: 2-oxoglutarate-dependent dioxygenase DAO-like [Brassica napus]	PSEFVDAEHPR	90.909
>gi|923755136|ref|XP_013675537.1|:280-290 PREDICTED: 2-oxoglutarate-dependent dioxygenase DAO-like [Brassica napus]	PSEFVDAEHPR	90.909
>gi|923719992|ref|XP_013664684.1|:280-290 PREDICTED: 2-oxoglutarate-dependent dioxygenase DAO-like [Brassica napus]	PSEFVDAEHPR	90.909
>gi|922545843|ref|XP_013600711.1|:280-290 PREDICTED: 2-oxoglutarate-dependent dioxygenase DAO-like [Brassica oleracea var. oleracea]	PSEFVDAEHPR	90.909
>gi|685367957|ref|XP_009117936.1|:280-290 PREDICTED: 2-oxoglutarate-dependent dioxygenase DAO-like [Brassica rapa]	PSEFVDAEHPR	90.909

>gi|685314120|ref|XP_009147659.1|:279-289 PREDICTED: probable 2-oxoglutarate-dependent dioxygenase AOP1 [Brassica rapa]	PEELVDAEHPR	90.909
>gi|685316163|ref|XP_009148695.1|:282-292 PREDICTED: 2-oxoglutarate-dependent dioxygenase DAO-like [Brassica rapa]	PSEFVDAEHPR	90.909
>gi|674936830|emb|CDX96865.1|:326-336 BnaA08g24080D [Brassica napus]	PSEFVDAEHPR	90.909
>gi|674949734|emb|CDX84043.1|:395-405 BnaC08g16020D [Brassica napus]	PSEFVDAEHPR	90.909
>gi|695051445|ref|XP_009413747.1|:336-346 PREDICTED: gibberellin 20 oxidase 1-D [Musa acuminata subsp. malaccensis]	PAELVDADHPR	81.818
>gi|296088490|emb|CBI37481.3|:183-193 unnamed protein product [Vitis vinifera]	PPELVDSEHPR	81.818
>gi|118484910|gb|ABK94321.1|:213-223 unknown [Populus trichocarpa]	PPELVDSEHPR	81.818
>gi|147781479|emb|CAN69444.1|:256-266 hypothetical protein VITISV_016474 [Vitis vinifera]	PPELVDSEHPR	81.818
>gi|743920686|ref|XP_011004396.1|:255-265 PREDICTED: 2-oxoglutarate-dependent dioxygenase DAO-like [Populus euphratica]	PPELVDSEHPR	81.818
>gi|224056727|ref|XP_002298993.1|:255-265 adventitious rooting related oxygenase family protein [Populus trichocarpa]	PPELVDSEHPR	81.818
>gi|566195567|ref|XP_002317640.2|:255-265 adventitious rooting related oxygenase family protein [Populus trichocarpa]	PPELVDSEHPR	81.818
>gi|225431637|ref|XP_002263124.1|:256-266 PREDICTED: 2-oxoglutarate-dependent dioxygenase DAO-like [Vitis vinifera]	PPELVDSEHPR	81.818
>gi|590711065|ref|XP_007049001.1|:257-267 2-oxoglutarate and Fe(II)-dependent oxygenase superfamily protein [Theobroma cacao]	PPELVDSEHPR	81.818
>gi|743887366|ref|XP_011038125.1|:258-268 PREDICTED: 2-oxoglutarate-dependent dioxygenase DAO-like [Populus euphratica]	PPELVDSEHPR	81.818
>gi|460374960|ref|XP_004233276.1|:259-269 PREDICTED: 2-oxoglutarate-dependent dioxygenase DAO [Solanum lycopersicum]	PPELVNAEHPR	81.818
>gi|694388066|ref|XP_009369758.1|:265-275 PREDICTED: 2-oxoglutarate-dependent dioxygenase DAO-like [Pyrus x bretschneideri]	PPELVDSEHPR	81.818
>gi|694388061|ref|XP_009369756.1|:265-275 PREDICTED: 2-oxoglutarate-dependent dioxygenase DAO-like [Pyrus x bretschneideri]	PPELVDSEHPR	81.818
>gi|694388042|ref|XP_009369750.1|:265-275 PREDICTED: 2-oxoglutarate-dependent dioxygenase DAO-like [Pyrus x bretschneideri]	PPELVDSEHPR	81.818

>gi|658054610|ref|XP_008363059.1|:265-275 PREDICTED: 2-oxoglutarate-dependent dioxygenase DAO-like [Malus domestica]	PPELVDSEHPR	81.818
>gi|657947856|ref|XP_008392065.1|:265-275 PREDICTED: 2-oxoglutarate-dependent dioxygenase DAO-like [Malus domestica]	PPELVDSEHPR	81.818
>gi|695080829|ref|XP_009387900.1|:562-572 PREDICTED: gibberellin 20 oxidase 1-D-like [Musa acuminata subsp. malaccensis]	PPELVDADHPR	81.818
>gi|565495888|ref|XP_006305583.1|:179-189 hypothetical protein CARUB_v10010246mg [Capsella rubella]	PEEMVDAEHPR	81.818
>gi|125590728|gb|EAZ31078.1|:212-222 hypothetical protein OsJ_15175 [Oryza sativa Japonica Group]	PGELVDGEHPR	81.818
>gi|641842951|gb|KDO61853.1|:257-267 hypothetical protein CISIN_1g036868mg [Citrus sinensis]	PAEFVDAEHPR	81.818
>gi|567922574|ref|XP_006453293.1|:257-267 hypothetical protein CICLE_v10009037mg [Citrus clementina]	PAEFVDAEHPR	81.818
>gi|567922576|ref|XP_006453294.1|:258-268 hypothetical protein CICLE_v10009037mg [Citrus clementina]	PAEFVDAEHPR	81.818
>gi|115458950|ref|NP_001053075.1|:260-270 Os04g0475600 [Oryza sativa Japonica Group]	**PGELVDGEHPR**	**81.818**
>gi|922545717|ref|XP_013600645.1|:262-272 PREDICTED: 2-oxoglutarate-dependent dioxygenase DAO-like [Brassica oleracea var. oleracea]	PSEFVNAEHPR	81.818
>gi|567132038|ref|XP_006392866.1|:279-289 hypothetical protein EUTSA_v10011658mg [Eutrema salsugineum]	PEEMVDAEHPR	81.818
>gi|747076935|ref|XP_011085561.1|:292-302 PREDICTED: 2-oxoglutarate-dependent dioxygenase DAO-like [Sesamum indicum]	PPELVDVEHPR	81.818
>gi|567151883|ref|XP_006417054.1|:262-272 hypothetical protein EUTSA_v10008310mg [Eutrema salsugineum]	PSEFVDAQHPR	81.818
>gi|674878202|emb|CDY53799.1|:247-257 BnaA06g01840D [Brassica napus]	PEELVDPEHPR	81.818
>gi|16118978|gb|AAL14687.1|:264-274 2-oxoglutarate-dependent dioxygenase [Arabidopsis halleri]	PEELVDEEHPR	81.818
>gi|922449065|ref|XP_013627893.1|:255-265 PREDICTED: probable 2-oxoglutarate-dependent dioxygenase AOP1.2 [Brassica oleracea var. oleracea]	PDEIVDAEHPR	81.818
>gi|727565328|ref|XP_010455020.1|:281-291 PREDICTED: probable 2-oxoglutarate-dependent dioxygenase AOP1.2 [Camelina sativa]	PEELVDEEHPR	81.818
>gi|727439110|ref|XP_010500908.1|:257-267 PREDICTED: probable 2-oxoglutarate-dependent dioxygenase AOP1 isoform X3 [Camelina sativa]	PEELVDEEHPR	81.818
>gi|923915384|ref|XP_013727228.1|:262-272 PREDICTED: 2-oxoglutarate-dependent dioxygenase DAO-like [Brassica napus]	PSEFVDVEHPR	81.818
>gi|731339915|ref|XP_010681112.1|:261-271 PREDICTED: 2-oxoglutarate-dependent dioxygenase DAO-like [Beta vulgaris subsp. vulgaris]	PSEFVDVEHPR	81.818

>gi|674893502|emb|CDY39340.1|:263-273 BnaC05g10390D [Brassica napus]	PSEFVDVEHPR	81.818
>gi|674238139|gb|KFK30904.1|:274-284 hypothetical protein AALP_AA6G041200 [Arabis alpina]	PEELVDEEHPR	81.818
>gi|727439108|ref|XP_010500907.1|:275-285 PREDICTED: probable 2-oxoglutarate-dependent dioxygenase AOP1 isoform X2 [Camelina sativa]	PEELVDEEHPR	81.818
>gi|685314118|ref|XP_009147658.1|:275-285 PREDICTED: probable 2-oxoglutarate-dependent dioxygenase AOP1 [Brassica rapa]	PDELVDEEHPR	81.818
>gi|922508768|ref|XP_013590757.1|:275-285 PREDICTED: probable 2-oxoglutarate-dependent dioxygenase AOP1 [Brassica oleracea var. oleracea]	PDELVDEEHPR	81.818
>gi|15219099|ref|NP_175691.1|:275-285 putative 2-oxoglutarate-dependent dioxygenase [Arabidopsis thaliana]	PDELVDEEHPR	81.818
>gi|567132034|ref|XP_006392865.1|:275-285 hypothetical protein EUTSA_v10011667mg [Eutrema salsugineum]	PDELVDEEHPR	81.818
>gi|565495504|ref|XP_006305391.1|:275-285 hypothetical protein CARUB_v10009783mg [Capsella rubella]	PDELVDEEHPR	81.818
>gi|727439106|ref|XP_010500906.1|:276-286 PREDICTED: probable 2-oxoglutarate-dependent dioxygenase AOP1 isoform X1 [Camelina sativa]	PEELVDEEHPR	81.818
>gi|470110454|ref|XP_004291498.1|:273-283 PREDICTED: probable 2-oxoglutarate-dependent dioxygenase AOP1 [Fragaria vesca subsp. vesca]	PKELVDEEHPR	81.818
>gi|16118889|gb|AAL14645.1|AF417857_1:276-286 AOP1 [Arabidopsis lyrata]	PEELVDEEHPR	81.818
>gi|674238138|gb|KFK30903.1|:277-287 hypothetical protein AALP_AA6G041100 [Arabis alpina]	PEELVDEEHPR	81.818
>gi|922563880|ref|XP_013610213.1|:279-289 PREDICTED: probable 2-oxoglutarate-dependent dioxygenase AOP1 [Brassica oleracea var. oleracea]	PEELVDEEHPR	81.818
>gi|674238136|gb|KFK30901.1|:279-289 hypothetical protein AALP_AA6G040900 [Arabis alpina]	PEELVDEEHPR	81.818
>gi|923684279|ref|XP_013654615.1|:280-290 PREDICTED: probable 2-oxoglutarate-dependent dioxygenase AOP1 [Brassica napus]	PDEIVDAEHPR	81.818
>gi|685340431|ref|XP_009107019.1|:280-290 PREDICTED: probable 2-oxoglutarate-dependent dioxygenase AOP1 [Brassica rapa]	PDEIVDAEHPR	81.818
>gi|674238137|gb|KFK30902.1|:280-290 hypothetical protein AALP_AA6G041000 [Arabis alpina]	PEELVDEEHPR	81.818
>gi|565463434|ref|XP_006289716.1|:283-293 hypothetical protein CARUB_v10003282mg [Capsella rubella]	PDELVDEEHPR	81.818
>gi|727427883|ref|XP_010467243.1|:289-299 PREDICTED: probable 2-oxoglutarate-dependent dioxygenase AOP1 [Camelina sativa]	PEELVDEEHPR	81.818
>gi|923804578|ref|XP_013688552.1|:279-289 PREDICTED: probable 2-oxoglutarate-dependent dioxygenase AOP1 [Brassica napus]	PEELVDEEHPR	81.818

>gi|116788351|gb|ABK24846.1|:308-318 unknown [Picea sitchensis]	PPELVDNEHPR	81.818
>gi|646283286|gb|AIB53819.1|:252-262 2-oxoacid-dependent dioxygenase [Paeonia suffruticosa]	PEELVDAENP R	81.818
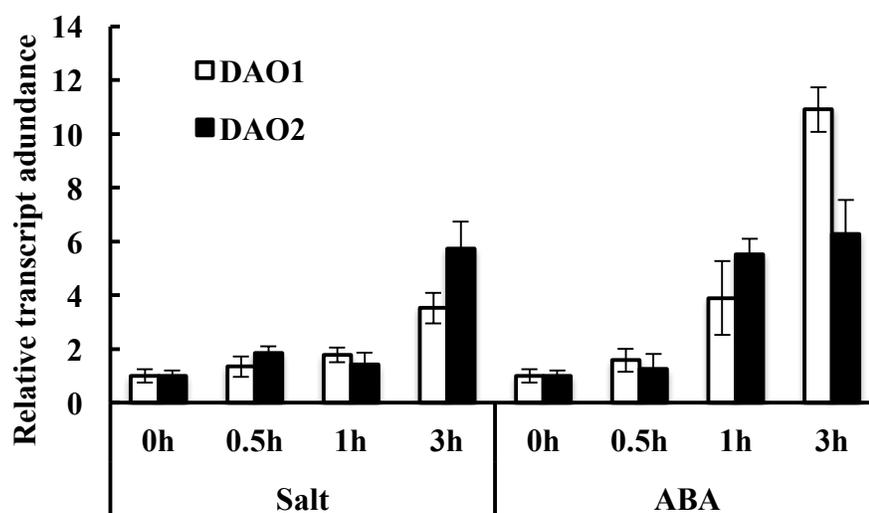
Appendix E. Time course of salt and ABA treatment induced transcript level response of *DAO1* and *DAO2* in *Arabidopsis* seedlings. 7-day-old seedlings were treated with 150 mM NaCl or 10 μM ABA from 0 to 3h. Each data point has 3 replicas (average± SD).

Appendix F. Primer list

Sal1-ACO2-F	GTGTCGACATGGAGAAGAACATGAAGTT
Xho1-ACO2-R	TTCTCGAGGAAAGTCTCTACGGCTGCT
ACO1-BamHI-F	ATAGGATCCGATGGTTTTGA TCAAAGAGAG
ACO1-Not1-R	AAGCGGCCGCGGCTGAATCCGCATTTC
Sal1-ACO3-F	GTGTCGACATGGAGATGAACATTAAG
Xho1-ACO3-R	AAGCGGCCGCTTAGAATGTCTCAACCAC
ACO4-BamHI-F	ATAGGATCCG ATGGAGAGTT TCCCGATCAT
ACO4-Not1-R	AAGCGGCCGC CGCAGTGGCCAATGGTC
SALK_027311C-LP	AGAAGCTGGAGACCACTGACC
SALK_027311C-RP	TCCCTCAATCCAATCTCAATG

SALK_044146C-LP	ATCCATCTGTTTTGGGGAAAC
SALK_044146C-RP	GATTCCGAGTACCCGAGTTTC
ACO2QRT-F1	GGCTTCTTTGAGATAGTGAACC
ACO2QRT-R1	GGGAGGTGACGAACGTAGAA
Salk_093162-F	TTCCCCACGGAATTAAGGTAC
Salk_093162-R	CAAGTCCATTGATAGCCTTCG
CS816250-F	GGTTTGGAGATAAGGCTCAGG
CS816250-R	CGCCTCGTTCTTATTAGGACC
Salk_209298 LP	TCCGTTTAGTTCCCCCATATC
Salk_209298 RP	AAAAGTCGTGATGTTTGGCAC
AtACT2-738 F	ACACTGTGCCAATCTACGAGGGTT
AtACT2-882 R	ACAATTTCCCGCTCTGCTGTTGTG
RTDAO1-F	ATCCGTTGCAAGTCCATTGA
RTDAO1-R	GTTACAGAGCTCCAAACGAAA
RTDAO2-F	AAAATTGGGCTCTACCACTCC
RTDAO2-R	TTGTGATAAACTCGACGCCTC
RTGH3.3-F	ACAATTCCGCTCCACAGTTC
RTGH3.3-R	ACGAGTTCCTTGCTCTCCAA
RTGH3.4 -F	CGTTGGAGATACGTGTGGTG
RTGH3.4-R	GCAGTTTCATGATCGGTGTG
RTGH3.5-F	GTCTTCGAGGACTGCTGCTT
RTGH3.5-R	ATGTCCCTGGCTCAACAATC
RTGH3.6-F	CCTTGTTCCGTTTGATGCTT
RTGH3.6-R	CGTGTTACCGTTCAAGCAGA
DAO1pro-F-SAC1	GAGCTCTCGTAGATTTCCGGCGAAGTT
DAO1pro-R-spe1	ACTAGTATCTTCAATGGAGAGGTTAAC
DAO2pro-F-SAC1	GAGCTCCCTTACTATGAAGCATTAGGTCT
DAO2pro-R-spe1	ACTAGTTATCTTCAATGAAAAGGCTT
CACC-DAO1-F	CACCATGGGGGAACTAAACGGAGTC
DAO1-R	TCATTTATCTAGTCCTGCATGG
CACC-DAO2-F	CACCATGGCGGAAGTAAATGGAGT
DAO2-R	TTAATCTATCTTTGGGACGTCAC
CACC-GUS -F	CACCATGTTACGTCCTGTAGAAACCC
GUS-R	TCATTGTTTGCCTCCCTGCT

References

Alonso, J.M., Stepanova, A.N., Leisse, T.J., Kim, C.J., Chen, H., Shinn, P., Stevenson, D.K., Zimmerman, J., Barajas, P., Cheuk, R., Gadrinab, C., Heller, C., Jeske, A., Koesema, E., Meyers, C.C., Parker, H., Prednis, L., Ansari, Y., Choy, N., Deen, H., Geralt, M., Hazari, N., Hom, E., Karnes, M., Mulholland, C., Ndubaku, R., Schmidt, I., Guzman, P., Aguilar-Henonin, L., Schmid, M., Weigel, D., Carter, D.E., Marchand, T., Risseeuw, E., Brogden, D., Zeko, A., Crosby, W.L., Berry, C.C., Ecker, J.R., 2003. Genome-wide insertional mutagenesis of Arabidopsis thaliana. Science 301, 653–7. doi:10.1126/science.1086391

Beffa, R., Martin, H. V., Pilet, P.-E., 1990. In Vitro Oxidation of Indoleacetic Acid by Soluble Auxin-Oxidases and Peroxidases from Maize Roots. PLANT Physiol. 94, 485–491. doi:10.1104/pp.94.2.485

Butler, E.D., 2000. Characterization of auxin-induced ARRO-1 expression in the primary root of Malus domestica. J. Exp. Bot. 51, 1765–1766. doi:10.1093/jexbot/51.351.1765

Butler, E.D., Gallagher, T.F., 1999. Isolation and characterization of a cDNA encoding a novel 2-oxoacid-dependent dioxygenase which is up-regulated during adventitious root formation in apple (Malus domestica "Jork 9") stem discs. J. Exp. Bot. 50, 551–552. doi:10.1093/jxb/50.333.551

Chae, H.S., Cho, Y.G., Park, M.Y., Lee, M.C., Eun, M.Y., Kang, B.G., Kim, W.T., 2000. Hormonal cross-talk between auxin and ethylene differentially regulates the expression of two members of the 1-aminocyclopropane-1-carboxylate

oxidase gene family in rice (Oryza sativa L.). Plant Cell Physiol. 41, 354–62.

Christie, J.M., Yang, H., Richter, G.L., Sullivan, S., Thomson, C.E., Lin, J., Titapiwatanakun, B., Ennis, M., Kaiserli, E., Lee, O.R., Adamec, J., Peer, W.A., Murphy, A.S., 2011. phot1 inhibition of ABCB19 primes lateral auxin fluxes in the shoot apex required for phototropism. PLoS Biol. 9, e1001076. doi:10.1371/journal.pbio.1001076

Clough, S.J., Bent, A.F., 1998. Floral dip: a simplified method for Agrobacterium-mediated transformation of Arabidopsis thaliana. Plant J. 16, 735–43.

Dharmasiri, N., Dharmasiri, S., Estelle, M., 2005. The F-box protein TIR1 is an auxin receptor. Nature 435, 441–445. doi:10.1038/nature03543

Ding, Z., Wang, B., Moreno, I., Dupláková, N., Simon, S., Carraro, N., Reemmer, J., Pěnčík, A., Chen, X., Tejos, R., Skůpa, P., Pollmann, S., Mravec, J., Petrášek, J., Zažímalová, E., Honys, D., Rolčík, J., Murphy, A., Orellana, A., Geisler, M., Friml, J., 2012. ER-localized auxin transporter PIN8 regulates auxin homeostasis and male gametophyte development in Arabidopsis. Nat. Commun. 3, 941. doi:10.1038/ncomms1941

Dinkel, H., Van Roey, K., Michael, S., Kumar, M., Uyar, B., Altenberg, B., Milchevskaya, V., Schneider, M., Kühn, H., Behrendt, A., Dahl, S.L., Damerell, V., Diebel, S., Kalman, S., Klein, S., Knudsen, A.C., Mäder, C., Merrill, S., Staudt, A., Thiel, V., Welti, L., Davey, N.E., Diella, F., Gibson, T.J., 2015. ELM 2016-data update and new functionality of the eukaryotic linear motif resource. Nucleic Acids Res. gkv1291–. doi:10.1093/nar/gkv1291

Durek, P., Schmidt, R., Heazlewood, J.L., Jones, A., MacLean, D., Nagel, A.,

Kersten, B., Schulze, W.X., 2010. PhosPhAt: the Arabidopsis thaliana phosphorylation site database. An update. Nucleic Acids Res. 38, D828–34. doi:10.1093/nar/gkp810

Egebo, L.A., Nielsen, S. V, Jochimsen, B.U., 1991. Oxygen-dependent catabolism of indole-3-acetic acid in Bradyrhizobium japonicum. J. Bacteriol. 173, 4897–901.

Farrow, S.C., Facchini, P.J., 2014. Functional diversity of 2-oxoglutarate/Fe(II)-dependent dioxygenases in plant metabolism. Front. Plant Sci. 5, 524. doi:10.3389/fpls.2014.00524

Finet, C., Jaillais, Y., 2012. Auxology: when auxin meets plant evo-devo. Dev. Biol. 369, 19–31. doi:10.1016/j.ydbio.2012.05.039

Gazaryan, I.G., Lagrimini, L.M., Ashby, G.A., Thorneley, R.N., 1996. Mechanism of indole-3-acetic acid oxidation by plant peroxidases: anaerobic stopped-flow spectrophotometric studies on horseradish and tobacco peroxidases. Biochem. J. 313 (Pt 3, 841–7.

Geisler, M., Blakeslee, J.J., Bouchard, R., Lee, O.R., Vincenzetti, V., Bandyopadhyay, A., Titapiwatanakun, B., Peer, W.A., Bailly, A., Richards, E.L., Ejendal, K.F.K., Smith, A.P., Baroux, C., Grossniklaus, U., Müller, A., Hrycyna, C.A., Dudler, R., Murphy, A.S., Martinoia, E., 2005. Cellular efflux of auxin catalyzed by the Arabidopsis MDR/PGP transporter AtPGP1. Plant J. 44, 179–94. doi:10.1111/j.1365-313X.2005.02519.x

Goda, H., Sasaki, E., Akiyama, K., Maruyama-Nakashita, A., Nakabayashi, K., Li, W., Ogawa, M., Yamauchi, Y., Preston, J., Aoki, K., Kiba, T., Takatsuto, S., Fujioka, S., Asami, T., Nakano, T., Kato, H., Mizuno, T., Sakakibara, H.,

Yamaguchi, S., Nambara, E., Kamiya, Y., Takahashi, H., Hirai, M.Y., Sakurai, T., Shinozaki, K., Saito, K., Yoshida, S., Shimada, Y., 2008. The AtGenExpress hormone and chemical treatment data set: experimental design, data evaluation, model data analysis and data access. Plant J. 55, 526–42. doi:10.1111/j.0960-7412.2008.03510.x

Gonzalez, N., Vanhaeren, H., Inzé, D., 2012. Leaf size control: complex coordination of cell division and expansion. Trends Plant Sci. 17, 332–40. doi:10.1016/j.tplants.2012.02.003

Grefen, C., Donald, N., Hashimoto, K., Kudla, J., Schumacher, K., Blatt, M.R., 2010. A ubiquitin-10 promoter-based vector set for fluorescent protein tagging facilitates temporal stability and native protein distribution in transient and stable expression studies. Plant J. 64, 355–365. doi:10.1111/j.1365-313X.2010.04322.x

Grunewald, W., Friml, J., 2010. The march of the PINs: developmental plasticity by dynamic polar targeting in plant cells. EMBO J. 29, 2700–14. doi:10.1038/emboj.2010.181

Hodges, M., 2002. Enzyme redundancy and the importance of 2-oxoglutarate in plant ammonium assimilation. J. Exp. Bot. 53, 905–916. doi:10.1093/jexbot/53.370.905

Hu, T., Dryhurst, G., 1997. Electrochemical and peroxidase O2-mediated oxidation of indole-3-acetic acid at physiological pH. J. Electroanal. Chem. 432, 7–18. doi:10.1016/S0022-0728(97)00227-1

Ishimaru, K., Hirotsu, N., Madoka, Y., Murakami, N., Hara, N., Onodera, H., Kashiwagi, T., Ujiie, K., Shimizu, B.-I., Onishi, A., Miyagawa, H., Katoh, E.,

2013. Loss of function of the IAA-glucose hydrolase gene TGW6 enhances rice grain weight and increases yield. Nat. Genet. 45, 707–11. doi:10.1038/ng.2612

Jackson, R.G., Kowalczyk, M., Li, Y., Higgins, G., Ross, J., Sandberg, G., Bowles, D.J., 2002. Over-expression of an Arabidopsis gene encoding a glucosyltransferase of indole-3-acetic acid: phenotypic characterisation of transgenic lines. Plant J. 32, 573–583. doi:10.1046/j.1365-313X.2002.01445.x

Jackson, R.G., Lim, E.K., Li, Y., Kowalczyk, M., Sandberg, G., Hoggett, J., Ashford, D.A., Bowles, D.J., 2001. Identification and biochemical characterization of an Arabidopsis indole-3-acetic acid glucosyltransferase. J. Biol. Chem. 276, 4350–6. doi:10.1074/jbc.M006185200

Jacobs, W.P., 1993. A search for some angiosperm hormones and their metabolites in Caulerpa paspaloides (Chlorophyta).

Jin, S.-H., Ma, X.-M., Han, P., Wang, B., Sun, Y.-G., Zhang, G.-Z., Li, Y.-J., Hou, B.-K., 2013. UGT74D1 is a novel auxin glycosyltransferase from Arabidopsis thaliana. PLoS One 8, e61705. doi:10.1371/journal.pone.0061705

Johnson, P.R., Ecker, J.R., 1998. The ethylene gas signal transduction pathway: a molecular perspective. Annu. Rev. Genet. 32, 227–54. doi:10.1146/annurev.genet.32.1.227

Joseph, F., 1985. Confidence Limits on Phylogenies: An Approach Using the Bootstrap [WWW Document]. Evolution (N. Y). URL http://www.jstor.org/stable/2408678?seq=1#page_scan_tab_contents (accessed 3.7.16).

Kai, K., Horita, J., Wakasa, K., Miyagawa, H., 2007. Three oxidative metabolites of

indole-3-acetic acid from Arabidopsis thaliana. Phytochemistry 68, 1651–63. doi:10.1016/j.phytochem.2007.04.030

Kepinski, S., Leyser, O., 2005. The Arabidopsis F-box protein TIR1 is an auxin receptor. Nature 435, 446–451. doi:10.1038/nature03542

Khan, S., Stone, J.M., 2007. Arabidopsis thaliana GH3.9 in Auxin and Jasmonate Cross Talk. Plant Signal. Behav. 2, 483–5.

Kilian, J., Whitehead, D., Horak, J., Wanke, D., Weinl, S., Batistic, O., D'Angelo, C., Bornberg-Bauer, E., Kudla, J., Harter, K., 2007. The AtGenExpress global stress expression data set: protocols, evaluation and model data analysis of UV-B light, drought and cold stress responses. Plant J. 50, 347–63. doi:10.1111/j.1365-313X.2007.03052.x

Kim, J.I., Murphy, A.S., Baek, D., Lee, S.W., Yun, D.J., Bressan, R. a., Narasimhan, M.L., 2011. YUCCA6 over-expression demonstrates auxin function in delaying leaf senescence in Arabidopsis thaliana. J. Exp. Bot. 62, 3981–3992. doi:10.1093/jxb/err094

Kim, J.I., Sharkhuu, A., Jin, J.B., Li, P., Jeong, J.C., Baek, D., Lee, S.Y., Blakeslee, J.J., Murphy, A.S., Bohnert, H.J., Hasegawa, P.M., Yun, D.-J., Bressan, R. a, 2007. yucca6, a dominant mutation in Arabidopsis, affects auxin accumulation and auxin-related phenotypes. Plant Physiol. 145, 722–735. doi:10.1104/pp.107.104935

Korasick, D.A., Enders, T.A., Strader, L.C., 2013. Auxin biosynthesis and storage forms. J. Exp. Bot. 64, 2541–55. doi:10.1093/jxb/ert080

Kowalczyk, M., Sandberg, G., 2001. Quantitative analysis of indole-3-acetic acid

metabolites in Arabidopsis. Plant Physiol. 127, 1845–53.

Kramer, E.M., Ackelsberg, E.M., 2015. Auxin metabolism rates and implications for plant development. Front. Plant Sci. 6, 1–8. doi:10.3389/fpls.2015.00150

Kubeš, M., Yang, H., Richter, G.L., Cheng, Y., Młodzińska, E., Wang, X., Blakeslee, J.J., Carraro, N., Petrášek, J., Zažímalová, E., Hoyerová, K., Peer, W.A., Murphy, A.S., 2012. The Arabidopsis concentration-dependent influx/efflux transporter ABCB4 regulates cellular auxin levels in the root epidermis. Plant J. 69, 640–54. doi:10.1111/j.1365-313X.2011.04818.x

LAEMMLI, U.K., 1970. Cleavage of Structural Proteins during the Assembly of the Head of Bacteriophage T4. Nature 227, 680–685. doi:10.1038/227680a0

Larkin, M.A., Blackshields, G., Brown, N.P., Chenna, R., McGettigan, P.A., McWilliam, H., Valentin, F., Wallace, I.M., Wilm, A., Lopez, R., Thompson, J.D., Gibson, T.J., Higgins, D.G., 2007. Clustal W and Clustal X version 2.0. Bioinformatics 23, 2947–8. doi:10.1093/bioinformatics/btm404

LeClere, S., Tellez, R., Rampey, R.A., Matsuda, S.P.T., Bartel, B., 2002. Characterization of a family of IAA-amino acid conjugate hydrolases from Arabidopsis. J. Biol. Chem. 277, 20446–52. doi:10.1074/jbc.M111955200

Ludwig-Muller, J., 2011. Auxin conjugates: their role for plant development and in the evolution of land plants. J. Exp. Bot. 62, 1757–1773. doi:10.1093/jxb/erq412

Martinez, S., Hausinger, R.P., 2015. Catalytic Mechanisms of Fe(II)- and 2-Oxoglutarate-dependent Oxygenases. J. Biol. Chem. 290, 20702–11. doi:10.1074/jbc.R115.648691

Mashiguchi, K., Tanaka, K., Sakai, T., Sugawara, S., Kawaide, H., Natsume, M.,

Hanada, A., Yaeno, T., Shirasu, K., Yao, H., McSteen, P., Zhao, Y., Hayashi, K., Kamiya, Y., Kasahara, H., 2011. The main auxin biosynthesis pathway in Arabidopsis. Proc. Natl. Acad. Sci. U. S. A. 108, 18512–7. doi:10.1073/pnas.1108434108

Michniewicz, M., Brewer, P.B., Friml, J.Í., 2007. Polar auxin transport and asymmetric auxin distribution. Arabidopsis Book 5, e0108. doi:10.1199/tab.0108

Mravec, J., Skůpa, P., Bailly, A., Hoyerová, K., Krecek, P., Bielach, A., Petrásek, J., Zhang, J., Gaykova, V., Stierhof, Y.-D., Dobrev, P.I., Schwarzerová, K., Rolcík, J., Seifertová, D., Luschnig, C., Benková, E., Zazímalová, E., Geisler, M., Friml, J., 2009. Subcellular homeostasis of phytohormone auxin is mediated by the ER-localized PIN5 transporter. Nature 459, 1136–40. doi:10.1038/nature08066

Murphy, A., Taiz, L., 1999. Localization and characterization of soluble and plasma membrane aminopeptidase activities in Arabidopsis seedlings. Plant Physiol. Biochem. 37, 431–443. doi:10.1016/S0981-9428(99)80048-5

Nagpal, P., Ellis, C.M., Weber, H., Ploense, S.E., Barkawi, L.S., Guilfoyle, T.J., Hagen, G., Alonso, J.M., Cohen, J.D., Farmer, E.E., Ecker, J.R., Reed, J.W., 2005. Auxin response factors ARF6 and ARF8 promote jasmonic acid production and flower maturation. Development 132, 4107–18. doi:10.1242/dev.01955

Nonhebel, H.M., Crozier, A., Hillman, J.R., 1983. Analysis of [14C] indole-3-acetic acid metabolites from the primary roots of Zea mays seedlings using reverse-phase high-performance liquid chromatography. Physiol. Plant. 57, 129–134. doi:10.1111/j.1399-3054.1983.tb00742.x

Normanly, J., 1997. Auxin metabolism. Physiol. Plant. 100, 431–442. doi:10.1111/j.1399-3054.1997.tb03047.x

Novák, O., Hényková, E., Sairanen, I., Kowalczyk, M., Pospíšil, T., Ljung, K., 2012. Tissue-specific profiling of the Arabidopsis thaliana auxin metabolome. Plant J. 72, 523–536. doi:10.1111/j.1365-313X.2012.05085.x

Ogawara, T., Higashi, K., Kamada, H., Ezura, H., 2003. Ethylene advances the transition from vegetative growth to flowering in Arabidopsis thaliana. J. Plant Physiol. 160, 1335–40. doi:10.1078/0176-1617-01129

Östin, A., Kowalyczk, M., Bhalerao, R.P., Sandberg, G., 1998. Metabolism of indole-3-acetic acid in Arabidopsis. Plant Physiol. 118, 285–296. doi:10.1104/pp.118.1.285

Panoli, A., Martin, M.V., Alandete-Saez, M., Simon, M., Neff, C., Swarup, R., Bellido, A., Yuan, L., Pagnussat, G.C., Sundaresan, V., 2015. Auxin Import and Local Auxin Biosynthesis Are Required for Mitotic Divisions, Cell Expansion and Cell Specification during Female Gametophyte Development in Arabidopsis thaliana. PLoS One 10, e0126164. doi:10.1371/journal.pone.0126164

Parry, G., Calderon-Villalobos, L.I., Prigge, M., Peret, B., Dharmasiri, S., Itoh, H., Lechner, E., Gray, W.M., Bennett, M., Estelle, M., 2009. Complex regulation of the TIR1/AFB family of auxin receptors. Proc. Natl. Acad. Sci. 106, 22540–22545. doi:10.1073/pnas.0911967106

Peer, W.A., Blakeslee, J.J., Yang, H., Murphy, A.S., 2011. Seven Things We Think We Know about Auxin Transport. Mol. Plant 4, 487–504. doi:10.1093/mp/ssr034

Peer, W.A., Cheng, Y., Murphy, A.S., 2013. Evidence of oxidative attenuation of auxin signalling. J. Exp. Bot. 64, 2629–2639. doi:10.1093/jxb/ert152

Pencik, A., Simonovik, B., Petersson, S. V., Henykova, E., Simon, S., Greenham, K., Zhang, Y., Kowalczyk, M., Estelle, M., Zazimalova, E., Novak, O., Sandberg, G., Ljung, K., 2013. Regulation of Auxin Homeostasis and Gradients in Arabidopsis Roots through the Formation of the Indole-3-Acetic Acid Catabolite 2-Oxindole-3-Acetic Acid. Plant Cell 25, 3858–3870. doi:10.1105/tpc.113.114421

Perrot-Rechenmann, C., 2010. Cellular responses to auxin: division versus expansion. Cold Spring Harb. Perspect. Biol. 2, a001446. doi:10.1101/cshperspect.a001446

Rampey, R.A., LeClere, S., Kowalczyk, M., Ljung, K., Sandberg, G., Bartel, B., 2004. A family of auxin-conjugate hydrolases that contributes to free indole-3-acetic acid levels during Arabidopsis germination. Plant Physiol. 135, 978–88. doi:10.1104/pp.104.039677

Ray, P.M., 1958. Destruction of Auxin. Annu. Rev. Plant Physiol. 9, 81–118. doi:10.1146/annurev.pp.09.060158.000501

Raz, V., Ecker, J.R., 1999. Regulation of differential growth in the apical hook of Arabidopsis. Development 126, 3661–8.

Reinecke, D.M., Bandurski, R.S., 1988. Oxidation of indole-3-acetic acid to oxindole-3-acetic acid by an enzyme preparation from Zea mays. Plant Physiol. 86, 868–872.

Robert, H.S., Crhak Khaitova, L., Mroue, S., Benková, E., 2015. The importance of localized auxin production for morphogenesis of reproductive organs and

embryos in Arabidopsis. J. Exp. Bot. 66, 5029–42. doi:10.1093/jxb/erv256

Sagee, O., Riov, J., Goren, R., 1990. Ethylene-enhanced catabolism of [C]indole-3-acetic Acid to indole-3-carboxylic Acid in citrus leaf tissues. Plant Physiol. 92, 54–60.

Saitou, N., Nei, M., 1987. The neighbor-joining method: a new method for reconstructing phylogenetic trees. Mol. Biol. Evol. 4, 406–25.

Sandberg, G., Ernstsen, A., 1987. Dynamics of indole-3-acetic acid during germination of Picea abies seeds. Tree Physiol. 3, 185–92.

Schmid, M., Davison, T.S., Henz, S.R., Pape, U.J., Demar, M., Vingron, M., Schölkopf, B., Weigel, D., Lohmann, J.U., 2005. A gene expression map of Arabidopsis thaliana development. Nat. Genet. 37, 501–6. doi:10.1038/ng1543

Schneider, C.A., Rasband, W.S., Eliceiri, K.W., 2012. NIH Image to ImageJ: 25 years of image analysis. Nat. Methods 9, 671–675. doi:10.1038/nmeth.2089

Sembdner, G., Gross, D., Liebisch, H.-W., Schneider, G., 1980. Hormonal Regulation of Development I: Molecular Aspects of Plant Hormones, in: MacMillan, J. (Ed.), . Springer Berlin Heidelberg, Berlin, Heidelberg, pp. 281–444. doi:10.1007/978-3-642-67704-5_5

Smolka, A., Welander, M., Olsson, P., Holefors, A., Zhu, L.-H., 2009. Involvement of the ARRO-1 gene in adventitious root formation in apple. Plant Sci. 177, 710–715. doi:10.1016/j.plantsci.2009.09.009

Staswick, P.E., Serban, B., Rowe, M., Tiryaki, I., Maldonado, M.T., Maldonado, M.C., Suza, W., 2005. Characterization of an Arabidopsis enzyme family that conjugates amino acids to indole-3-acetic acid. Plant Cell 17, 616–27.

doi:10.1105/tpc.104.026690

Stepanova, A.N., Yun, J., Robles, L.M., Novak, O., He, W., Guo, H., Ljung, K., Alonso, J.M., 2011. The Arabidopsis YUCCA1 flavin monooxygenase functions in the indole-3-pyruvic acid branch of auxin biosynthesis. Plant Cell 23, 3961–73. doi:10.1105/tpc.111.088047

Suzuki, Y., Kawarada, A., 2014. Products of Peroxidase Catalyzed Oxidation of Indolyl-3-acetic Acid. Agric. Biol. Chem.

Sztein, A.E., Cohen, J.D., Slovin, J.P., Cooke, T.J., 1995. Auxin Metabolism in Representative Land Plants. Am. J. Bot. 82, 1514. doi:10.2307/2446179

Takase, T., Nakazawa, M., Ishikawa, A., Kawashima, M., Ichikawa, T., Takahashi, N., Shimada, H., Manabe, K., Matsui, M., 2004. ydk1-D, an auxin-responsive GH3 mutant that is involved in hypocotyl and root elongation. Plant J. 37, 471–83.

Tamura, K., Stecher, G., Peterson, D., Filipski, A., Kumar, S., 2013. MEGA6: Molecular Evolutionary Genetics Analysis version 6.0. Mol. Biol. Evol. 30, 2725–9. doi:10.1093/molbev/mst197

Tan, X., Calderon-Villalobos, L.I.A., Sharon, M., Zheng, C., Robinson, C. V., Estelle, M., Zheng, N., 2007. Mechanism of auxin perception by the TIR1 ubiquitin ligase. Nature 446, 640–645. doi:10.1038/nature05731

Tanaka, K., Hayashi, K., Natsume, M., Kamiya, Y., Sakakibara, H., Kawaide, H., Kasahara, H., 2014. UGT74D1 catalyzes the glucosylation of 2-oxindole-3-acetic acid in the auxin metabolic pathway in Arabidopsis. Plant Cell Physiol. 55, 218–28. doi:10.1093/pcp/pct173

Tiwari, S.B., Wang, X.J., Hagen, G., Guilfoyle, T.J., 2001. AUX/IAA proteins are active repressors, and their stability and activity are modulated by auxin. Plant Cell 13, 2809–22.

Tognetti, V.B., Van Aken, O., Morreel, K., Vandenbroucke, K., van de Cotte, B., De Clercq, I., Chiwocha, S., Fenske, R., Prinsen, E., Boerjan, W., Genty, B., Stubbs, K.A., Inzé, D., Van Breusegem, F., 2010. Perturbation of indole-3-butyric acid homeostasis by the UDP-glucosyltransferase UGT74E2 modulates Arabidopsis architecture and water stress tolerance. Plant Cell 22, 2660–79. doi:10.1105/tpc.109.071316

Vanneste, S., Friml, J., 2009. Auxin: a trigger for change in plant development. Cell 136, 1005–16. doi:10.1016/j.cell.2009.03.001

Vernoux, T., Besnard, F., Traas, J., 2010. Auxin at the shoot apical meristem. Cold Spring Harb. Perspect. Biol. 2, a001487. doi:10.1101/cshperspect.a001487

Voß, U., Wilson, M.H., Kenobi, K., Gould, P.D., Robertson, F.C., Peer, W.A., Lucas, M., Swarup, K., Casimiro, I., Holman, T.J., Wells, D.M., Péret, B., Goh, T., Fukaki, H., Hodgman, T.C., Laplaze, L., Halliday, K.J., Ljung, K., Murphy, A.S., Hall, A.J., Webb, A.A.R., Bennett, M.J., 2015. The circadian clock rephases during lateral root organ initiation in Arabidopsis thaliana. Nat. Commun. 6, 7641. doi:10.1038/ncomms8641

Xuan, W., Audenaert, D., Parizot, B., Möller, B.K., Njo, M.F., De Rybel, B., De Rop, G., Van Isterdael, G., Mähönen, A.P., Vanneste, S., Beeckman, T., 2015. Root Cap-Derived Auxin Pre-patterns the Longitudinal Axis of the Arabidopsis Root. Curr. Biol. 25, 1381–8. doi:10.1016/j.cub.2015.03.046

Zádníková, P., Petrásek, J., Marhavy, P., Raz, V., Vandenbussche, F., Ding, Z., Schwarzerová, K., Morita, M.T., Tasaka, M., Hejátko, J., Van Der Straeten, D., Friml, J., Benková, E., 2010. Role of PIN-mediated auxin efflux in apical hook development of Arabidopsis thaliana. Development 137, 607–617. doi:10.1242/dev.041277

Záveská Drábková, L., Dobrev, P.I., Motyka, V., 2015. Phytohormone Profiling across the Bryophytes. PLoS One 10, e0125411. doi:10.1371/journal.pone.0125411

Zenser, N., Ellsmore, A., Leasure, C., Callis, J., 2001. Auxin modulates the degradation rate of Aux/IAA proteins. Proc. Natl. Acad. Sci. 98, 11795–11800. doi:10.1073/pnas.211312798

Zhang, S., Wu, J., Yuan, D., Zhang, D., Huang, Z., Xiao, L., Yang, C., 2014. Perturbation of auxin homeostasis caused by mitochondrial FtSH4 gene-mediated peroxidase accumulation regulates arabidopsis architecture. Mol. Plant 7, 856–73. doi:10.1093/mp/ssu006

Zhao, Y., Christensen, S.K., Fankhauser, C., Cashman, J.R., Cohen, J.D., Weigel, D., Chory, J., 2001. A role for flavin monooxygenase-like enzymes in auxin biosynthesis. Science 291, 306–9. doi:10.1126/science.291.5502.306

Zhao, Z., Zhang, Y., Liu, X., Zhang, X., Liu, S., Yu, X., Ren, Y., Zheng, X., Zhou, K., Jiang, L., Guo, X., Gai, Y., Wu, C., Zhai, H., Wang, H., Wan, J., 2013. A role for a dioxygenase in auxin metabolism and reproductive development in rice. Dev. Cell 27, 113–22. doi:10.1016/j.devcel.2013.09.005